NASA CR-132480

A.R.A.P. REPORT NO. 219

SUBCRITICAL FLUTTER TESTING AND SYSTEM IDENTIFICATION

(NASA-CR-132480) SUBCRITICAL FLUTTER TESTING AND SYSTEM IDENTIFICATION (Aeronautical Research Associates of Princeton) 113 p HC $4.50 CSCL 01C

N74-34471

Unclas
G3/02 51093

by

John C. Houbolt

Prepared under Contract No. NAS1-11672 by

Aeronautical Research Associates of Princeton, Inc.
50 Washington Road, Princeton, New Jersey 08540

for

NATIONAL AERONAUTICS AND SPACE ADMINISTRATION

August 1974

TABLE OF CONTENTS

SUBCRITICAL FLUTTER TESTING AND SYSTEM IDENTIFICATION

By John C. Houbolt

SUMMARY

Treatment is given of system response evaluation, especially in application to subcritical flight and wind tunnel flutter testing of aircraft. An evaluation is made of various existing techniques, in conjunction with a companion survey report. Theoretical and analog experiments are made to study the identification of system response characteristics. Various input excitations are considered. New techniques for analyzing response are explored, particularly in reference to the prevalent practical case where unwanted input noise is present, such as due to gusts or wind tunnel turbulence. Further developments are also made of system parameter identification techniques.

Theory on the subject is extended, and many aspects of identifying system response characteristics are given in handbook summary fashion.

INTRODUCTION

An important and vital phase of the aeroelastic study of aircraft is the substantiation of flutter by means of subcritical flight flutter or wind tunnel tests. Because of the commonality of the problem to aircraft designs, a major conference was held on the subject in May 1958 in Washington, D.C. Until recently, little had been done toward maintaining a summary of the various techniques used, or how they compare; essentially the companies have independently pursued and developed their own individual schemes.

Communications, smaller group meetings, and conference papers indicate that there is much mutual interest in the subject, that a number of different methods are being used, and that a survey and critique of these methods would be valuable. Design considerations of the space shuttle system emphasize the need for and timeliness of such a survey.

In the aeroelastic analysis of the shuttle configuration many questions naturally arise. What subcritical flight flutter techniques are presently being used, and has the ever increasing modern computer developments led to improvements in the techniques? A significant question is whether the techniques used on aircraft are suitable for studying the flutter problem of the shuttle. It is realized that the flight parameters for the shuttle will be in a constantly changing state. Thus, steady-state-type flutter testing techniques may not be applicable, and those techniques based on transient excitation may be

the only type suitable. If present techniques do not appear suitable in application to the space shuttle, then research must be undertaken to develop flight flutter prediction methods which will be applicable.

These needs led to the study effort that is covered in this report, sponsored by Langley Research Center of NASA. Part of the effort was directed toward making a survey, reference 1. This reference should be regarded as a companion to this report. Treatment herein deals with the evaluation of various sub-critical flutter testing techniques, with the set up and conduct of numerical and analog experiments of various schemes, with the development of improved procedures, especially for the case where input noise is present, such as due to turbulence or buffeting, and with the development of system identification techniques. The report is also intended to be, in part, a handbook, since many notions used in system response evaluation are summarized.

It is of interest to note that the survey and work of this report brought out the fact that not only is there much interest in flight flutter testing in the United States, but a very deep rooted interest in England and other European countries as well, and that, in fact, several other survey-type papers on the subject have recently been written, references 2, 3, and 4.

SYMBOLS

a	a constant; elastic axis position from leading edge; lift curve slope
$A(\omega)$	real part of frequency response function
b	a constant; wing span
$B(\omega)$	imaginary part of frequency response function
c	wing chord
$C(\omega)$	amplitude of frequency response function
e	exponential function, position of c-g relative to the elastic axis, positive aft
e_f	distance of force application from elastic axis, positive forward
e_o	distance of accelerometer from elastic axis, positive forward
f	frequency in cps

$F(t)$	input force
$F_y(\omega)$	Fourier transform of function y ; generally, the subscript denotes the function
h	impulse response function
h_s	response due to $F = \frac{\sin \omega_o t}{\omega_o t}$
$H(\omega)$	frequency response function, $H = A + iB$
k	reduced frequency, $k = \frac{\omega c}{2V}$
k_m	mass radius of gyration
L	lift
m	mass; an integer
n	an integer
p	operator $\frac{\partial}{\partial t}$; a root
q	dynamic pressure, $q = \frac{1}{2} \rho V^2$
r	nondimensional elastic axis position, $r = \frac{e}{c}$
r_o	nondimensional location of accelerometer, $r_o = \frac{e_o}{c}$
r_f	nondimensional location of input force, $r_f = \frac{e_f}{c}$
$R_y(t)$	correlation function of y
s	nondimensional time, $s = \frac{2Vt}{c}$
t	time
V	velocity
w	nondimensional deflection, $w = \frac{y}{c}$
$y(t)$	general displacement response function
$y_n(t)$	response due to noise
z	deflection at accelerometer location
β	damping coefficient
β_{cr}	critical damping coefficient
δ	Dirac delta function

ϵ	time interval; also used to denote error
λ	characteristic root
μ	mass parameter
ν	measure of velocity, $\nu = \frac{2V}{c}$
ρ	air density
σ	reduced velocity, $\sigma = \frac{2V}{\omega_r c}$
τ	time
ϕ	angular displacement
$\phi_y(\omega)$	power spectrum of the function y
ω	circular frequency
ω_o	undamped frequency; a cut-off frequency
ω_r	reference frequency

GENERAL THEORETICAL RELATIONS

This section presents a listing of the principal general relations that are appropriate in the treatment of the response of linear systems to various forcing functions, and especially in application to subcritical flutter testing. For the most part, little associated discussion is given. Some derivation is given where it is felt appropriate, especially where the relationships are not generally known or used. The equations are formulated in terms of basic concepts that are involved in describing the response characteristics of a structure, such as the impulse function, the frequency response function, correlation functions, and Fourier transform relations. Some of the equations presented may appear as new developments.

General.- Let the general governing differential equation for response be given by

$$D_1 y = D_2 F \tag{1}$$

where D_1 and D_2 are differential operators, and y is the response to the forcing function F. For a simple damped mass oscillator equation (1) is

$$m\ddot{y} + \beta\dot{y} + Ky = F$$

If the input force is a Dirac impulse function at $t = 0$, equation (1) defines the impulse response function h for displacement as follows:

$$D_1 h = D_2 \delta(0) \tag{2}$$

For a unit sinusoidal input, $F = e^{i\omega t}$, and with

$$y = He^{i\omega t}$$

equation (1) yields the frequency response function

$$H(\omega) = A(\omega) + iB(\omega) \tag{3}$$

according to the equation

$$(\Delta_1 + i\Delta_2)(A + iB) = N_1 + iN_2 \tag{4}$$

where Δ_1, N_1 and Δ_2, N_2 are the real and imaginary parts that are associated with the operators D_1 and D_2. The A component of H is symmetrical with respect to the frequency ω, the B component is antisymmetrical.

The h and H functions are related by the Fourier transform pair

$$H = \int_{-\infty}^{\infty} he^{-i\omega t}\, dt \tag{5}$$

$$h = \frac{1}{2\pi} \int_{-\infty}^{\infty} He^{i\omega t}\, d\omega \tag{6}$$

Since h is zero for $t < 0$, and because of the symmetry properties of A and B, it may be shown that the following relations also apply

$$h = \frac{2}{\pi} \int_{0}^{\infty} A \cos \omega t\, d\omega$$

$$h = \frac{2}{\pi} \int_{0}^{\infty} B \sin \omega t\, d\omega$$

Useful limit properties of the H and h functions are

$$H(0) = \int_{0}^{\infty} h\, dt \tag{7}$$

$$h(0) = \frac{1}{\pi} \int_{0}^{\infty} A\, dt \tag{8}$$

The impulse response functions $\dot{h}$ and $\ddot{h}$, for velocity and for acceleration, follows as derivatives of h, and are defined by the relations

$$\dot{h} = \frac{1}{2\pi} \int_{-\infty}^{\infty} i\omega(A + iB)e^{i\omega t}\, d\omega$$

$$= \frac{1}{2\pi} \int_{-\infty}^{\infty} H_1 e^{i\omega t}\, d\omega$$

$$H_1 = \int_{-\infty}^{\infty} \dot{h} e^{-i\omega t}\, dt = A_1 + iB_1$$

$$\ddot{h} = -\frac{1}{2\pi} \int_{-\infty}^{\infty} \omega^2(A + iB)e^{i\omega t}\, d\omega$$

$$= \frac{1}{2\pi} \int_{-\infty}^{\infty} H_2 e^{i\omega t}\, d\omega$$

$$H_2 = \int_{-\infty}^{\infty} \ddot{h} e^{-i\omega t}\, dt = A_2 + iB_2$$

where

$$\left.\begin{aligned} A_1 &= -\omega B \\ B_1 &= \omega A \\ A_2 &= -\omega^2 A \\ B_2 &= -\omega^2 B \end{aligned}\right\} \qquad (9)$$

By the superposition theorem, the solution of equation (1) for any general forcing function F is given by

$$y = \int_{-\infty}^{\infty} F(\tau)h(t - \tau)\, d\tau \qquad (10)$$

The Fourier transform of this equation is

$$F_y(\omega) = H(\omega)F_F(\omega) \qquad (11)$$

where F_y and F_F denote the Fourier transforms, respectively, of y and F. Similar expressions in terms of $\dot{h}$, $\ddot{h}$, H_1, and H_2 apply for the response variables $\dot{y}$ and $\ddot{y}$. If each side of this equation is multiplied by its complex conjugate, the result is

$$F_y \bar{F}_y = H\bar{H}\, F_F \bar{F}_F$$

which leads to the well known spectral equation

$$\phi_y = |H|^2 \phi_F \tag{12}$$

relating the input spectrum ϕ_F to the output spectrum ϕ_y through the amplitude squared of the frequency response function.

A specific response equation.- A specific form of equation (1) that is of prime concern in later sections of this report is

$$y^V + a_4 y^{IV} + a_3 \dddot{y} + a_2 \ddot{y} + a_1 \dot{y} + a_1 y = b_3 \dddot{F} + b_2 \ddot{F} + b_1 \dot{F} + b_1 F \tag{13}$$

With

$$y = y_o e^{i\omega t} = (A + iB) e^{i\omega t}$$

and

$$F = e^{i\omega t}$$

this equation yields

$$(\Delta_1 + i\Delta_2)(A + iB) = N_1 + iN_2$$

where

$$\left.\begin{aligned} \Delta_1 &= \omega^4 a_4 - \omega^2 a_2 + a_o \\ \Delta_2 &= \omega^5 - \omega^3 a_3 + \omega a_1 \\ N_1 &= -\omega^2 b + b_o \\ N_2 &= -\omega^3 b_3 + \omega b_1 \end{aligned}\right\} \tag{14}$$

Solution for A and B yields the results

$$\left.\begin{aligned} A &= \frac{N_1\Delta_1 + N_2\Delta_2}{\Delta_1^2 + \Delta_2^2} \\ B &= \frac{N_2\Delta_1 - N_1\Delta_2}{\Delta_1^2 + \Delta_2^2} \\ C^2 = A^2 + B^2 &= \frac{N_1^2 + N_2^2}{\Delta_1^2 + \Delta_2^2} \end{aligned}\right\} \tag{15}$$

Another solution of importance, but which has not grown into popular use, is the solution for impedance $\frac{1}{A + iB}$ (instead of for admittance $A + iB$). It is noted that

$$\frac{1}{A + iB} = \frac{A - iB}{C^2}$$

From equations (15) and (9), it follows that

$$\left.\begin{aligned} \frac{A}{C^2} &= \frac{N_1\Delta_1 + N_2\Delta_2}{N_1^2 + N_2^2} = \frac{-\omega^2 A_2}{C_2^2} \\ \frac{B}{C^2} &= \frac{N_2\Delta_1 - N_1\Delta_2}{N_1^2 + N_2^2} = \frac{-\omega^2 B_2}{C_2^2} \\ \left(\frac{A}{C^2}\right)^2 + \left(\frac{B}{C^2}\right)^2 &= \frac{1}{C^2} = \frac{\Delta_1^2 + \Delta_2^2}{N_1^2 + N_2^2} \quad ; \quad C_2^2 = A_2^2 + B_2^2 \end{aligned}\right\} \qquad (16)$$

These equations are of special significance in the treatment of flutter.

A special type response function.- Let the input force be taken as $F = \frac{\sin \omega_o t}{\omega_o t}$; this is a simple but very special input force which has not received the recognition it deserves, and which gives a response that has many important and useful characteristics. For this force, equation (11) becomes

$$F_y(\omega) = H \times$$

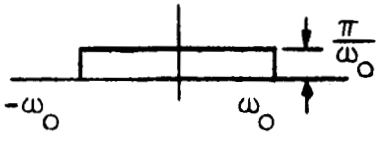

where, symbolically, the notation indicates that F_y is simply H truncated by the "box car" function. The actual response, the inverse transform of F_y, is herein denoted as h_s, and appears as

$$h_s = \int_{-\infty}^{\infty} \frac{\sin \omega_o \tau}{\omega_o \tau} h(t - \tau)\, d\tau \qquad (17)$$

Thus if the frequency response function of a system is known, and is sharply cut off to zero beyond a frequency ω_o, then the "impulse" function that is associated with the truncated frequency response function is simply the response of the

system to an input force equal to $\frac{\sin \omega_o t}{\omega_o t}$; as ω_o is made larger, the more and more h_s approaches h .

Significant differential equations in terms of correlation functions.- Several equations are developed here which are not generally known but which should be of great help in system identification studies.

Let the input force be $h(-t)$, which is the impulse response function folded around to fall along the negative t axis. By equation (10), the response would be

$$y = \int_{-\infty}^{\infty} h(-\tau)h(t - \tau)\, d\tau$$

which, in turn, may be written

$$y = \int_{-\infty}^{\infty} h(\tau)h(t + \tau)\, d\tau \tag{18}$$

This equation is, however, to within some constant, the definition of the autocorrelation function of $h(t)$. Thus, the autocorrelation function of h is the response of the system to a force input of $h(-t)$, or

$$D_1 R_h = D_2 h(-t) \tag{19}$$

A related equation is associated with the response of the system to pure white noise. Thus, if the input is white noise, equation (12) becomes

$$\phi_{y_n} \propto |H|^2$$

since ϕ_F is flat. The inverse transform of this equation is

$$R_{y_n} = \int_{-\infty}^{\infty} h(\tau)h(t + \tau)\, d\tau$$

which is the same as equation (18). Thus, the correlation function of the response due to white noise is seen to be the same as the autocorrelation function of the impulse function h .

An equation involving the cross-correlation between any input and the associated response is also of significance. The Fourier transform of equation (1) is

$$(\Delta_1 + i\Delta_2)F_y = (N_1 + iN_2)F_F$$

Multiply both sides by $\bar{F}_F$, the complex conjugate of F_F ; the result is

$$(\Delta_1 + i\Delta_2)F_y\bar{F}_F = (N_1 + iN_2)\bar{F}_F F_F$$

which immediately leads to the spectral equation

$$(\Delta_1 + i\Delta_2)\phi_{Fy} = (N_1 + iN_2)\phi_F \tag{20}$$

where ϕ_{Fy} is the cross-spectrum between the force and the response, and ϕ_F is the spectrum of the input force. The inverse transform of this spectral equation is

$$D_1 R_{Fy} = D_2 R_F \tag{21}$$

Thus, if the autocorrelation function of an input F is applied to the system as an input force, the response is the cross-correlation function between F and the response y due to F .

Some significant equalities and transforms.- Some equalities and transforms of importance are listed here to close out this section. They are given without proof or derivation.

Two basic Fourier transforms:

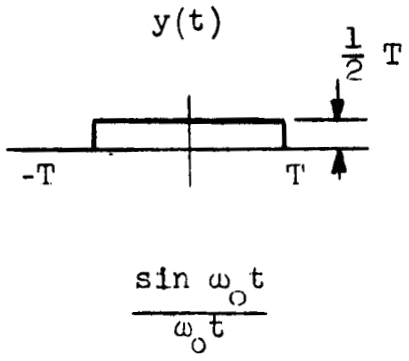

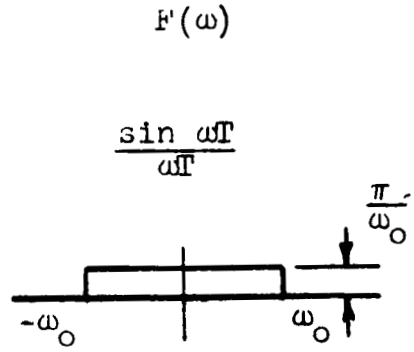

Convolution:

$$\int_{-\infty}^{\infty} \frac{\sin \omega_1 \tau}{\omega_1 \tau} \frac{\sin \omega_2(t-\tau)}{\omega_2(t-\tau)}\, d\tau = \frac{\sin \omega_1 t}{\omega_1 t} \quad \text{for} \quad \omega_2 > \omega_1$$

$$= \frac{\sin \omega_2 t}{\omega_2 t} \quad \text{for} \quad \omega_1 > \omega_2$$

$$\int_{-\infty}^{\infty} \sin \omega_1 \tau \frac{\sin \omega_2(t-\tau)}{\omega_2(t-\tau)}\, d\tau = \sin \omega_1 t \quad \text{for} \quad \omega_2 > \omega_1$$

$$= \frac{1}{2} \sin \omega_1 t \quad \text{for} \quad \omega_2 = \omega_1$$

$$= 0 \quad \text{for} \quad \omega_2 < \omega_1$$

Properties of a specific h function:

The impulse response function h for a simple damped mass oscillator is

$$h = \frac{1}{m\omega_d} e^{-\frac{\beta}{\beta_{cr}}\omega_o t} \sin \omega_d t \qquad (22)$$

where

$$\omega_d = \omega_o \sqrt{1 - \frac{\beta^2}{\beta_{cr}^2}}$$

The autocorrelation of this function, see equation (18), is

$$R_h = \frac{1}{4m^2\omega_o^3 \frac{\beta}{\beta_{cr}}} e^{-\frac{\beta}{\beta_{cr}}\omega_o t} \left[\cos \omega_d t + \frac{\frac{\beta}{\beta_{cr}}}{\sqrt{1 - \frac{\beta^2}{\beta_{cr}^2}}} \sin \omega_d t \right] \qquad (23)$$

as reference 5 also shows. The derivative of R_h is

$$\dot{R}_h = -\frac{1}{4m^2\omega_o\omega_d \frac{\beta}{\beta_{cr}}} e^{-\frac{\beta}{\beta_{cr}}\omega_o t} \sin \omega_d t \qquad (24)$$

Interestingly, $\dot{R}_h$ is seen to be equal, within a constant, to h (equation 22)). It would be of interest to study what type systems have h functions that obey this property.

CHARACTERISTICS OF VARIOUS INPUTS

Spectral content.- Figure 1 indicates in summary fashion the spectral characteristics that are associated with various inputs that are of concern in subcritical flutter testing.

Four distinctly different functions, the δ function, white noise, a swept sine, and $\frac{\sin \omega_o t}{\omega_o t}$, are seen to lead to an ostensibly flat power spectra. Besides the δ function, which is difficult to achieve in practice, the only function which leads to a truly flat power spectrum, and which extends to zero frequency is the $\frac{\sin \omega_o t}{\omega_o t}$ function. The white noise spectrum is usually quite jagged. The spectrum for a swept sine has large lobes at the low and high frequency ends. The

contrast between the swept sine and the $\frac{\sin \omega_o t}{\omega_o t}$ is interesting; the swept sine function has constant amplitude but varying frequency; the $\frac{\sin \omega_o t}{\omega_o t}$ function has a constant frequency but varying amplitude. The $\frac{\sin \omega_o t}{\omega_o t}$ function is a very attractive function for use in system identification studies and has not been exploited sufficiently. Because in the limit as $\omega_o \to \infty$ the $\frac{\sin \omega_o t}{\omega_o t}$ function approaches the δ function, it is suggested that $\frac{\sin \omega_o t}{\omega_o t}$ be termed the impulse sine function for ready identification purposes.

Classification of the swept sine function.- The swept sine function has become rather popular for use in subcritical flutter testing, reference 1. The rate of sweep or total duration is one of the prime variables; with some tests the sweep rate is fast, in others the rate is quite slow. For discussion and testing purposes, it appears desirable to make a classification of the rate or duration of sweep. The rate of change of frequency depends of course on the frequency range covered and the duration required to make the sweep. For the testing of most aircraft systems, however, it appears that classification can be based mainly on duration alone. The following classification is suggested:

1) Fast sweep - one made with a duration of about 5 seconds.

2) Moderate sweep - duration of around 1 minute.

3) Slow sweep - duration of around 5 minutes.

Each of these sweeps has certain advantages, and certain deficiencies, depending on the application. Results later in the report will try to bring out some of the relative merits.

Related differential equations.- It is perhaps of interest to note that differential equations associated with various swept sine wave laws, and with the impulse sine function, may be identified. This section shows, in the nature of an aside, the construction of these differential equations.

Consider the differential equation solution to be of the following general form

$$y = e^{f(t)} \sin g(t) \tag{25}$$

where $f(t)$ and $g(t)$ are any functions of interest. If the first and second derivative of equation (25) are formed, and if

these derivatives are combined in linear fashion with the function y, then the following differential equation may be shown as a result

$$\ddot{y} - \left(2\dot{f} + \frac{\ddot{g}}{\dot{g}}\right)\dot{y} + \left(-\ddot{f} + \dot{f}^2 + \dot{g}^2 + \dot{f}\frac{\ddot{g}}{\dot{g}}\right) y = 0 \qquad (26)$$

Equation (25) is thus a solution of this differential equation. The differential equation for various swept sine laws and for the impulse sine function follow directly from these equations.

Linear sweep law:

Consider that the solution is the swept sine wave often used as a forcing function in subcritical flutter testing, namely

$$y = \sin\theta = \sin(a + bt)t \qquad (27)$$

where instantaneous frequency is defined as

$$\omega = \frac{d\theta}{dt}$$

or

$$\omega = a + 2bt \qquad (28)$$

In terms of the beginning frequency ω_o and the end frequency ω_1, after a sweep of T seconds, a and b are

$$a = \omega_o$$

$$b = \frac{\omega_1 - \omega_o}{2}\frac{1}{T}$$

so that

$$\omega = \omega_o + (\omega_1 - \omega_o)\frac{t}{T}$$

Equation (25) reduces to equation (27) for

$$f(t) = 0$$

$$g(t) = (a + bt)t$$

By equation (26), then, the differential equation yielding equation (25) as a solution is

$$\ddot{y} - \frac{2b}{a + 2bt}\dot{y} + (a + 2bt)^2 y = 0 \qquad (29)$$

Linear sweep down:

For this case

$$y = \sin (a - bt)t \tag{30}$$

or $f(t) = 0$, and $g(t) = (a - bt)t$. Equation (26) thus indicates the associated differential equation to be

$$\ddot{y} + \frac{2b}{a - 2bt} \dot{y} + (a - 2bt)^2 y = 0 \tag{31}$$

Exponential sweep:

Let $$\omega = \omega_o e^{at}$$

so that

$$\theta = g(t) = \int \omega dt = \frac{\omega_o}{a} e^{at}$$

Through equation (26), with $f(t) = 0$, the swept sine

$$y = \sin \left(\frac{\omega_o}{a} e^{at} \right) \tag{32}$$

is thus found to be defined by the differential equation

$$\ddot{y} - a\dot{y} + \omega_o^2 e^{2at} y = 0 \tag{33}$$

Linear period sweep:

For this case

$$\omega = \frac{1}{a - bt}$$

or

$$\theta = g(t) = \int \omega dt = \frac{-1}{b} \log (a - bt)$$

and

$$y = \sin \left[- \frac{1}{b} \log (a - bt) \right] \tag{34}$$

By equation (26) with $f(t) = 0$, the differential equation is found to be

$$\ddot{y} - \frac{b}{a - bt} \dot{y} + \frac{1}{(a - bt)^2} y = 0 \tag{35}$$

The impulse sine function:

With $f(t) = - \log \omega t$

$g(t) = \omega t$

equation (25) defines the impulse sine function

$$y = \frac{\sin \omega t}{\omega t} \tag{36}$$

By equation (26), the associated differential equation is found to be

$$\ddot{y} + \frac{2}{t} \dot{y} + \omega^2 y = 0 \tag{37}$$

This equation is a special case of Bessel's differential equation, with the solution

$$y = t^{-\frac{1}{2}} Z_{-\frac{1}{2}}(-\omega t)$$

The function

$$y = \frac{\cos \omega t}{\omega t}$$

is also a solution.

Other second-order time-varying systems:

Equation (26), and the subcases given by equations (29), (31), (33), (35), and (37), are noted to be associated with linear systems with time-varying parameters. As a further aside, it may be noted that equation (26) may be useful in the study of various second-order systems having time-varying properties.

A common approach in dealing with time-varying systems is to model the system and then to seek approximate solutions to the modeled system. Reference 6 is an excellent treatise along these lines. Consideration of equations (25) and (26) suggests an approach which is just the opposite. Thus, it is supposed that the solution is known; from the solution the differential equation is derived. This differential equation is then examined to see whether it represents the system being studied, or at least is a close approximation to the system.

Consider, for example, $f(t) = - \beta t$ and $g(t) = \omega t$; equation (26) then indicates the well known damped oscillator equation

$$\ddot{y} + 2\beta\dot{y} + (\omega^2 + \beta^2)y = 0$$

In this case, a time invariant second-order system is implied by the choices for f and g. By contrast, suppose $f(t) = at + bt^2$, $g(t) = \omega t$; in this case, equation (26) indicates

$$\ddot{y} - (2a + 4bt)\dot{y} + \left[-2b + (a + 2bt)^2 + \omega^2\right]y = 0$$

This equation is noted to apply to a system with a linear change in damping and a quadratic change in frequency. If, further, a and b are small relative to ω, then the coefficient of y is roughly a constant. The equation would then represent a good approximation to a system with a linear change in damping. The nature of the homogeneous response behavior of such a system is in turn automatically given by equation (25).

SECOND-ORDER SYSTEM UNDER CONSTANT FREQUENCY EXCITATION

In studying the response characteristics of structures, one of the primary goals is to identify the frequencies and damping values of the various modes. Common or popular ways of identifying these quantities are summarized in this section in terms of a second-order system.

Figure 2 depicts a popular type construction involving the frequency response function, and specifically in the form of a plot of B against A. This presentation is often referred to as the Kennedy-Pancu method, reference 7. Much discussion on this type construction is also given in reference 8. For a second-order system, the A's and B's are given by

Displacement,

$$A + iB = \frac{\frac{F}{m\omega_o^2}}{1 - x^2 + igx}$$

Velocity,

$$A_1 + iB_1 = \frac{ix\,\frac{F}{m\omega_o}}{1 - x^2 + igx}$$

Acceleration,

$$A_2 + iB_2 = \frac{-x^2\,\frac{F}{m}}{1 - x^2 + igx}$$

where $x = \frac{\omega}{\omega_o}$, and $g = 2\frac{\beta}{\beta_{cr}}$

Characteristically, the plots for all three quantities resemble circles, and indeed the plot for velocity is a true circle. The resonant frequency is identified at the position on the "circle" where there is greatest arc length swept for equal frequency increments. Damping is found in two ways: the diameter of the circle is $1/g$ (assuming the response at zero frequency has been normalized to unity), or by the equation

$$g = \frac{2\Delta\omega}{\omega_o \tan \frac{\phi}{2}} \tag{38}$$

where ω_o is the resonant frequency.

The plot in figure 2d illustrates the results obtained if there is a mixture of viscous damping and structural "g" type damping; specifically, the frequency response function is given by

$$A + iB = \frac{\frac{F}{m\omega_o^2}}{1 - x^2 + i(gx + g_s)}$$

All results shown in figure 2 are for $g = 2\frac{\beta}{\beta_{cr}} = .1$ and $g_s = .1$, and are presented on the assumption that the factors $\frac{F}{m\omega_o^2}$, $\frac{F}{m\omega_o}$, and $\frac{F}{m}$ are unity.

Other means for evaluating frequency and damping are shown in figure 3 (again for a second-order system). The top sketch represents C^2, the square of the amplitude of the frequency response function. The resonant frequency is associated with the peak of the curve. Damping may be found as shown, either from the peak value (if $\frac{F}{m\omega_o^2}$ is known) or from the width at the half-height position. As shown in the bottom of the figure, the h function, or the response that ensues after suddenly cutting off a resonant excitation, is still another way to estimate frequency and damping. The frequency is evaluated from the period T; damping is estimated from the decay of the peaks. The curves presented are based on viscous damping and provide a quick way for estimating damping from successive peak values.

Figure 4 illustrates the impedance method which is another good way for estimating frequency and damping, although the schemes haven't been pursued greatly. The plots represent $\frac{B}{C^2}$ vs. $\frac{A}{C^2}$ and $\frac{1}{C}$ vs. ω. For a second-order system, these quantities are defined by

$$\frac{A}{C^2} = \left(1 - x^2\right) \frac{m\omega_o^2}{F}$$

$$\frac{B}{C^2} = - gx \frac{m\omega_o^2}{F}$$

$$\frac{1}{C} = \left[\left(1 - x^2\right)^2 + g^2x^2\right]^{1/2} \cdot \frac{m\omega_o^2}{F}$$

Damping and frequency are found as shown (again presented on the basis that $m\omega_o^2/F$ is unity).

Figure 5 is provided as a convenient reference figure to indicate the basic characteristics of the impulse response and frequency response functions for displacement, velocity, and acceleration for a second-order system.

RESULTS FOR SIMPLE SYSTEMS WITH TIME-VARYING INPUTS

The nature of the results that are obtained through use of swept sine and impulsive sine excitations are brought out in this section. Most of the results given have been obtained through study of a simple damped mass oscillator system, with an undamped frequency $f_o = 9.95$ cps , and a $\frac{\beta}{\beta_{cr}} = .05$.

Figure 6 shows the results for a fast swept sine run, sweeping up from 4.8 cps to 24 cps in 4 seconds. The top figure is the input force, the second the response. The figure at lower left represents the autocorrelation of the input force; the function is seen to be composed of two $\frac{\sin \omega t}{\omega t}$ type functions, thus implying a flat-type spectrum between an upper and a lower frequency. The figure on bottom right represents the autocorrelation function R_y of the response y . If the input force has a truly white spectrum, then R_y can be shown to be the same as the autocorrelation function of the h function, see equation (23) and reference 5. Further, it is also found that, at least for a single degree of freedom system, frequency and damping indicated by the R_h function are the same as for the h function. It is of interest to note that processing in this case involves use of the response only; the establishment of R_y provides a ready means for estimating system frequency and damping.

Figure 7 shows results for h as obtained from the y function of figure 6 by a randomdec-type technique (ref. 9). In contrast to the randomdec process described in reference 9, the process advocated here is developed in terms of functions that result from zero-crossings considerations; figure 7(a)

illustrates the zero-crossings technique for constructing the randomdec signature. The thesis is that the randomdec signal so obtained is the impulse response function h. The result shown in figure 7(b) represents the sum of only 20 functions, starting at the point marked a in figure 6. As seen, the beginning portion represents quite well the decaying sine wave characteristic of the h function for a second-order system. The results at larger time values cannot be considered reliable because the randomdec summation involved only 20 terms. Here is a case where a moderate sweep rate would be better for randomdec purposes. If a moderate sweep had been used, then the summation could have involved many more terms, with the consequence that h function derived would also be accurate at larger time values.

Figure 8 presents results obtained by sweeping down from 24 cps to 4.8 cps in 4 seconds. The autocorrelation function of the response y is found to be virtually the same as for the sweep-up run of figure 6.

Figure 9 presents the sweep-up results for the system with zero damping, and is given to show the caution that must be used in interpreting the autocorrelation function. The function shown in figure 9 indicates that the system appears to have some damping. The response y, however, shows a persistence in oscillations, or ringing, after the resonance frequency is passed. This is a tip-off that the system has little or no damping. Here again, if a moderate sine sweep had been used, then many more cycles of persistence would be indicated, which in turn would lead to a nondecaying autocorrelation function.

Figure 10 applies to a fourth-order system wherein two modes have frequencies close together; in this case $f_1 = 9.95$ and $f_2 = 10.73$ cps. The response y appears as in figures 6 and 8, but the autocorrelation function of y is seen to exhibit a beat pattern, as might be expected (see ref. 10). The high frequency and beat frequency seen can be used to estimate the system frequencies. The estimation of damping for each of the modes, however, is not easy. Techniques for handling the damping evaluation for such situations are in need of development.

Figure 11 shows the response that results due to use of an impulsive sine input. Shown at the bottom of the figure is the randomdec signature for h that is obtained from the response y (as outlined in fig. 7). The h obtained is virtually a true replica of the exact h for the system. This figure shows that the use of the impulsive sine function can be a powerful tool for use in evaluating system response characteristics.

The following table summarizes the frequencies and damping values that are indicated by the various evaluation techniques for the second-order system that was studied.

	ω	$\frac{\beta}{\beta_{cr}}$
Exact	9.95 cps	.05
By R_y , sweep up	9.92	.051
Randomdec of y , sweep up	9.92	.050
By R_y , sweep down	9.92	.051
From h , impulsive sine	9.96	.048

THEORETICAL FLUTTER MODEL

As an aid in the study of various subcritical flutter testing techniques, a theoretical flutter reference model was developed. This model was used to provide exact answers; the model was also set up on an analog machine so as to provide a means for simulating subcritical testing. This section describes the theoretical model used.

Differential Equation Formulation of Nonsteady Aerodynamic Forces

A novel approach is given here for approximating the air forces that develop on an airfoil having nonsteady motion. The development automatically accounts for lag in lift effects, but avoids having to give explicit consideration to the commonly used F and G functions that are due to Theodorsen and Garrick for an oscillating airfoil.

A study of oscillating airfoil theory and results for two-dimensional incompressible flow indicates that the basic lift forces on the airfoil may be represented as shown in the following sketch

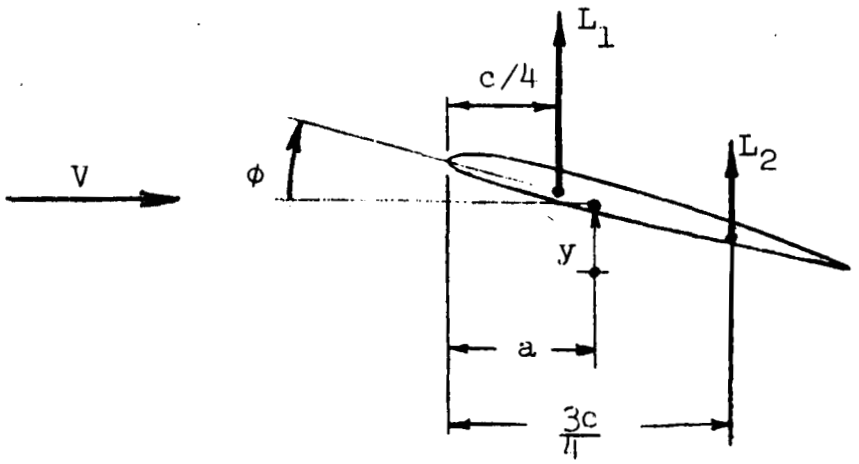

where a refers to the position of the elastic axis of the airfoil system. Besides L_1 and L_2, an additional force and a moment associated with the inertia of the air act on the airfoil; these inertia forces will be neglected in this treatment and will be assumed to be taken into account simply as additions to the mass and rotary inertia of the airfoil. Expressions for L_1 and L_2 may be written

$$L_1 = \frac{a}{2}\rho cVb\int_{-\infty}^{t}\left[V\phi - \dot{y} + c\left(\frac{3}{4} - \frac{a}{c}\right)\dot{\phi}\right]h_a(t-\tau)d\tau \tag{39}$$

$$L_2 = \frac{a\rho c^2 Vb}{8}\dot{\phi} \tag{40}$$

where h_a refers to the lift that develops at the quarter chord position due to an impulsive change in angle of attack at the 3/4-chord position, and b is airfoil span.

The growth in lift on an airfoil following a step-function change in angle of attack is often given in approximation by an equation of the form

$$1 - \phi(t) = 1 - a_1 e^{-b_1 t} \tag{41}$$

Sometimes two or more exponential terms are included, but for present purposes a single term is considered adequate. A good approximation for a wing of finite aspect ratio is, in fact, (see ref. 11)

$$1 - \phi(t) = 1 - .6e^{-.3s}$$

where $s = \frac{2Vt}{c}$.

The derivative of equation (41) yields h_a, thus

$$h_a = (1 - a_1)\delta(0) + a_1 b_1 e^{-b_1 t} \tag{42}$$

where $\delta(0)$ signifies a Dirac function at $t = 0$.

The substitution of this equation into equation (39) gives

$$L_1 = \frac{a}{2}\rho cVb\left[\left(1 - a_1\right)y(t) + a_1 b_1\int_{-\infty}^{t} y(\tau)e^{-b_1(t-\tau)}\,d\tau\right] \tag{43}$$

where $Y = V\phi - \dot{y} + c\left(\frac{3}{4} - \frac{a}{c}\right)\dot{\phi}$. The derivative of L_1 is

$$\dot{L}_1 = \frac{a}{2}\rho cVb\left[\left(1 - a_1\right)\dot{Y} - a_1 b_1^2 \int_{-\infty}^{t} Y(\tau)e^{-b_1(t-\tau)}\,d\tau + a_1 b_1 Y\right] \tag{44}$$

If equation (43) is multiplied by b_1, and the result is added to equation (44), the following simple result, void of any integrals, is found

$$\dot{L}_1 + b_1 L_1 = \frac{a}{2}\rho cVb\left[\left(1 - a_1\right)\dot{Y} + b_1 Y\right] \tag{45}$$

The development of the equations for flutter (or any arbitrary motion) can now proceed on the basis of this equation, rather than through a formulation which involves the F and G functions; nonsteady aerodynamic effects will automatically be taken into account. Note, a similar development can be made with two exponential terms in equation (41); equation (45) would then appear as a second-order differential equation for L_1.

Equations for Flutter Model

Consider the aeroelastic system depicted by the following sketches

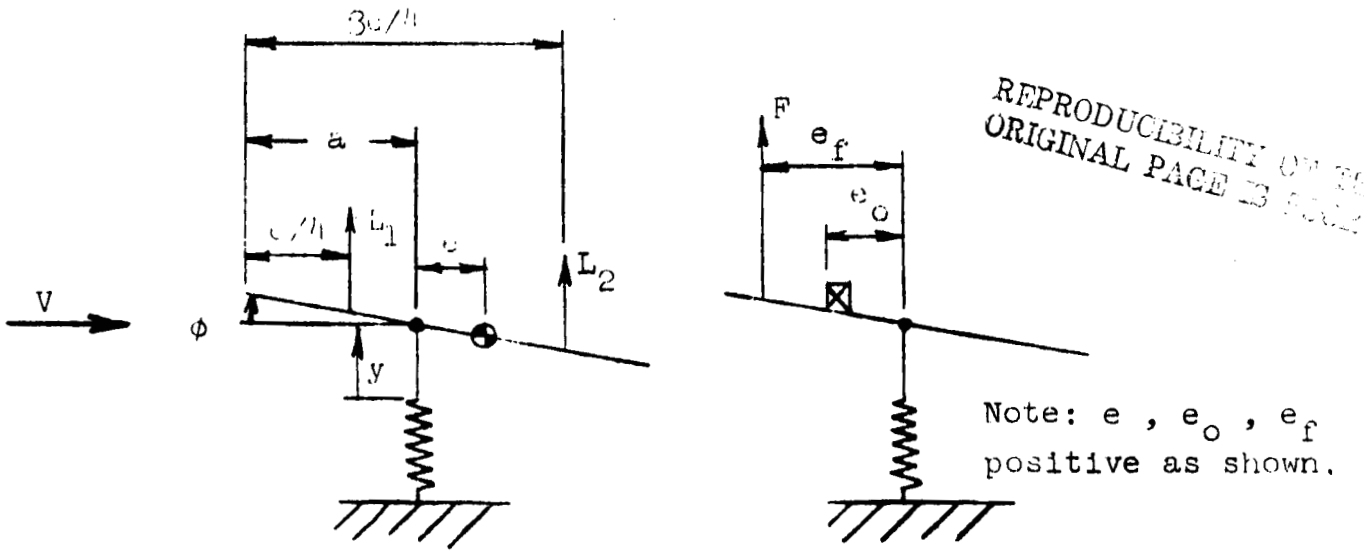

The quantity a denotes the elastic axis position; e represents the distance of the mass c-g from the elastic axis; e_f is the distance of external force application from the elastic axis, and e_o denotes the position of a response transducer, such as an accelerometer, relative to the elastic axis position.

On the basis of equations (40) and (45), the equations for motion of the system can be shown to be

$$\begin{vmatrix} \mu p^2 + \mu k_y^2 & -\mu r p^2 - \frac{1}{2} p & -1 \\ -\mu r p^2 & \mu \frac{k_m^2}{c^2} p^2 + \frac{1}{2} r_2 p + \mu \frac{k_m^2}{c^2} k_\phi^2 & -r_1 \\ 2a_2 p^2 + 2b_2 p & -2r_2 a_2 p^2 - (a_2 + 2b_2 r_2) p - b_2 & p + b_2 \end{vmatrix} \begin{Vmatrix} w \\ \phi \\ u \end{Vmatrix} = \frac{F}{2\pi q S} \begin{vmatrix} 1 \\ r_f \\ 0 \end{vmatrix} \tag{46}$$

where

$$\mu = \frac{m}{m_1} \quad ; \quad m_1 = \frac{\pi}{4} c^2 \rho b$$

$$k_y = \frac{\omega_y c}{2V} \quad ; \quad \omega_y = \sqrt{\frac{k_y}{m}}$$

$$k_\phi = \frac{\omega_\phi c}{2V} \quad ; \quad \omega_\phi = \sqrt{\frac{k_\phi}{m k_m^2}}$$

$$r = \frac{e}{c}$$

$$r_1 = \frac{a}{c} - \frac{1}{4}$$

$$r_2 = \frac{3}{4} - \frac{a}{c}$$

$$r_f = \frac{e_f}{c}$$

$$a_2 = 1 - a_1$$

$$b_2 = \frac{b_1 c}{2V}$$

and where

$$p = \frac{d}{ds} \quad ; \quad s = \frac{2Vt}{c}$$

$$w = \frac{y}{c}$$

$$u = \frac{L_1}{2\pi q S}$$

$$q = \frac{1}{2} \rho V^2$$

S = wing area = cb

The response quantities of interest herein are for displacement and acceleration at the pickup location e_o. These quantities are defined as

$$z = w + \frac{e_o}{c}\phi \tag{47}$$

$$\ddot{z} = \ddot{w} + \frac{e_o}{c}\ddot{\phi} \tag{48}$$

From equations (46) the solution for z is found to take the form

$$a_5 z^V + a_4 z^{IV} + a_3 \dddot{z} + a_2 \ddot{z} + a_1 \dot{z} + a_o z = b_3 \dddot{F} + b_2 \ddot{F} + b_1 \dot{F} + b_o F \tag{49}$$

which is the basis for equation (13) presented earlier (equation (13) is the result of normalizing by the coefficient a5). Functions (14) and frequency response solutions (15) and (16) are thus applicable to equation (49). If the right-hand side is set equal to zero, and z is assumed to be $e^{\lambda t}$, the following characteristic equation of the system is found

$$\Delta = a_5\lambda^5 + a_4\lambda^4 + a_3\lambda^3 + a_2\lambda^2 + a_1\lambda + a_o = 0$$

The roots of this equation, $\lambda = \beta + i\omega$, are a key to the system response characteristics. If λ is taken as $i\omega$, the characteristic equation yields the real and imaginary parts

$$\Delta_1 = \omega^4 a_4 - \omega^2 a_2 + a_o$$

$$\Delta_2 = \omega^5 a_5 - \omega^3 a_3 + \omega a_1$$

as defined also by equations (14).

Equations (46) (or equation (49)) were evaluated for a number of specific cases to provide exact reference results. The equations were also set up on an analog machine so as to provide a means for simulating subcritical flutter testing. Some of the exact results are presented in the following section; analog results will appear later.

Theoretical Results Indicated by Flutter Model

All of the theoretical results given herein are based on the following parameter choice

$$\mu = 10$$

$$\frac{k_m^2}{c^2} = .1$$

$$\frac{a}{c} = .35$$

$$r_1 = .1$$

$$r_2 = .4$$

$$a_2 = .6$$

$$b_2 = .3$$

In all but one case, the uncoupled torsion frequency ω_ϕ was taken as 10 cps, the uncoupled bending frequency ω_y was taken as 2 cps; in the lone case $\omega_y = \omega_\phi$. The variable parameters were as follows

$$\sigma = \frac{1}{k_r} = \frac{2V}{\omega_r c} \quad ; \quad (\omega_r \text{ is a reference freq.})$$

$$r = \frac{e}{c}$$

$$r_o = \frac{e_o}{c}$$

$$r_f = \frac{e_f}{c}$$

In all the results to follow, the reference frequency ω_r was taken as 10 cps.

System roots.- A common way to evaluate flutter speed and frequency is to solve for the roots ω_n of

$$\Delta_1 = 0$$

$$\Delta_2 = 0$$

as a function of airspeed V ; the roots of Δ_1 and Δ_2 are referred to here as quasi-flutter roots, since they are fictitious values for all speeds except the flutter speed. A flutter condition is defined when the roots of Δ_1 and Δ_2 are equal. Figure 12 shows illustrative behavior patterns for the roots of Δ_1 and Δ_2 due to variations in $\frac{e}{c}$. Note that, in agreement with results shown by other investigations, no flutter is found with the mass c.g. in a forward position, $\frac{e}{c} = -.1$. It is also to be noted that if a sixth-order system instead of a fifth-order system were being studied, then the branch labeled Δ_2 would become the Δ_1 branch.

Figure 13 is for the lone case where $\omega_y = \omega_\phi$; this situation leads to a very low flutter speed, as has often been observed.

Illustrations of the behavior patterns of the true roots, as obtained from the characteristic equation, are shown in figure 14. These roots are of physical significance since they indicate the damping and frequency of the various modes that are present in any response excitation. Flutter occurs when one of the damping values (β) becomes zero (crosses from positive to negative damping). Figures 14(c) through (e) are examples of a slow approach to flutter, since the damping degrades to zero in a slow fashion as airspeed is increased. For such cases a flutter speed prediction can usually be made by extrapolating the damping results. Figures 14(a) and (b) illustrate the behavior for an abrupt or explosive type of flutter. The damping may appear well behaved, but then with a very small speed increase can suddenly degrade to a positive value. These cases are very difficult, or impossible, to predict in practice, and are the cases that cause grave concern in flight flutter and wind tunnel testing. A comparison of figures 14(a) and (b) is interesting. In one case, the frequencies of two modes cross, while the corresponding damping values diverge; in the other case, the damping values cross, while the frequencies approach one another but then diverge. For the other cases shown in figure 14, the frequencies tend to come together, but no crossing is noted.

Figure 15 shows a comparison of the true and quasi-roots for frequencies. Figure 15(a) shows that for a mild approach to flutter (figure 14(c), the true roots and quasi-roots are markedly different (a true and quasi-root are of course the same at flutter). Figures 15(b) and (c), which apply to an explosive-type flutter, as seen in figures 14(a) and (b), show that one branch of the quasi-roots is close to the true roots. This fact, and other characteristics that are seen in figures 15(b) and (c), as contrasted to figure 15(a), suggest that perhaps there may be a "tip-off" at subcritical speeds as to whether or not the flutter may be explosive. At least three distinct patterns may be noted.

1) A quasi-root branch falls close to the true roots.

2) The top portions of the quasi-root branches tend to remain parallel over a large speed range.

3) The quasi-root branches tend to coalesce near one another (the coalescence points aren't separated greatly along the x-axis direction).

Whether all these three characteristics must appear simultaneously, or whether any one is sufficient to indicate the likelihood of an explosive flutter, is not known. Further study to investigate these tentative observations is considered desirable.

Coefficients of the governing differential equation.- There is another promising possibility for extrapolating results forward to estimate the flutter speed, which should apply whether

the approach to flutter is mild or of an explosive type. The scheme is based on the notion of identifying system parameters in a more complete way than identifying damping and frequency values only. Specifically, one concept is to identify the coefficients a_n in the governing differential equation of motion, equation (49). The problem may be stated as follows. Suppose the response z due to a given excitation force F is established; is it then possible to use z and F to estimate the coefficients a_n, thus establishing the differential equation. If the coefficients are known, then the complete response characteristics can be determined. Involved also is the notion that perhaps there is a more orderly variation of the coefficients a_n with air speed than found for the damping or frequency values. Thus, the concept advanced is that of identifying the coefficients a_n at several subcritical speeds assuming a certain order model applies, and then extrapolating these coefficients to higher speeds, and in turn to use the extrapolated values to predict the flutter speed. As a way of gaining some insight to this concept, a specific evaluation of the coefficients in equation (49) was made through use of equations (46). Airspeed and elastic axis location were left as variables, the other parameters were given the specific values indicated previously in this section. The results found are as follows:

$$
\begin{aligned}
a_5\omega_r^5 &= 10 - 100r^2 \\
\frac{a_4}{\sigma}\omega_r^4 &= 5.72 - 30r^2 - 8.6r \\
a_3\omega_r^3 &= 10.4 + (.66 - 9.3r)\sigma^2 \\
\frac{a_2}{\sigma}\omega_r^2 &= 4.3808 - (.15 + 3r)\sigma^2 \\
a_1\omega_r &= .4 + .5904\sigma^2 \\
\frac{a_o}{\sigma} &= .1 - .012\sigma^2
\end{aligned}
\qquad (50)
$$

where $\sigma = \frac{2V}{\omega_r c}$. The coefficients are noted to be invariant or have a simple quadratic variation with respect to the airspeed. Figure 16 shows the variation of the coefficients, normalized to make a_5 unity, for $r = \frac{e}{c} = .1$ and $\frac{e}{c} = .3$. Since the variation with speed is orderly, and since the theoretical model indicates the type of variation that each coefficient should exhibit (flat or parabolic), reliable extrapolation to higher airspeeds ought to be possible. The question is: "How well can the coefficients be evaluated from

measured response data?" The circled points on figure 16(a) represent estimations from response data, and will be discussed further in a subsequent section.

Results of the form presented in figures 16(a) and 16(b) may have a special significance in predicting what type of flutter may be encountered, that is, whether flutter will be of the mild type or of the explosive type. Part (a) applies to a mild type flutter, see β_2 curve of figure 14(d). The variation of the coefficient with airspeed is seen to be slight. By contrast, part (b), which applies to an explosive flutter case (see β_2 curve in figure 14(a)), shows a much greater change of the coefficients with airspeed, especially the a_3 and a_2 coefficients. Marked changes in the coefficients therefore appear to be a clue or a "tip-off" that explosive-type flutter can be expected.

Frequency response results.- Figure 17 presents representative results for frequency response as obtained from the theoretical model. Some results that were obtained from the analog computer are also indicated. The following table serves to show the parameters that apply to each figure:

Fig.	$\nu = \frac{2V}{c}$	$\frac{e}{c}$	$\frac{e_f}{c}$	$\frac{e_o}{c}$	
17(a)	60	.1	-.1	.1	Analog results also
17(b)	100	.1	-.1	.1	
17(c)	100	.1	.1	.1	
17(d)	100	.1	.1	-.3	
17(e)	100	.3	.1	.1	

The general intent is to show the variation in the frequency response function as brought about by changes in air speed, elastic axis position, and in the locations of the applied excitation force and the measuring transducer.

Figures 17(a) and (b) also include the results that were obtained from the analog computer set-up of the system. The results indicate that the analog system duplicates the theoretically exact equations of motion quite accurately.

Figure 18 shows the nature of the plots that are obtained when use is made of the impedance values $\frac{A}{C^2}$ and $\frac{B}{C^2}$, rather than A and B. The contrast with figure 4, which applies to a simple second-order system, is to be noted. The loops in the impedance loci plots are associated with the higher frequency modes of the higher order flutter system. Damping is measured by the closeness of the loops to the origin. Flutter occurs when a loop passes through the origin, thereby indicated zero damping.

Figure 19(a) presents impedance results in the form of $\frac{1}{C_2}$ (see equations (16)) versus frequency. The dips or valleys in the curve are of special signficance, since the horizontal position indicates a mode resonant frequency, while the distance of the dip from the horizontal axis indicates the damping of the mode. The right side of the figure indicates the manner of using these valleys to extrapolate to the flutter speed. In this case, an extrapolated value precisely the same as the exact value is indicated. This figure is considered a significant type plot, since it gives a fairly complete picture of the development of a flutter mode, allows both damping and frequency to be tracked readily, and leads to a fairly direct extrapolation to predict flutter. Figure 19(a) applies to a "mild" flutter case. The question naturally arises as to whether a similar type extrapolation procedure would be valid for an "explosive"-type flutter situation. In figure 19(b) results are given for an explosive case, specifically, the case covered by figure 14(a). The marked curvature of the curve is perhaps a clue that the flutter may be of the explosive type. It is seen that the variation of the $\frac{1}{C_2}$ curve is not as gradual as for the mild flutter case of figure 19(a); the variation is not nearly as abrupt, however, as is noticed for the β_2 damping curve of figure 14(a). Thus, this extrapolation procedure shows promise of applying to the explosive cases as well as the mild flutter cases.

A $\frac{\sin \omega_o t}{\omega_o t}$ VANE FORCE GENERATOR

Oscillating vanes attached to the wing structure are used quite often as a means for generating an excitation force for subcritical flutter testing. The vanes are usually driven in a swept sine fashion to produce a swept sine force. By means of the simple form offered by equation (45), it is possible to derive an equation for vane motion which allows the generation of various prescribed excitation forces.

Consider equations (39) and (40) in application to a vane executing rotary motion only about some axis (see sketch preceding equation (39)). The total lift on the vane is set equal to the desired vane force F, thus

$$L = L_1 + L_2 = F$$

From this equation the following relation may be derived

$$\dot{L}_1 + b_1 L_1 + \dot{L}_2 + b_1 L_2 = \dot{F} + b_1 F$$

Through means of equations (40) and (45), and the equation for Y following equation (43) (with the y motion suppressed), this equation may be written

$$\frac{c}{2V}\left(\frac{1}{\rho} + 2a_2 r_2\right)\ddot{\phi} + \left(a_2 + \frac{1}{\rho} b_2 + 2b_2 r^2\right)\dot{\phi} + b_1\phi = \frac{1}{2\pi qS}\left(\dot{F} + b_1 F\right) \tag{51}$$

Solution of this equation for ϕ for a stipulated F yields the vane rotational motion that is necessary to produce F. Equation (51) thus leads to a ready means for generating an impulsive sine excitation. In this case F is set equal to $\frac{\sin \omega_o t}{\omega_o t}$; the associated solution describes the vane motion that is required to produce a vane excitation force of $\frac{\sin \omega_o t}{\omega_o t}$. It is noted that this development applies for the case of a fixed wing; application to the case of a flexible or movable wing should be satisfactory, however, as long as the force being applied to the wing is measured.

DEDUCTION OF SYSTEM RESPONSE CHARACTERISTICS

This section outlines the development of various techniques for identifying the basic response characteristics of a subcritical flutter system. Attention is focused mainly on the frequency response function H, and the impulse response function h. A primary objective of forced excitation testing is to derive such functions accurately so that

a) damping and frequencies can be identified reliably,

b) or that a much more detailed system identification may be made, such as the reliable evaluation of the coefficients of the governing equation of motion.

One of the biggest problems of flutter testing is that of coping with an unknown "noise" input, such as due to atmospheric turbulence in flight flutter testing, or due to tunnel noise in wind tunnel testing. Since noise excitation represents such a serious obstacle in deducing accurate and reliable response characteristics, considerable attention was directed towards developing means for eliminating or masking noise effects. For this effort, use was made of an analog computer in conjunction with various input force generators and system response analyzers. This analog simulation proved invaluable, since many different schemes could be investigated rather quickly and repeatedly.

Surprisingly, a number of different ways for coping with the noise problem were found, each having different merits. In the development of the procedures, the following interrelated questions were kept in mind (it is suggested that these points also be kept in mind as the results are read).

1. What type of input is required?

2. What record durations are required?

3. Can reliable results be obtained from a single record?

4. Should results be obtained in the form of a single record of relatively long duration, or should the analysis be based on numerous records of short duration?

5. How much time is required to analyze the results?

Point 5 is, of course, of prime concern in flight flutter and wind tunnel testing. Shut-down time, or ground time, between test points to await data analyses is not considered desirable in general. The desire is to make a test, analyze the results in a matter of seconds or minutes so that tests can proceed almost immediately to the next point.

The following section describes the analog simulation system that was used. In the subsequent sections results obtained from the analog simulation study are described. The ideal situation of no noise in the input is described first. The following sections then describe 11 different schemes that were developed to eliminate, or at least minimize, the noise problem; 4 deal with discrete-frequency testing, 5 with time-varying excitation, and 2 deal with the use of response information alone due to noise (ironically, noise response can be used to establish noise-free response characteristics).

Analog Set-Up and Associated Excitation and Measuring Equipment

This section gives a brief description of the analog set-up that was used to simulate subcritical flutter testing of an airplane; whether the tests be in flight or in a wind tunnel.

Figure 20(a) is a block diagram indicating the various pieces of equipment used. Four types of excitation input were used, a sine wave generator, a swept sine generator, a tape recorder which could supply any specified input such as the $\frac{\sin \omega t}{\omega t}$ function, and a noise generator. In general, the noise input was treated as an unknown (nonmeasurable) quantity. The analog system was a representation of equations (46). Low-pass filters were used on both the input and output signals to ensure that the spectral content of the signals did not go beyond a certain frequency (to avoid aliasing). The Fourier analyzer was used as a ready means for processing the signals. The scope display and strip charts allowed for a "quick look" data analysis.

The printer and plotter allowed for the recording of data. Figure 20(b) shows the analog schematic that was derived from equations (46), and which was used for wiring the analog computer.

Figure 21 is a picture of the simulated flutter testing system, set up at the Langley Research Center of NASA. While equipment from a number of different sources would be suitable for use, the following listing indicates the specific hardware used.

EAI PACE	TR-48 Analog/hybrid computer
Hewlett-Packard	5451 Fourier Analyzer
	5466A Analog to digital converter
	5475A Control unit
	2100A Computer
	H01-3722A Noise generator
	5460A Display unit
	H51-18A Oscilloscope
	ASR35 Teletype Corp. printer
	7046A x-y recorder
	5323A Automatic counter
	3403C True rms voltmeter
Sangamo	Sabre III tape recorder
Tektronix	R564B Storage oscilloscope
Spectral Dynamics	SD112 Voltmeter log converter
	SD127 MZ/TFA control
	SD104A-5 Sweep oscillator
	SD109B Co/Quad analyzer
	SD105B Amplitude servo/monitor
	SD122 Tracking filter
Rockland	1022F Dual Hi/Lo filter
Datagraph	5-510 CEC Strip chart recorder
	1-511 CEC D.C. preamp.

The following sections deal with results obtained from the analog simulation just described. Most of the results given are for the following choice in parameters

$$\nu = \frac{2V}{c} = 100$$

$$\frac{e}{c} = .1$$

$$\frac{e_o}{c} = .1$$

$$\frac{e_f}{c} = .1$$

Cases which depart from these values are so indicated. Because of the limited storage capacity of the Fourier analyzer used, most of the runs involving the use of the Fourier analyzer were made covering a duration of 5 seconds only. Swept sine studies were therefore restricted to fast sweeps only.

Noise-Free Inputs

Four techniques are described here for establishing H or h when the input is free of noise.

Dwell.- Figure 22 illustrates the frequency response results that were obtained by a frequency dwell technique. In this case, the excitation force is set at a certain level and at specified frequencies. The response and input force are analyzed jointly by means of a Co-Quad analyzer to yield A, the component of the response in phase with the sinusoidal excitation force, and B, the component 90 degrees out of phase. This is a good technique if the time of dwell at each frequency is not a limiting factor.

Swept sine input with Co-Quad analyzer.- Figure 23 is typical of the results that are obtained by use of a swept since force input and the use of a Co-Quad analyzer to establish A and B as in the dwell case. The main trouble with this method is that results depend on the sweep rate, and whether the sweep is up or down. Generally, a sweep up tends to distort peaks towards the right of the correct value, while a sweep down distorts peaks to the left. Damping indicated is higher than actual. To avoid distortion, a very slow sweep rate must be used, and in such cases the dwell technique might just as well be used.

Fourier transform approach using a swept sine input.- The basis for this approach is equation (11). A swept sine input, which covers the frequency range of interest, is used for excitation purposes. The frequency response function is then evaluated from the Fourier transforms of F and y according to the equation

$$H = \frac{F_y}{F_F} \tag{52}$$

Results generally do not depend on the rate of sweep.

Figure 24 illustates some analog results that were deduced by this procedure. The top sketch applies to H_2, and h, as might be obtained through acceleration measurements. The second sketch from the top applies to H and h, as would be obtained from strain gage measurements. The sketch near the center illustrates a novel way to evaluate the function ω^2. If the functions H_2 and H are perfectly formed, then the ratio $\frac{H_2}{H}$ should evaluate to ω^2, see equations (9). The sketch shows the ratio as obtained from the analog results; the nearness to an ω^2 variation is not bad, considering that no attempt was made to establish H_2 and H as accurately as possible. Both H_2 and H are of interest in practice; the lower frequency modes tend to be emphasized by the H function, while the higher frequency modes are emphasized by H_2. The bottom sketch on the figure applies to H_1 and h.

Impulsive sine excitation.- Figure 25 shows the nature of the response that was obtained from an impulsive sine excitation. Figure 26 shows the h_s function that was obtained for a slightly impure impulsive sine force input; also shown is the associated frequency response function. The rather sharp cut-off of the function due to the use of an impulsive sine input is noted.

Discrete Frequency Testing with Noise in the Input

Frequency dwell.- Figure 27 shows results obtained using the Co-Quad analyzer. Noise causes the A_2 (Co) and B_2 (Quad) evaluations to be time varying. Results from tests at discrete frequencies thus lead to vertical marks, or ink blots, as shown. Time of dwell at each frequency was from 30 to 60 seconds. Statistically, it seems reasonable that the centroid of each ink blot should correspond to the noise-free situation. Results for no noise are indicated by horizontal tics and, indeed, these tics appear associated with the centroid location.

The curves on the figure are the result of sweep up and sweep down tests, using a Co-Quad analyzer to establish A_2 and B_2. It is seen that, with input noise present, such tests are of little value.

Figure 28 shows results obtained by using different averaging times in the Co-Quad analyzer. The curves represent transfer loci obtained by sweeping up and sweeping down with no noise present. The "random walk" patterns shown below are due to a noisy input and represents results that would appear at the specific locations A and B of the transfer locus if frequency dwells were conducted at the frequencies indicated. It is seen that increased averaging time greatly reduces the size of the random walk pattern obtained; these results thus show the effect of using longer record lengths to "average out" noise effects. The consequence, of course, is a much increased testing time. Errors due to sweep rate and averaging time of the Co-Quad analyzer are treated in reference 12.

Correlation of input and output.- The top sketch of figure 29 denotes a discrete frequency input excitation. The second sketch is the response recorded; it is composed of the response to F as well as the response due to the unknown noise excitation. If the noise and applied force are uncorrelated, which they should be in this case, then the technique of formulating the cross-correlation function between the input force F and the response y should lead to noise elimination. The bottom sketch is the cross-correlation function found. It is seen to be quite clear and regular. A comparison of R_{Fy} with F in turn allows for the accurate evaluation of A and B for the frequency considered. These results are for only 5 seconds of record. Longer time durations would lead to even better results for R_{Fy}.

Peak shifting.- In figure 30, F denotes a discrete frequency input force; y represents the measured response. If the sinusoidal curves were not present on the figure, y would seem to be a response to noise only; it contains, however, a definite sinusoidal component. The concept of using peak shifting or peak enhancement can be stated with reference to F . Consider first the trace as given, next consider a like F function and shift it so as to align peak b with a , consider another like F function and shift to make peak c align with a , and so on; then add all the results. The result is the trace labeled ΣF . Note, shifting on the Fourier analyzer system is such to cause the information that is shifted off the left side to spill around in belt fashion and appear on the right side. Summations in the overlap region are thus not valid; because of this overlap problem, the ends of the Σ trace have been cleared. Next, do the same operations with the y function, using precisely the same shifts as for the F function. The result is Σy . Frequency response information can then be evaluated from the ΣF and Σy functions.

The concept in this technique is that the shifting and adding operations causes the meaningful or intelligent part of the record to be enhanced, amplified, or reinforced, while the noise level remains the same. Note, the addition of a number of uncorrelated noise records should give a result which is similar to any one record. Thus, if an average value of the summation is formed, then the peak level should be the same as the original peak level, but the noise content should be decreasing as $\frac{1}{n}$, where n is the number of samples involved.

The establishment of a fairly clean sine wave, as indicated by the Σy , from the rather noisy function y indicates the usefulness of this peak shifting technique. The result is for only 12 additions; a larger number would lead to an improved quality for the Σy .

Ensemble averaging.- This technique is based on the concept of adding together a number of independently generated records, with the additions being made so that the input records start in the same way (phase maintained). As in the peak shifting technique, the ensemble sum of the output should show a decreasing noise content as the number in the ensemble is increased. Figure 31 illustrates the procedure. The top sketch denotes a single input record, the second sketch the measured response. The records at the bottom shows the ensemble sum for F and y as obtained from an ensemble size of 30. Note how the noise in the output has been reduced. Frequency response information follows from the ΣF and Σy records.

Time-Varying Excitation with Noise in the Input

The use of a swept sine input and the Fourier transform relation given by equation (52) leads to results of the type shown in figure 32 when an unknown noise is present in the

input. This figure should be compared with the no-noise analog result, figures 22 and 26, and with the corresponding exact result, figure 17(c). This figure vividly illustrates the problem brought about by input noise. With results of the type shown, it is virtually hopeless to deduce meaningful response characteristics. Techniques for obviating the noise problem are therefore of great interest.

Clearing or weighting of the h function.- It is to be noted that throughout this report, discussions of H or h are essentially synonymous, since, as equations (5) and (6) show, knowledge of one function automatically defines the other. The use of equation (52) leads first to H, but h then follows directly. Certain features in figure 32 are worth noting. The position labeled a on $\ddot{h}$ appears to be the point where the correct or noise-free $\ddot{h}$ function would have decayed to near zero. Beyond this point the information shown is mostly due to noise. In turn, most of the jaggedness in the A_2 and B_2 functions is due to the erratic behavior of h beyond a point such as a. The simple technique of clearing the h function beyond the point a is thus suggested as an easy means for vastly improving the noise problem, reference 13. A rectangular truncation is implied, having unity out to a selected time, and zero thereafter. Figure 33 illustrates results of this type clearing process. The results on top is another example of the type of results shown in figure 32, and are for the raw data. Clearing the h function beyond a point corresponding to a on figure 32, and then rederiving H leads to the results shown in the middle. A great improvement is noted; noise effects are still present, but at least some indications of frequencies and damping are present. The bottom sketch applies to the no-noise case and is included for comparative purposes.

References 3 and 13 indicate the use of an exponential weighting function on the raw h function, and then re-evaluating H, as a means for minimizing noise. Figure 34 shows results obtained by this approach. This technique appears to be quite effective in eliminating noise effects. The introduction of a weighting function of course causes distortions in the derived H function. Corrections that account for the weighting function must subsequently be made to the deduced damping values. Fortunately, these corrections are easy to make when an exponential function is used, since the correction is simply to subtract out the apparent damping that has been added by the weighting function. Other weighting functions are not recommended, since the corrections are not known or cannot be made.

Cross-spectrum between F and y.- The theory for this technique is as follows. The response due to an applied excitation and due to the noise environment may be written as

$$y = y_F + y_n = \int (F + F_n)h(t - \tau)d\tau \qquad (53)$$

where F_n is the unknown input noise and y_n is the associated noise contamination in the response. The Fourier transform of y is

$$F_y = F_{y_F} + F_{y_n} = (F_F + F_{F_n})H$$

If this equation is multiplied through by the complex conjugate $\bar{F}_F$, then the following spectrum equation is indicated

$$\phi_{Fy_F} + \phi_{Fy_n} = (\phi_F + \phi_{FF_n})H \tag{54}$$

Because there is no correlation between F and F_n, however, both the cross spectra ϕ_{Fy_n} and ϕ_{FF_n} should vanish. The equation then yields

$$H = \frac{\phi_{Fy_F}}{\phi_F} \tag{55}$$

which appears as a completely noise-free result. The technique is thus to form the cross-spectrum ϕ_{Fy} between the applied input and the measured response, and to divide by the input spectrum ϕ_F to obtain H.

Typical results are shown in figure 35 for the case of a swept sine excitation. A substantial improvement is noted. The illustration is not a fair test of the approach, however, because of the very short record lengths that had to be used. The results shown in figure 35 represent only 2.5 seconds of data, because correlation was involved. In spite of this limitation, a marked improvement in the noise problem is noted. It is felt that record lengths of about 30 seconds (a moderate sweep) are needed for this correlation technique, and that if such lengths were involved, then almost perfect results would be obtained. The author considers this to be one of the best techniques available for eliminating noise effects.

Peak shifting.- A peak shifting technique similar to that described under discrete frequency testing with noise in the input is also possible for a swept sine input excitation. In this case, shifts are based on the peaks of the swept sine input function; the shifts for the response are taken identical to the shifts of the input. The sum of the input shifts is treated then as a single input function, and the sum of the shifted output functions is treated as a corresponding single response function. Note, the concept that solutions for linear systems may be linearly added is involved. The summed results are treated by equation (52) as though they represented a single response run. Results obtained are shown in figure 36. Relative to figure 32, a vast improvement is found. Here again though, as with the correlation example, the test of the technique is not fair. The short record length available allowed only a small number of peaks to be summed. Thus, enhancement of the meaningful signal part was not sufficient to "average out" the noise. Record lengths of around 30 seconds (moderate

sweeps) should allow construction with many peak shifts and should make this a powerful technique.

Ensemble averaging.- The previous techniques are based on the use of a single record only. By contrast, an ensemble averaging technique involves the use of many sweep runs. The idea is simply to evaluate H or h for each of the runs and then to add the results to form an ensemble average. The concept is that noise effects will "average out" to zero. Results for an ensemble of 20 sweep runs, each of 5 seconds duration, are shown in figure 37. The figure gives the results for both $\ddot{h}$ and $\dot{h}$, and for values of $\nu = \frac{2V}{c} = 60$, 80, 100, and 110. The value of ν for flutter is 117. This technique is seen to be very effective in leading to reduced noise effects; the penalty is the problem of having to make many repeated runs.

If 20 to 30 runs, each of 5 seconds duration are needed, then a total test time of 100 to 150 seconds is implied for each test point (one speed), not counting reset times between runs. A total time of 150 seconds approaches but is still smaller than the sweep duration runs of 4 minutes that are often used in flight tests. The question is raised: "Would a single run of only about 50 seconds, analyzed by the correlation or peak shifting technique, be better?" Unfortunately, this question can not be answered at the moment.

Figure 37(a) also includes the result for $|H_2|^2$, which also represents the spectrum of $\ddot{h}$. This function is seen to be quite clean, and of all the functions shown, allows for the easiest evaluation of system damping and frequency. The frequency is indicated by the location of the peak, the damping by the width at half-peak height, see figure 3.

Combined ensemble averaging and h weighting.- Some of the methods described here can of course be used in combination. Figure 38 shows the results obtained by an ensemble averaging of only 5 runs, with the subsequent use of the exponential weighting function technique. The resulting curves are quite smooth, but correction of the data must of course be kept in mind; the results shown should be compared with the exact results shown in figure 17(c).

Ensemble averaging using response to noise only.- The treatment following equation (19) indicates that the autocorrelation function of the response to white noise is the same as the autocorrelation function of the impulse function h. This fact suggests that a useful result might be derivable by working with noise response records only. Autocorrelation functions of the response to noise alone were established for a number of individual runs. The result of adding together 20 such functions is shown in figure 39. The agreement with the result shown in figure 37 is remarkable. Damping and frequency appear to be readily identifiable. The Fourier transform of

the autocorrelation function is shown as the second function from the top. The smoothness of this function indicates that the results are essentially noise-free response results for the system. The Fourier transform of the right half of R_y is often of interest. This result is shown at the bottom of the figure.

Use of the randomdec technique.- The randomdec technique is another means for deriving system response characteristics from noise response information only. The technique described in figure 7 was applied to the noise response of the flutter system. Results are shown in figure 40; these results are to be compared with the h results shown in figure 24.

The randomdec technique may be applied to acceleration noise response results, but the construction does not lead to a system physical function. The reasons is that the Dirac function usually found with h functions, see figure 5, are not accounted for properly. The randomdec signature found from acceleration should give, however, an indication of system frequency and damping.

SYSTEM PARAMETER IDENTIFICATION

Most of the techniques used for evaluating frequency and damping of the various modes of a multimode system are based on the behavior of a single degree of freedom system. When the modal frequencies are well separated, reasonably good estimates of frequencies and damping probably result, but even in such cases, the values deduced are really only "pseudo" estimates of the true values. When frequencies are close together, identification becomes uncertain or impossible, or estimates may be in large error. The identification of the parameters of a system in greater detail is therefore desirable. The establishment of the coefficients of the governing differential equation of motion (see equation (13)) from response measurements is, for example, an extended step to better system identification. With these coefficients, all response characteristics of the system can be evaluated, whether frequencies are close together or not. The accuracy of the determination of the coefficients is of course a factor.

This section describes three means for evaluating system parameters in greater detail from response measurements. References 14 through 17 represent noteworthy treatments of the subject.

Collocation using the frequency response function.- Assume that the system under consideration is a 5th-order system, so that equation (13) applies. The frequency response equation for displacement response indicated by this equation is

$$\left[\omega^4 a_4 - \omega^2 a_2 + a_o + i\left(\omega^5 - \omega^3 a_3 + \omega a_1\right)\right](A + iB) =$$

$$- \omega^2 b_2 + b_o + i\left(-\omega^3 b_3 + \omega b_1\right) \qquad (56)$$

which when expanded leads to

$$\omega^4 A a_4 - \omega^2 A a_2 + A a_o + \omega^3 B a_3 - \omega B a_1 + \omega^2 b_2 - b_o = \omega^5 B \qquad (57)$$

$$\omega^4 B a_4 - \omega^2 B a_2 + B a_o - \omega^3 A a_3 + \omega A a_1 + \omega^3 b_3 - \omega b_1 = -\omega^5 A \qquad (58)$$

The multiplication through of equation (56) by $A - iB$ and division by $C^2 = A^2 + B^2$ leads to the following two alternative forms

$$\omega^4 a_4 - \omega^2 a_2 + a_o + \omega^3 \frac{B}{C^2} b_3 + \omega^2 \frac{A}{C^2} b_2 - \omega \frac{B}{C^2} b_1 - \frac{A}{C^2} b_o = 0 \qquad (59)$$

$$- \omega^3 a_3 + \omega a_1 + \omega^3 \frac{A}{C^2} b_3 - \omega^2 \frac{B}{C^2} b_2 - \omega \frac{A}{C^2} b_1 + \frac{B}{C^2} b_o = - \omega^5 \qquad (60)$$

The collocation solution proceeds by using these equations singly or jointly to solve for the a_n and b_n coefficients. Consider equation (57) for example; five a_n and two b_n coefficients appear in this equation. Measured values of A and B are substituted in this equation at seven different values of ω, leading to seven linear simultaneous equations with unknowns a_n and b_n. Solution is then made for these coefficients. Or, five frequency values may be used in equation (57) and four in equation (58), giving nine simultaneous equations in terms of the total of nine unknown coefficients.

A test of the approach was made by using values of A and B as obtained from the exact solution, equation (49). The coefficients evaluated were in good agreement with the original coefficient used to obtain the A and B values; this comparison is shown in figure 16, where the circled points refer to the coefficients as evaluated by the collocation procedure. This comparison indicates that the scheme works, at least in principle.

Analog values of A and B were also used to check the procedure. Some of the results obtained were good, some were bad, depending on the frequency locations chosen. Figure 41 indicates a few of the results obtained, and shows the quasi-roots that were obtained from the deduced coefficients in comparison to the exact quasi-roots. The results indicate that perhaps the best procedure to use is to evaluate the

coefficients several times for different frequency choices (the evaluation is very quick since only a few simultaneous linear equations are involved) and then to average the results.

To check further on the collocation procedure, a sensitivity study was made to establish how sensitive the coefficients a_n and b_n were to assumed changes in A and B. Figure 42 indicates the results of this study. The study started with the exact values of A and B. These values were given random variations through use of a random number generator. With the varied values, solution was made for the a_n and b_n coefficients. This experiment was repeated 100 times. The σ_A value in figure 42 represents the standard deviation of all the variations of the A and B values; the σ_a value, the standard deviation of all the variations found for the a_n and b_n values. This figure shows that the coefficients are quite sensitive to the A and B values used (roughly, a magnification in errors of 200).

Least squares difference equation approach.- The difference equation equivalent of equation (13) may be written as

$$y_{n+5} + a_4 y_{n+4} + a_3 y_{n+3} + a_2 y_{n+2} + a_1 y_{n+1} + a_o y_n = b_4 F_{n+4} + b_3 F_{n+3} + b_2 F_{n+2} + b_1 F_{n+1} \qquad (61)$$

where the y's and F's represent equally spaced values with interval ϵ. The a_n and b_n coefficients used here are not the same as the coefficients in equation (13), but rather are some combination of these coefficients. Assume the y_n and F_n values are measured values as obtained from a test, and rewrite equation (61) in the form

$$y_{n+5} + a_4 y_{n+4} + a_3 y_{n+3} + a_2 y_{n+2} + a_1 y_{n+1} + a_o y_n - b_4 F_{n+4} - b_3 F_{n+3} - b_2 F_{n+2} - b_1 F_{n+1} = \epsilon_n$$

where ϵ_n represents a possible error because the y_n and F_n values are not exact. The coefficients a_n and b_n are now found using a least squares process involving the error ϵ_n. The problem statement appears as

$$E = \sum \epsilon_n^2 = \min.$$

Minimization yields

$$\frac{\partial E}{\partial a_m} = \sum_{n=1}^{k} \epsilon_n y_{n+m} = 0 \qquad (62)$$

$$\frac{\partial E}{\partial b_m} = \sum_{n=1}^{k} \epsilon_n F_{n+m} = 0 \qquad (63)$$

thus leading to nine linear simultaneous equations in nine unknowns. Solution yields the desired values of a_n .

With the solution for the a_n values, the roots of the characteristic equation of the difference equation may be found. Assume the right-hand side of equation (61) is zero and let $y = e^{\lambda t} = e^{\lambda n \epsilon}$; the result is

$$p^5 + a_4 p^4 + a_3 p^3 + a_2 p^2 + a_1 p + a_o = 0 \qquad (64)$$

where $p = e^{\lambda \epsilon}$. Solution of this equation yields the roots

$$p_n = c_n \pm i d_n$$

Roots which approximate the roots of the characteristic equation of equation (26) may be now established as follows. Let $\lambda = \beta \pm i\omega$ represent these approximate roots; then

$$e^{(\beta_n \pm i\omega_n)\epsilon} = p_n = c_n \pm i d_n \qquad (65)$$

Solution for β_n and ω_n yields

$$\tan \omega_n \epsilon = \frac{d_n}{c_n} \qquad (66)$$

$$e^{2\beta_n \epsilon} = c_n^2 + d_n^2 \qquad (67)$$

Application of this least squares procedure was made to the $\ddot{h}$, $R_{\ddot{h}}$ and $R_{\dot{h}}$ functions, as given in figure 37. Since these functions represent homogeneous solution of equation (13), no F_n terms had to be considered; that is, equations (63) were not involved. Note, the initial values of the functions were not used so as to avoid the problem of their Dirac function type beginning. Results obtained for ω_n and β_n for the value of $\nu = 110$ are shown in the following table. The estimates for the first mode show a considerable variation; second mode values, however, are in good confirmation. It should be kept in mind that these limited results do not represent a fair test of this difference equation approach. First, the spacing ϵ was rather large; a value of $\epsilon = .02$ sec. was used, and thus one cycle of the higher frequency mode is represented by only six points. Second, the maximum number of points used was only 64. And, thirdly, there is very little response of the first mode present in the $\ddot{h}$ functions.

From:	$\ddot{h}$			$R_h^{\ddot{}}$			$R_h^{\dot{}}$			Exact
N	16	32	64	16	32	64	16	32	64	
$\left(\frac{\beta}{\beta_{cr}}\right)_1$	-1.38	-1.53	-1.38		-4.36	-1.97	-.864	-.786	-.689	.925
f_1	5.93	5.56	6.04		2.13	4.45	3.50	3.52	3.85	4.15
$\left(\frac{\beta}{\beta_{cr}}\right)_2$	-.036	-.033	-.036	- 029	-.030	-.031	-.032	-.033	-.033	.031
f_2	8.03	7.98	8.01	8.00	8.01	8.02	7.97	7.96	7.95	8.05

Differential equation solution by least squares.- An interesting least squares solution can be made in the time plane, but which makes use of frequency plane information. Consider equation (13) in the following form

$$y^{V} + a_4 y^{IV} + a_3 \dddot{y} + a_2 \ddot{y} + a_1 \dot{y} + a_o y - b_3 \dddot{F} - b_2 \ddot{F} - b_1 \dot{F} - b_o F = \epsilon(t) \tag{68}$$

where ϵ represents an error due to the use of measured y and F values. Assume that the response data have been processed to lead to $y = h_s$, see equation (17). The function h_s corresponds to the response due to $F = \frac{\sin \omega_o t}{\omega_o t}$, and falls out in a straightforward natural way when processing is made on the basis of the Fourier transform relation, equation (52). Note, this analysis, although presented in terms of h_s and $F = \frac{\sin \omega_o t}{\omega_o t}$, is not restricted to these functions alone.

The coefficients a_n and b_n are now evaluated through use of a least squares statement involving ϵ, thus

$$E = \int_{t_1}^{t_2} \epsilon^2(t)dt = \text{Min.} \tag{69}$$

$$\frac{\partial E}{\partial a_n} = \int_{t_1}^{t_2} \epsilon \frac{\partial^n y}{\partial t^n} dt = 0 \tag{70}$$

$$\frac{\partial E}{\partial b_n} = \int_{t_1}^{t_2} \epsilon \frac{\partial^n F}{\partial t^n} dt = 0 \tag{71}$$

Equations (70) and (71) give simultaneous linear equations in terms of the a_n and b_n coefficients, which then allows their evaluation to be made.

Equations (70) and (71) may be converted to a more amenable form as follows. With limits extending from $t = -\infty$ to $t = \infty$, the integrals which appear in the simultaneous equations may be written in three general forms

$$\left.\begin{aligned} A_{mn} &= \int_{-\infty}^{\infty} \frac{\partial^m y}{\partial t^m}\,\frac{\partial^n y}{\partial t^n}\,dt \\ B_{mn} &= \int_{-\infty}^{\infty} \frac{\partial^m y}{\partial t^m}\,\frac{\partial^n F}{\partial t^n}\,dt \\ C_{mn} &= \int_{-\infty}^{\infty} \frac{\partial^m F}{\partial t^m}\,\frac{\partial^n F}{\partial t^n}\,dt \end{aligned}\right\} \qquad (72)$$

Use is now made of two significant Fourier transform theorems, namely

1. The Fourier transform of $\frac{d^n y}{dt^n}$ is $(i\omega)^n F_y$, where F_y is the Fourier transform of y

2. $\int_{-\infty}^{\infty} F_1(f)F_2(\mp f)df = \int_{-\infty}^{\infty} y_1(t)y_2(\mp t)dt$ where $\omega = 2\pi f$

With these theorems, equations (72) become

$$\left.\begin{aligned} A_{mn} &= \frac{i^m(-i)^n}{2\pi}\int_{-\infty}^{\infty} \omega^{m+n}\,|F_y|^2 d\omega \\ B_{mn} &= \frac{i^m(-i)^n}{2\pi}\int_{-\infty}^{\infty} \omega^{m+n}\,F_y\bar{F}_F\,d\omega \\ C_{mn} &= \frac{i^m(-i)^n}{2\pi}\int_{-\infty}^{\infty} \omega^{m+n}\,|F_F|^2 d\omega \end{aligned}\right\} \qquad (73)$$

For the $y = h_s$ function, let

$$F_y = F_{h_s} = A + iB \quad , \quad \text{with} \quad C^2 = A^2 + B^2$$

and for the $F = \frac{\sin \omega_o t}{\omega_o t}$ function it is known that

$$F_F = \frac{\pi}{\omega_o} \quad , \quad -\omega_o < \omega < \omega_o$$

$$= 0 \quad , \quad \omega < -\omega_o \text{ and } \omega > \omega_o$$

Equations (73) thus become simply

$$A_{mn} = \frac{i^m(-i)^n}{\pi} \int_0^\infty \omega^{m+n} C^2 d\omega \quad , \quad m+n \text{ even}$$

$$= 0 \quad , \quad m+n \text{ odd}$$

$$B_{mn} = \frac{i^m(-i)^n}{\omega_o} \int_0^\infty \omega^{m+n} A \, d\omega \quad , \quad m+n \text{ even}$$

$$= \frac{i^{m+1}(-i)^n}{\omega_o} \int_0^\infty \omega^{m+n} B \, d\omega \quad , \quad m+n \text{ odd}$$

$$C_{mn} = \frac{i^m(-i)^n \pi}{\omega_o^2} \frac{1}{m+n+1} \omega_o^{m+n+1} \quad , \quad m+n \text{ even}$$

$$= 0 \quad , \quad m+n \text{ odd}$$

Through means of equations (72) through (74), it is possible to write equations (70) and (71) as follows

$$\begin{vmatrix} D_8 & 0 & -D_6 & 0 & D_4 & F_7 & E_6 & -F_5 & -E_4 \\ 0 & D_6 & 0 & -D_4 & 0 & -E_6 & F_5 & E_4 & -F_3 \\ -D_6 & 0 & D_4 & 0 & -D_2 & -F_5 & -E_4 & F_3 & E_2 \\ 0 & -D_4 & 0 & D_2 & 0 & E_4 & -F_3 & -E_2 & F_1 \\ D_4 & 0 & -D_2 & 0 & D_0 & F_3 & E_2 & -F_1 & -E_o \\ F_7 & -E_6 & -F_5 & E_4 & F_3 & G_6 & 0 & -G_4 & 0 \\ E_6 & F_5 & -E_4 & -F_3 & E_2 & 0 & G_4 & 0 & -G_2 \\ -F_5 & E_4 & F_3 & -E_2 & -F_1 & -G_4 & 0 & G_2 & 0 \\ -E_4 & -F_3 & E_2 & F_1 & -E_o & 0 & -G_2 & 0 & G_o \end{vmatrix} \begin{vmatrix} a_4 \\ a_3 \\ a_2 \\ a_1 \\ a_o \\ b_3 \\ b_2 \\ b_1 \\ b_o \end{vmatrix} = \begin{vmatrix} 0 \\ D_8 \\ 0 \\ -D_6 \\ 0 \\ -E_8 \\ F_7 \\ E_6 \\ -F_5 \end{vmatrix}$$

(75)

where

$$D_n = \int_0^\infty \omega^n C^2 \, d\omega$$

$$E_n = \int_0^\infty \omega^n A \, d\omega$$

$$F_n = \int_0^\infty \omega^n B \, d\omega$$

$$G_n = \frac{1}{m + n + 1} \omega_o^{m+n+1}$$

Solution of these equations leads to the differential equation coefficients a_n and b_n. The symmetry of equations (75), and repeated appearance of the D_n, E_n and F_n coefficients should be noted. In all, only 14 such coefficients need evaluation (the four F_n values are known). One of the appealing merits of this approach is that the D_n's and E_n's may be evaluated automatically by the Fourier analyzer that is being used to analyze the response. Solution for the a_n values should therefore be quite easy and quick.

A minor test of equations (75) was made using only approximate values for D_n, E_n and F_n; results for a_n were, however, in reasonable agreement with the corresponding exact values. Further study of the soundness of this least squares technique is worthwhile.

CONCLUDING REMARKS

Main emphasis in this report has been on the development of improved subcritical flutter testing techniques, whether in flight or in the wind tunnel, and particularly in reference to the situation where input noise is present. Discussion was given to a certain extent as the material was presented. Some additional observations are made here in the form of concluding remarks.

Frequency and damping evaluation:

A number of different schemes were outlined for deducing frequency and damping from response measurements. Mode frequency is identified quite well by most all of the techniques. Damping determination, however, is more nebulous. The transfer locus scheme, which hopefully leads to identifiable circles, is popularly quoted but the author does not favor this approach too highly. The diameter of a circle obtained from acceleration measurements is, for example, $\frac{1}{g}\frac{F}{m}$ (assuming of course that

behavior is that of a single degree of freedom system). Thus, explicit g evaluation from the diameter is precluded because the unknown $\frac{F}{m}$ is also involved (m, in general, is some generalized mass value). Actually, it would be better to use equation (38) to evaluate g (if the center of the apparent circle can be fixed), and then to use the diameter to evaluate $\frac{F}{m}$. The methods preferred are those shown in figure 3, and particularly the scheme involving use of the width of the spectrum peak at half power. This scheme is simple and direct, and subjective interpretation is a minimum. (Note, with g established by the width of the peak, the height in turn may be used to estimate $\frac{F}{m}$.) The scheme of deducing damping from a randomdec signature is also considered good and reliable. It is to be noted that all of the schemes are subject to a common problem; specifically, all the methods for deducing frequencies and damping are open to question for the situation where two (or more) frequencies of the system are close together. Means of being able to detect when frequencies are close together and, in turn, of deducing the frequencies and damping are in need of further development.

Deduction of H or h:

As indicated, a number of methods may be used for obviating the input noise problem. The ensemble averaging technique is attractive but requires a substantial number of repetitive runs. The use of exponential weighting of the h function appears satisfactory, but schemes which do not lead to distortion of the data, which then require correction, are judged preferable. The cross-correlation approach (equation (21) and equation (55)), and the peak shifting technique seem the most appealing on the overall. The technique of using the response only, as obtained from a "white" noise environment, and forming the autocorrelation function, with ensemble averaging, is quite intriguing and should be used where possible; in this case, a function representing the autocorrelation function of h is found. In general, randomdec signatures may be interpreted as h only for displacement response. Randomdec signatures obtained from velocity or acceleration response are not strictly the h or h functions because step functions or Dirac functions at the origin are not reproduced (see h and h in figure 5). Damping and frequencies as established from the randomdec signatures for velocity or acceleration response should, however, be representative of actual system response characteristics.

System identification:

A variety of possible system identification schemes were developed, but attention was restricted herein to three approaches. The collocation scheme is quite simple but suffers from the fact that the frequency values chosen for response

matching is so arbitrary. The question of how to handle the two equations in combination (one associated with the real part of the solution, one with the imaginary part) is somewhat of a mystery. The difference equation approach is considered good and quite attractive. An analogous scheme, reported in references 2 and 13, appears to be highly regarded. The differential equation approach, which makes use of frequency plane information, needs more corroborative study, but is considered quite promising.

A final word is given with respect to subcritical flutter testing techniques which differ from the type discussed herein. Tacit in the schemes mentioned in this report is the assumption that the air density is constant, and that tests proceed on an incremental increase in air speed basis. Reference 17 describes procedures for testing on an increase of air density basis, holding speed essentially constant. Figure 43, taken from this reference, shows the excellent success that was obtained in extrapolating to flutter through use of a density increase approach. This technique is still considered to be a good and useful approach and should be kept in mind in any further development studies of subcritical flutter testing.

Application to the space shuttle:

Flight of the space shuttle will represent a situation of a time-varying system, since dynamic pressure and Mach number in particular will change rapidly with time, see figure 7, of reference 1. The question that naturally arises is whether the methods discussed in this report, which apply mainly to time invariant systems, can be used for subcritical flutter evaluation of the shuttle system. With respect to the various methods, the following recommendations are made. During the transonic region of flight (where the dynamic pressure will be nominally about 75% of q_{max}), the random forcing input associated with the transonic flow will probably be strong enough to excite a sizable random response. It follows then that two of the methods discussed herein might be useful in evaluating the shuttle response characteristic. One is to break the record up into 5-second segments (on the assumption that the system is nearly time-invariant during such an interval) and then to form the autocorrelation function of the response for each segment. The second approach is to form the randomdec signature from the random response record.

At maximum dynamic pressure, the Mach number will nominally be around 1.5. It is not known at this time whether the flow during this period will be rough enough to cause random excitation. If tests indicate that the flow should still be "rough," then the same two means for analyzing the data should be used.

To ensure that system excitation can be obtained over all regions of flight, it is desirable to have aerodynamic vanes or inertial shakers installed. The excitation recommended is to go through a sine sweep, first up, and then down, in continuous succession. Sweep durations of 5 seconds are suggested. Each five seconds of response information could then be analyzed to deduce H and h through means of the method involving the Fourier transform of the output response to the Fourier transform of the input force. In this case, the procedure involving the peak shifting technique would appear ideally suited. Note, the time-varying aspect more or less precludes any ensemble averaging approach. The auto-correlation of the response due to the sweeps should also be obtained as an additional means for evaluation of the response characteristics.

In summary, three approaches appear useful for subcritical flutter test evaluation of the space shuttle system, namely

1) The autocorrelation of system response, whether the response is due to a natural random excitation or due to a controlled force excitation.

2) The randomdec signature approach.

3) The use of the peak shifting approach.

REFERENCES

1. Rosenbaum, Robert, "Survey of Aircraft Subcritical Flight Flutter Testing Methods," NASA CR-132479, May 1974.

2. Baird, E.F. and Clark, W.B., "Recent Developments in Flight Flutter Testing in the United States," AGARD Report No. 596.

3. Baldock, J.C.A. and Skingle, C.W., "Flutter Technology in the United Kingdom - A Survey," AIAA Paper No. 73-330.

4. Dat, Rolland, "The Theoretical and Experimental Methods Used in France for Flutter Prediction," AIAA Paper No. 73-329.

5. Kandianis, F., "Frequency Response of Structures and the Effects of Noise on its Estimates from the Transient Response," J. Sound Vib., 15(2), March 1971, pp. 203-215.

6. Reed, Wilmer H., III, "Effects of a Time-Varying Test Environment on the Evaluation of Dynamic Stability with Application to Flutter Testing," J. of the Aero/Space Sciences, Vol. 25, No. 7, July 1958.

7. Kennedy, Charles C. and Pancu, C.D.P., "Use of Vectors in Vibration Measurement and Analysis," J. of the Aeronautical Sciences, Vol. 14, No. 11, November 1947.

8. de Vries, Gerhard and Beatrix, Christian, "General Measuring Processes of Vibratory Characteristics of Lightly Damped Linear Structures," Progress in Aeronautical Sciences, Vol. 9, Pergamon Press, Oxford and New York, 1968.

9. Cole, Henry A., Jr., "On-Line Failure Detection and Damping Measurement of Aerospace Structures by Random Decrement Signatures," NASA CR-2205, March 1973.

10. White, R.G., "Evaluation of the Dynamic Characteristics of Structures by Transient Testing," J. Sound Vib., 15(2), March 1971, pp. 147-161.

11. Houbolt, John C., "A Recurrence Matrix Solution for the Dynamic Response of Aircraft in Gusts," NACA TN 2060, March 1950.

12. Reed, W. H., III, Hall, A.W., and Barker, L.E.J., "Analog Techniques for Measuring the Frequency Response of Linear Physical Systems Excited by Frequency-Sweep Inputs," NASA TN D-508, October 1960.

13. Newman, K.W., Skingle, C.W., and Gaukroger, D.R., "The Development of Rapid-Testing Techniques for Flutter Experiments," Royal Aircraft Establishment, Tech. Report No. 73067, May 1973.

14. Waisanen, P.R. and Perangelo, H.J., "Real Time Flight Flutter Testing via Z-Transform Analysis Technique," AIAA Paper No. 72-784.

15. Gaukroger, D.R., Skingle, C.W., and Heron, K.H., "Numerical Analysis of Vector Response Loci," J. of Sound and Vib., 29(3), 1973, pp. 341-353.

16. Heron, K.H., Gaukroger, D.R., and Skingle, C.W., "The Derivation of Equations of Motion from Response Data and its Application in Flutter Testing," Royal Aircraft Establishment, Tech. Report No. 73051, June 1973.

17. Taylor, Lawrence W., Jr. and Iliff, Kenneth W., "Systems Identification Using a Modified Newton-Raphson Method - A FORTRAN Program," NASA TN D-6734, May 1972.

18. Houbolt, John C. and Rainey, A. Gerald, "On the Prediction of Critical Flutter Conditions from Subcritical Response Data and Some Related Wind-Tunnel Experience," presented at the Flight Flutter Testing Symposium, Wash., D.C., May 15-16, 1958.

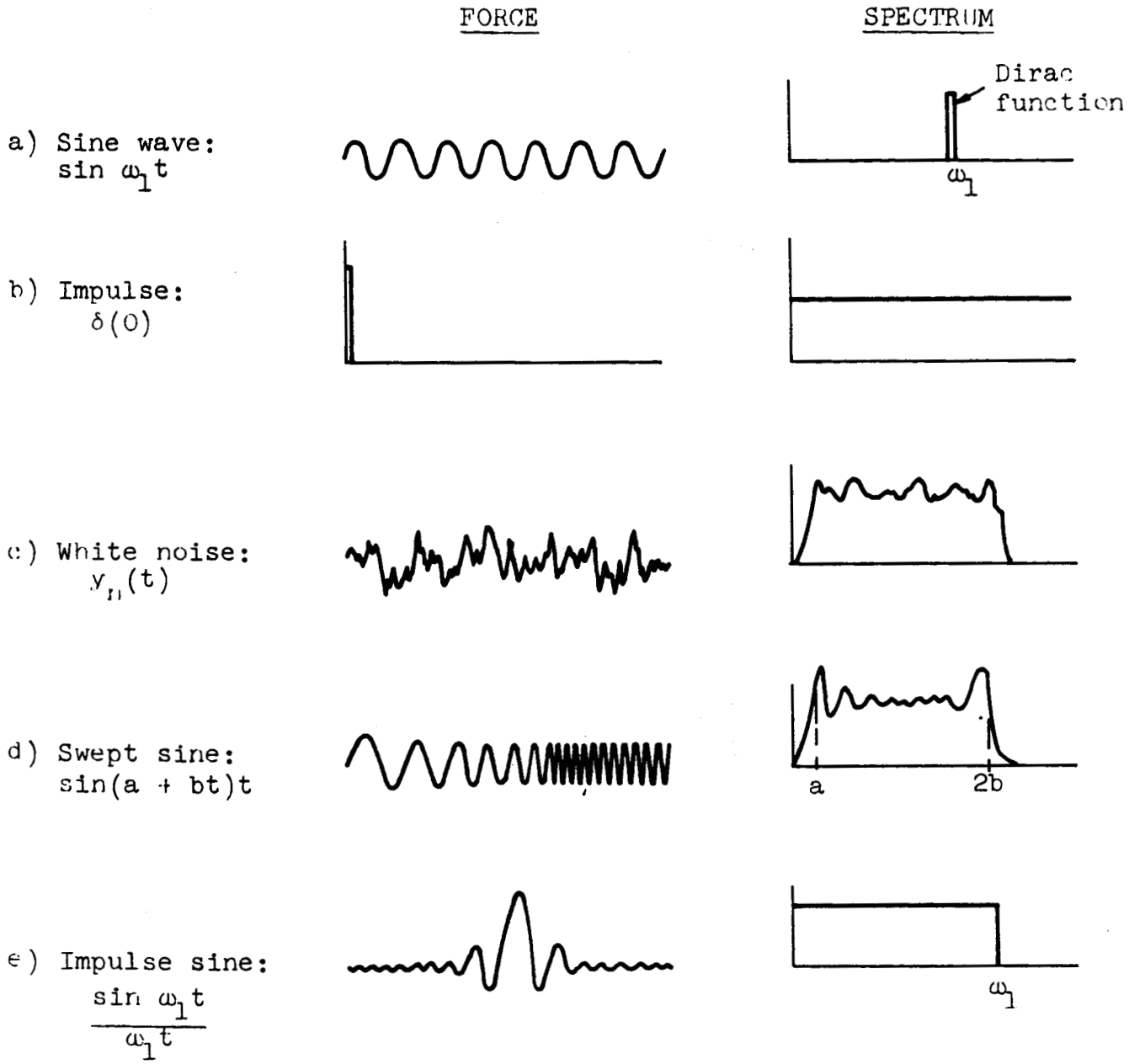

Fig. 1.- Spectra for various input forces.

f) Swept sine (same as d)

g) Swept triangular wave

h) Swept square wave

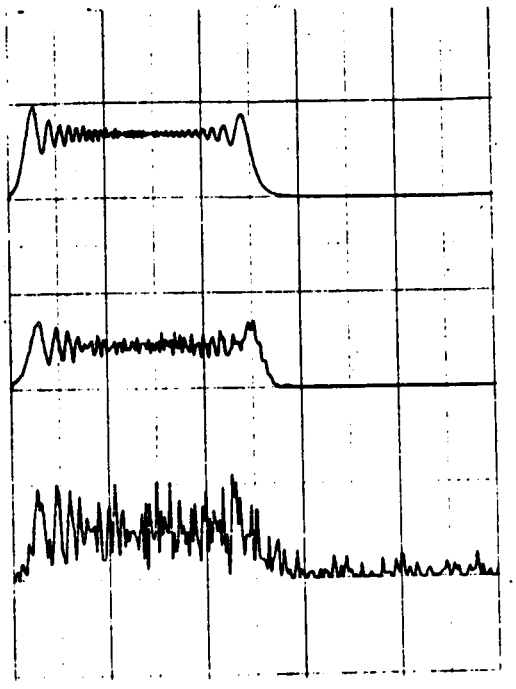

Fig. 1.- (Concluded)

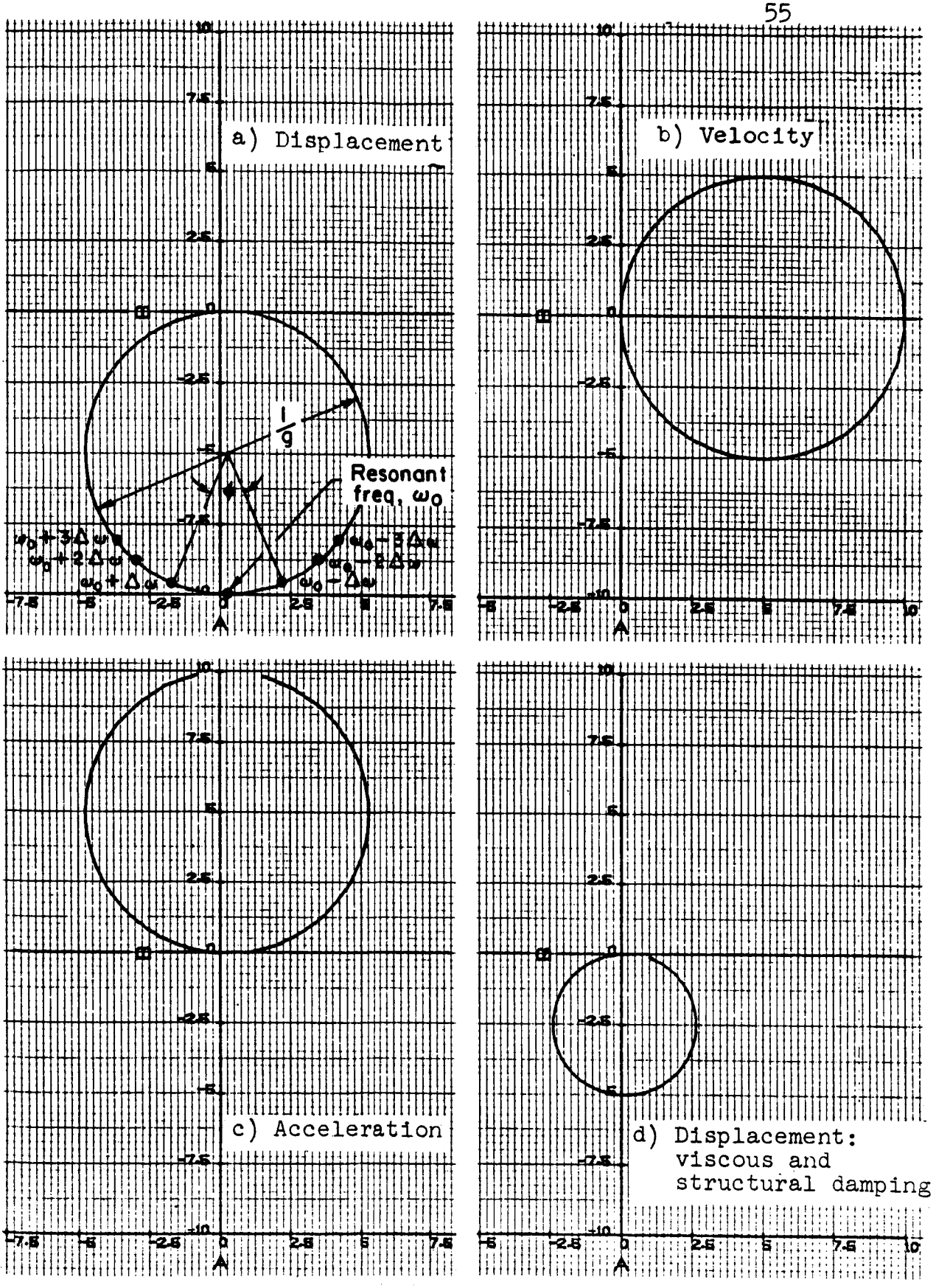

Fig. 2.- Illustrative transfer loci (admittance) as obtained from damped mass oscillator.

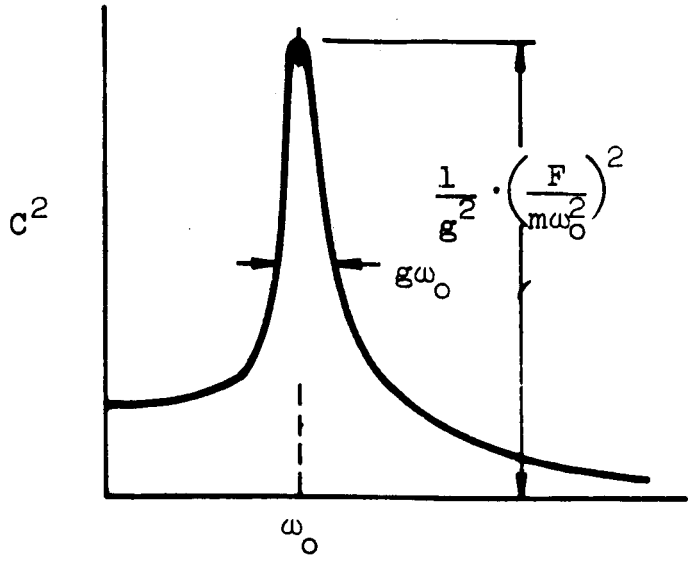

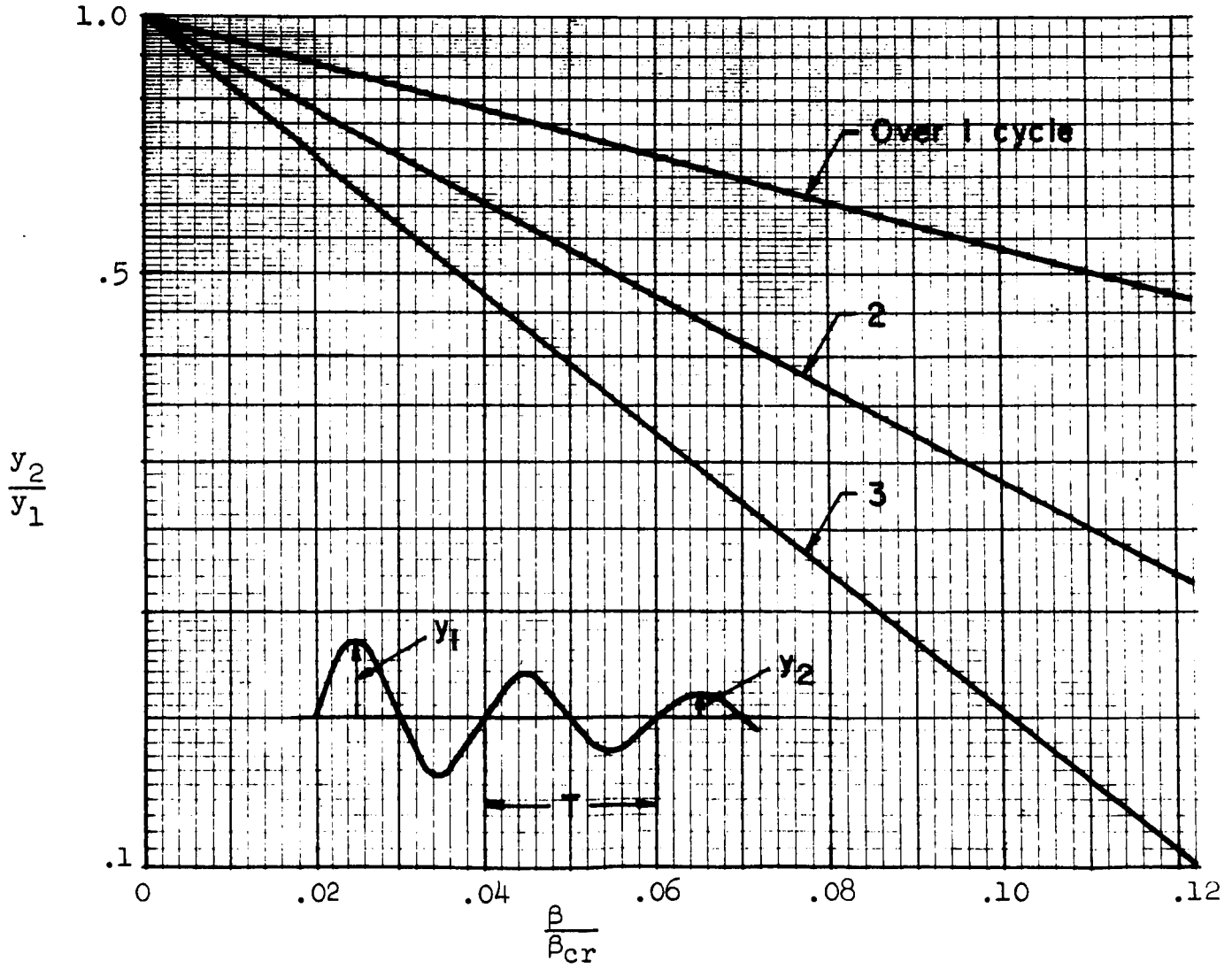

Fig. 3.- Frequency and damping as obtained from the frequency response function or from the decaying free oscillation.

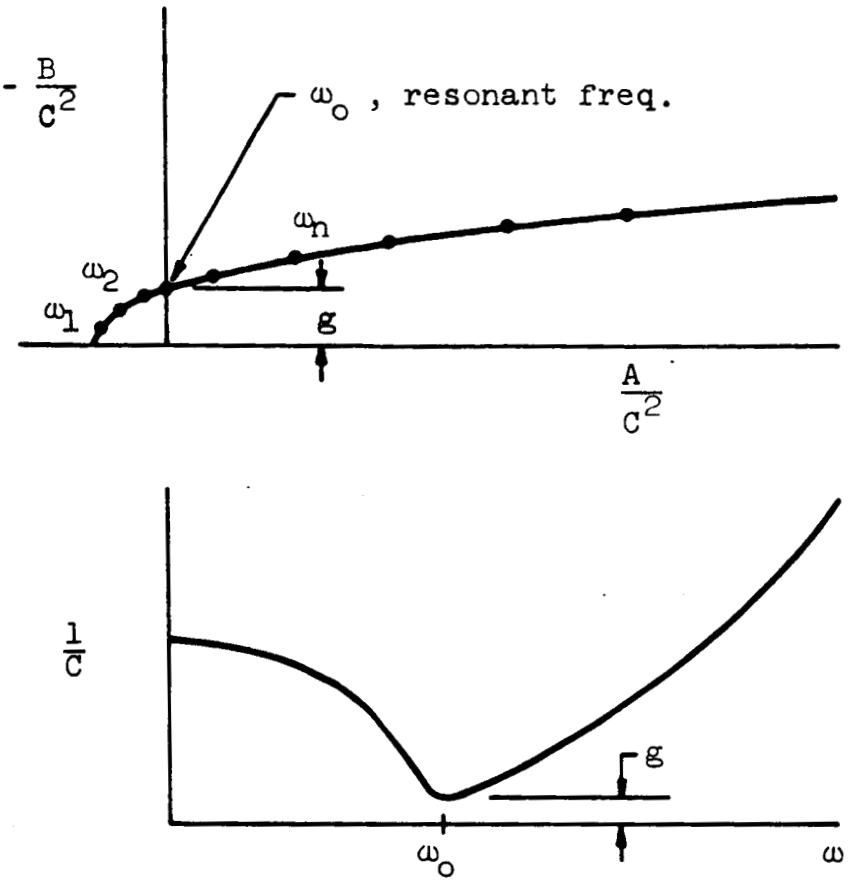

Fig. 4.- Frequency and damping by use of impedance curves.

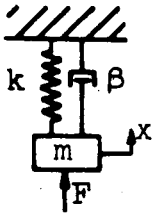

$$m\ddot{x} + \beta\dot{x} + kx = F$$

F = 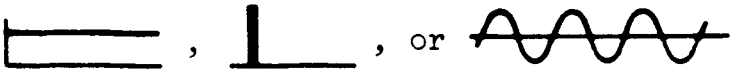 , or

Response to unit step

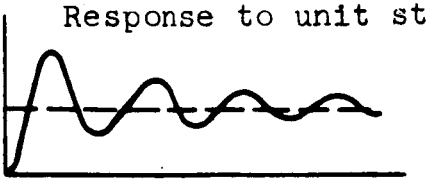

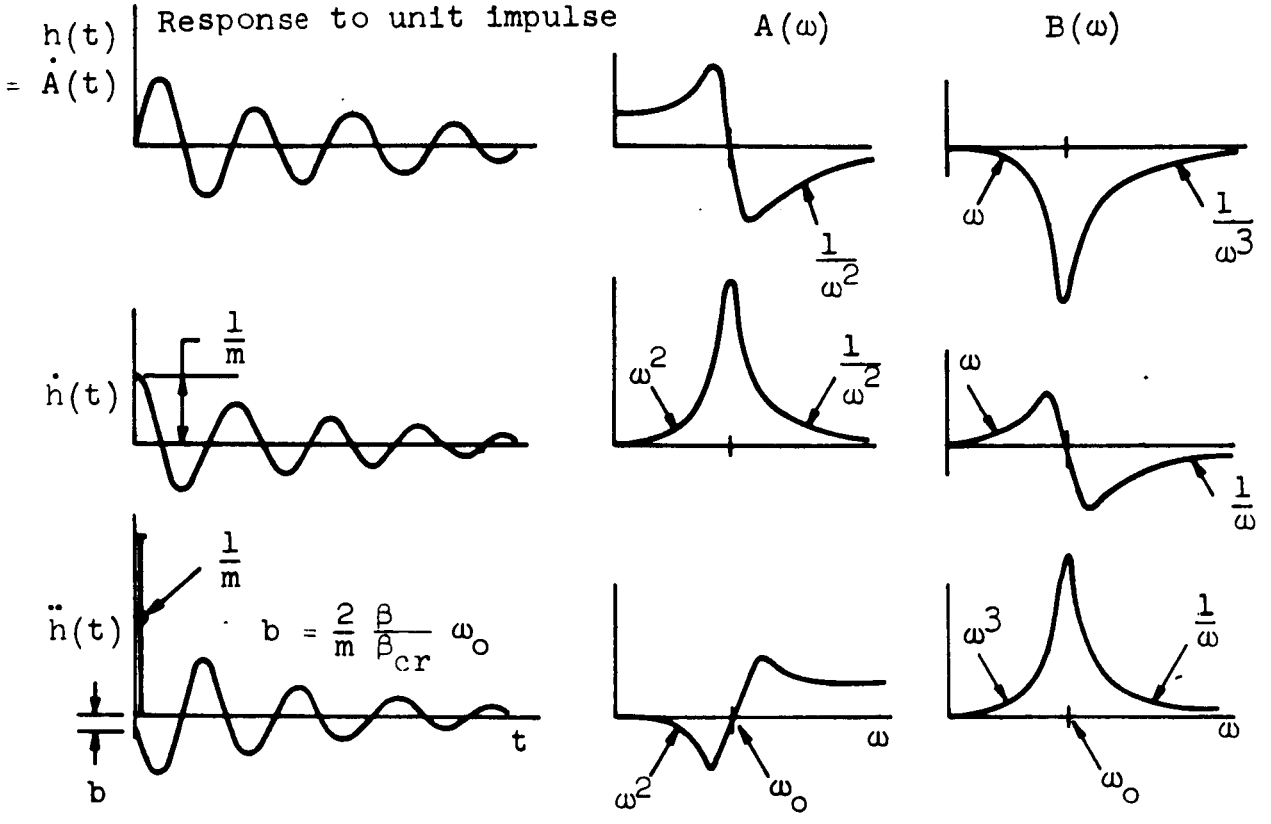

NOTE: $h = \frac{1}{m\omega_1} e^{-\frac{\beta}{\beta_{cr}}\omega_o t} \sin \omega_1 t$

$$\omega_1 = \omega_o \sqrt{1 - \frac{\beta^2}{\beta_{cr}^2}} \quad ; \quad \omega_o = \sqrt{\frac{k}{m}} \quad ; \quad \beta_{cr} = 2\sqrt{km}$$

$H(\omega) = A(\omega) + iB(\omega)$; (A(t) not to be confused with A(ω))

Fig. 5.- Impulsive and frequency response characteristics of a simple mass oscillator.

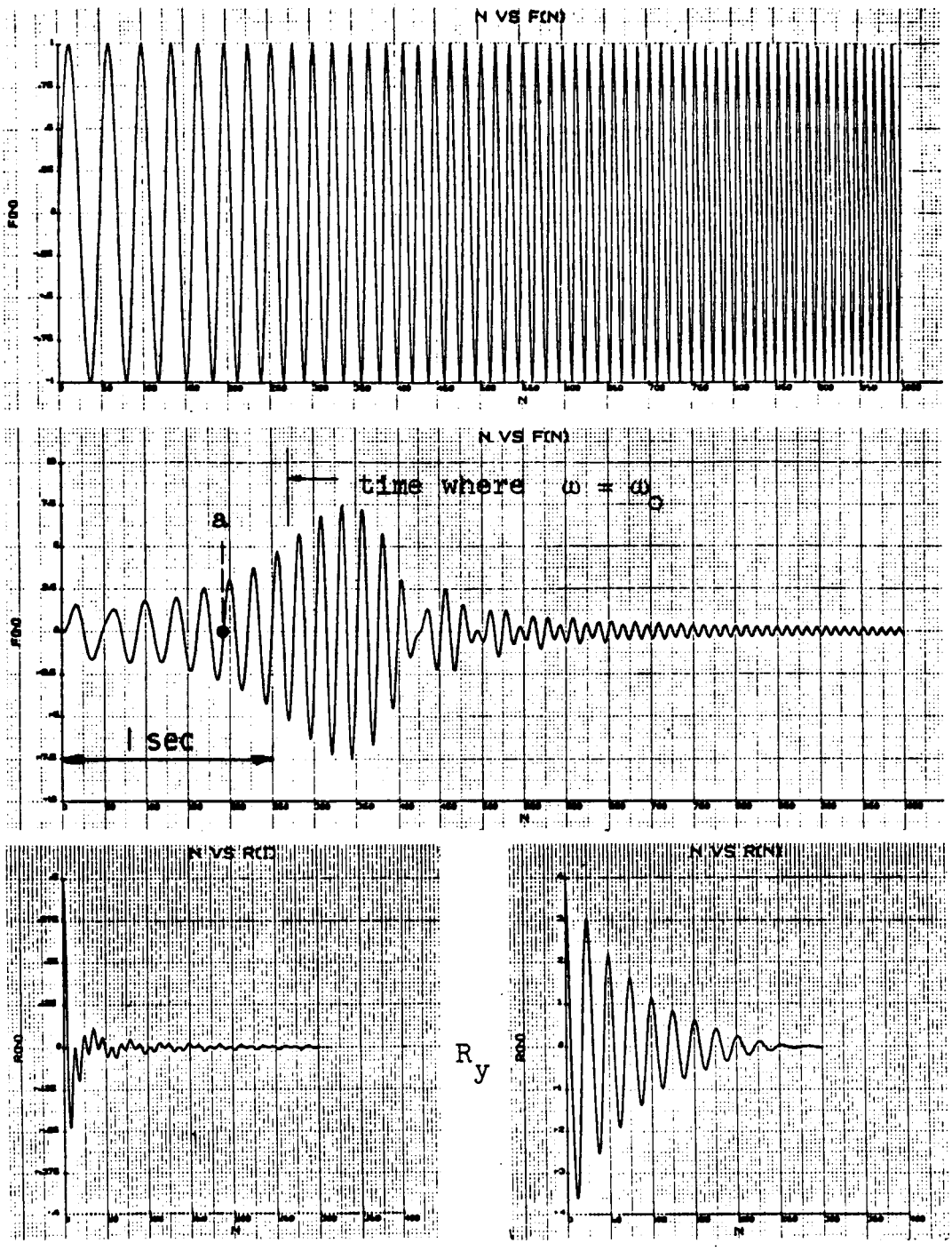

Fig. 6.- Results for 2nd-order system due to swept sine wave (sweep up).

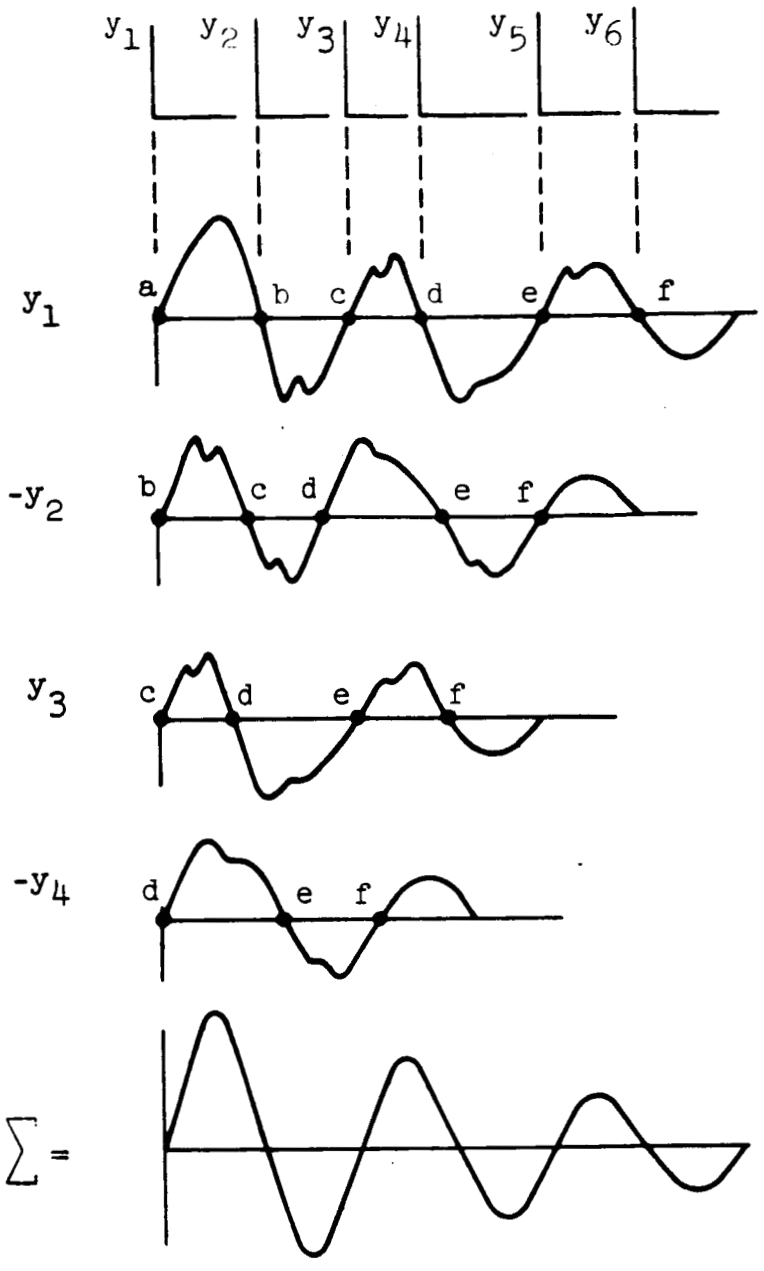

a) "Randomdec" process to derive h function

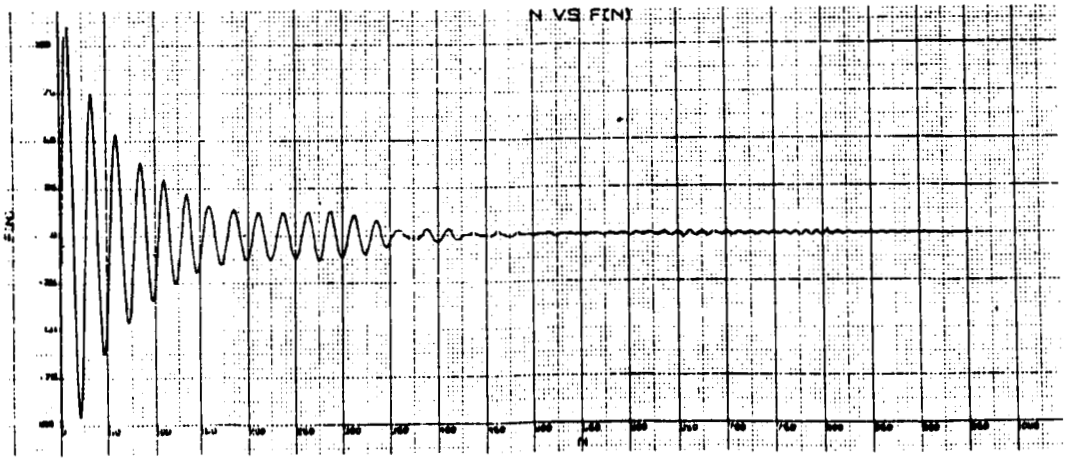

b) Randomdec signal for h obtained from y in figure 6

Fig. 7.- Establishment of h by randomdec technique.

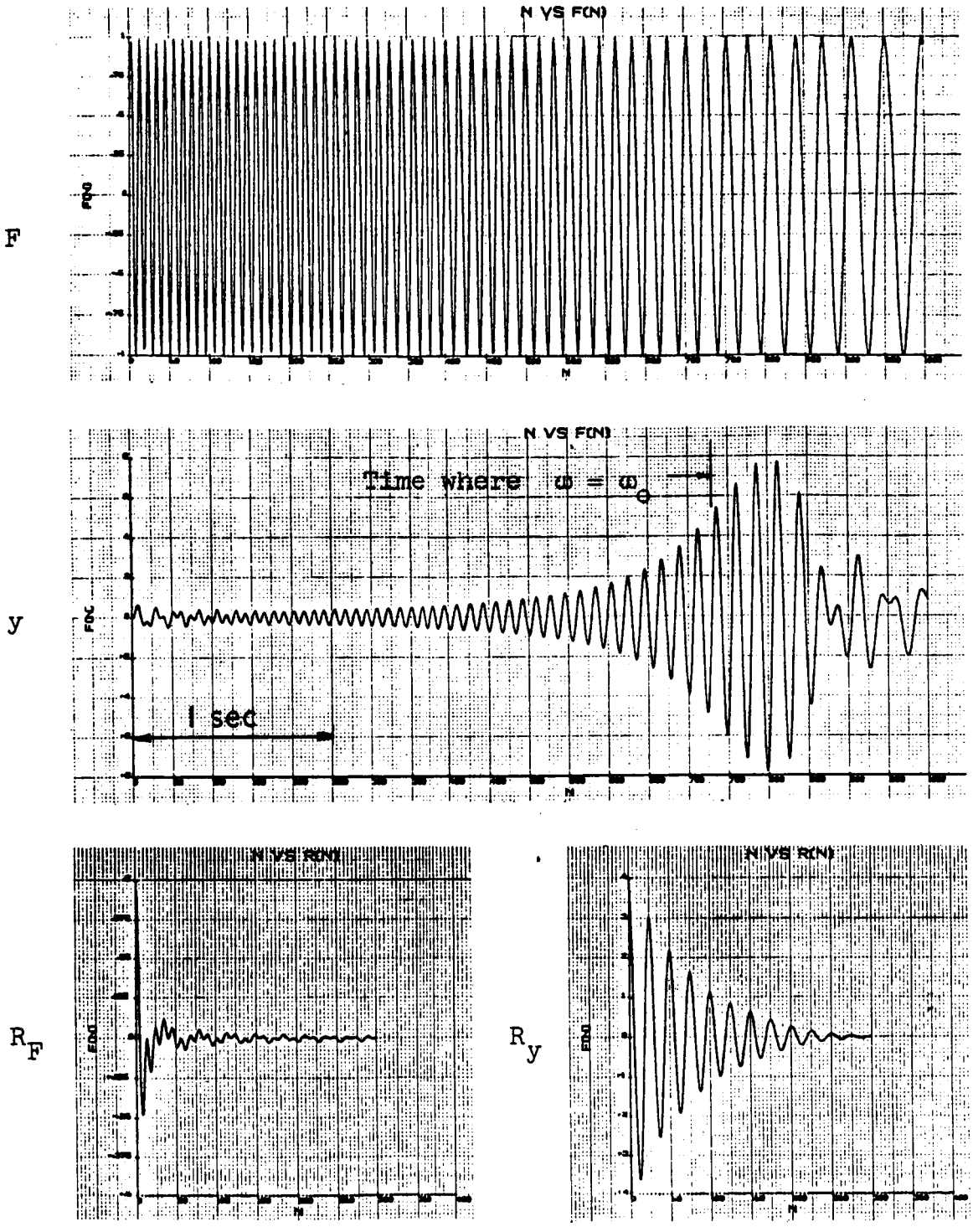

Fig. 8.- Results for 2nd-order system due to swept sine wave (sweep down).

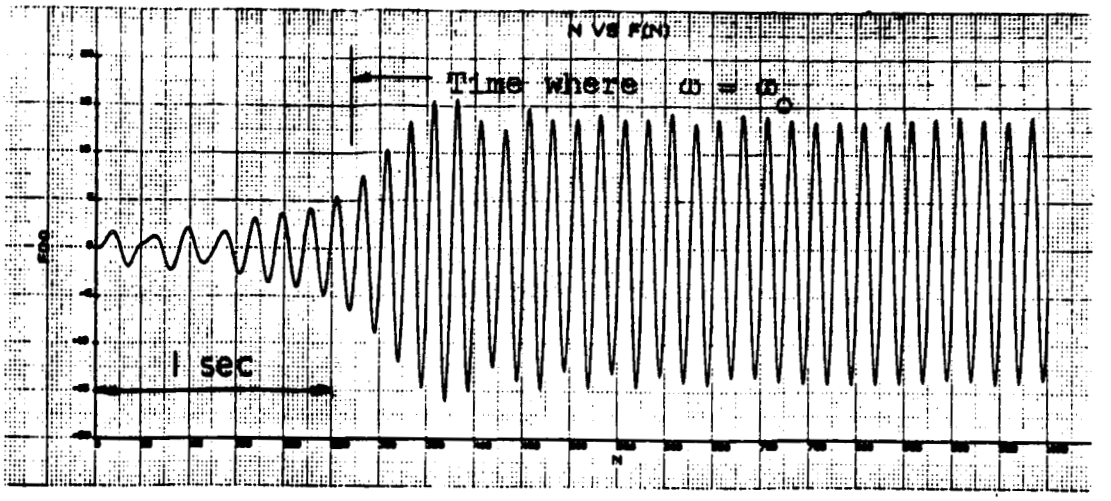

y

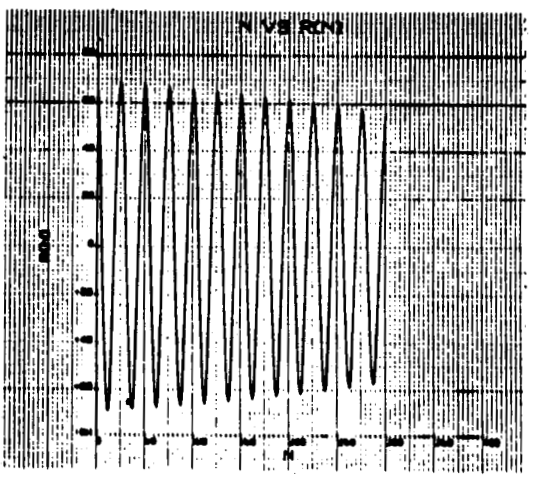

R_y

Fig. 9.- Results for 2nd-order system with zero damping due to swept sine wave (sweep up).

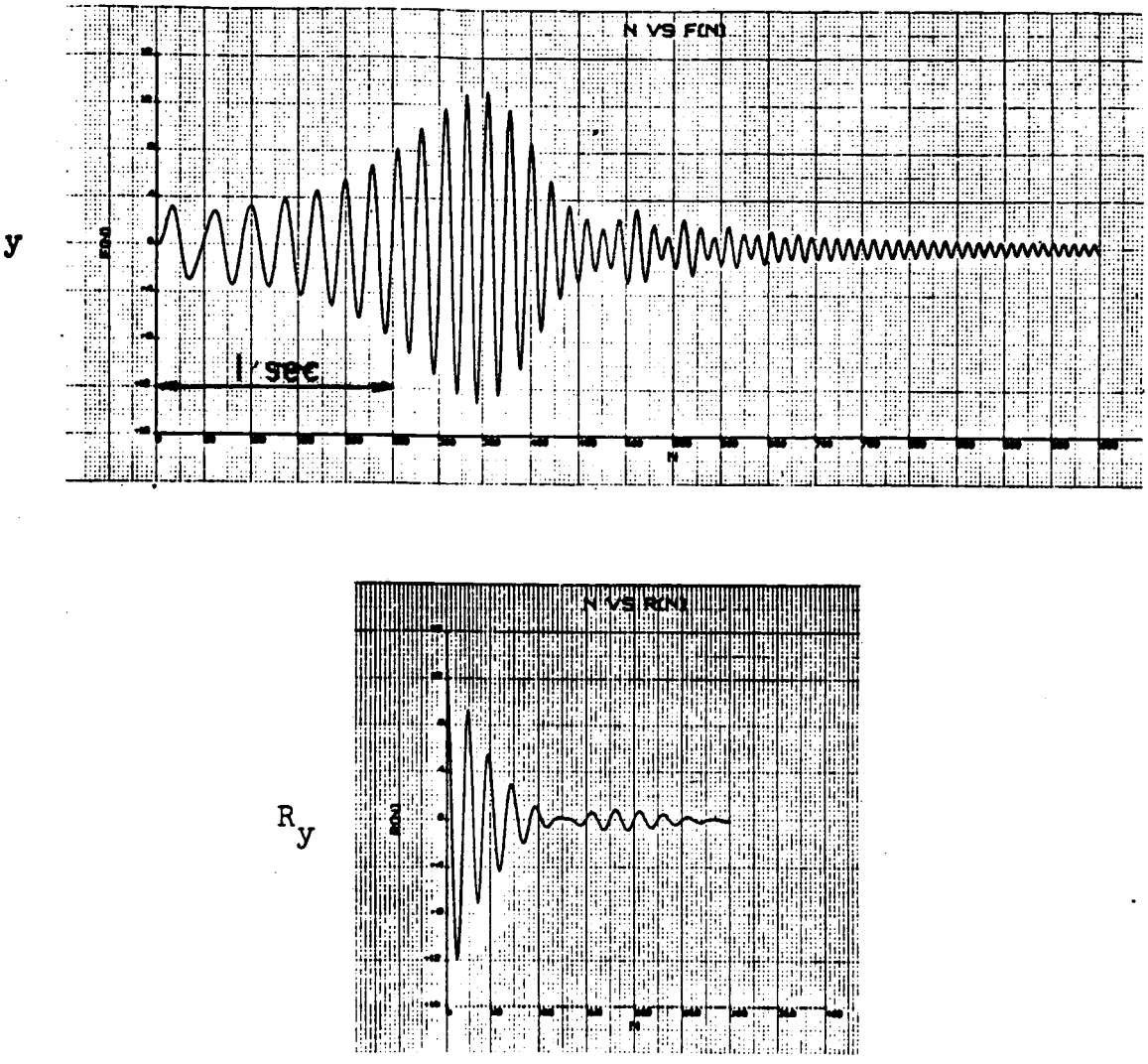

Fig. 10.- Results for 4th-order system with two frequencies close together due to swept sine wave (sweep up).

F

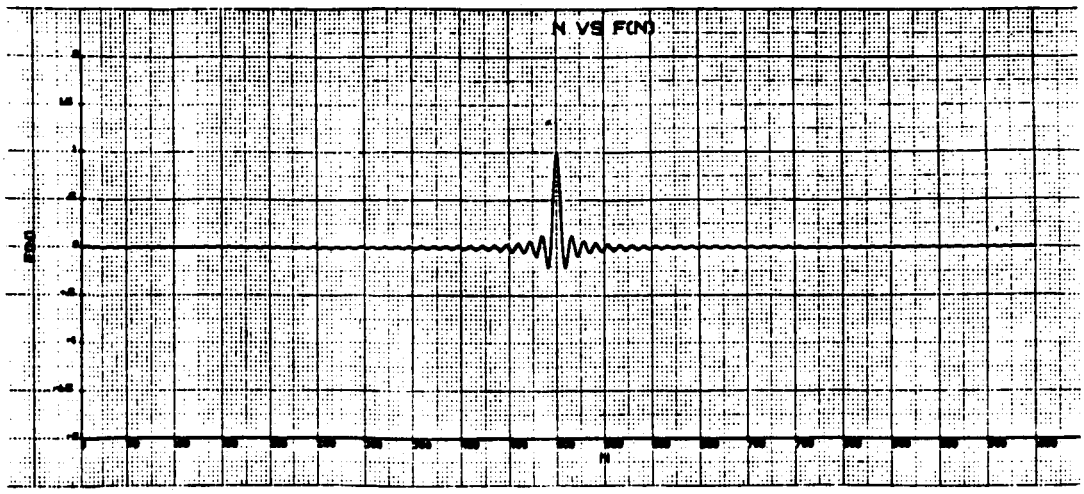

y

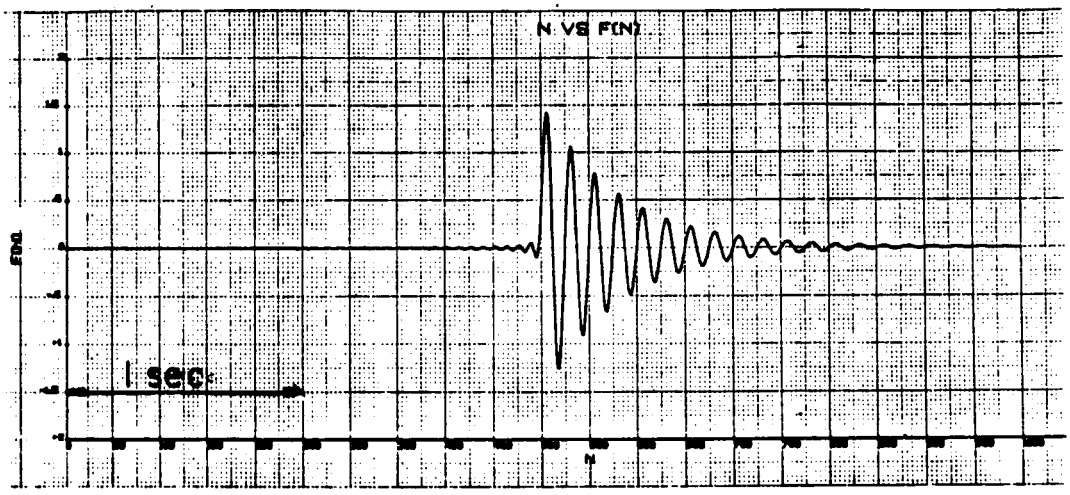

h

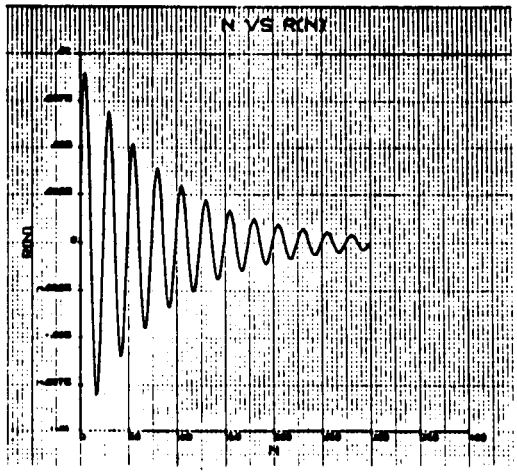

Fig. 11.- Results for 2nd-order system due to impulsive sine input.

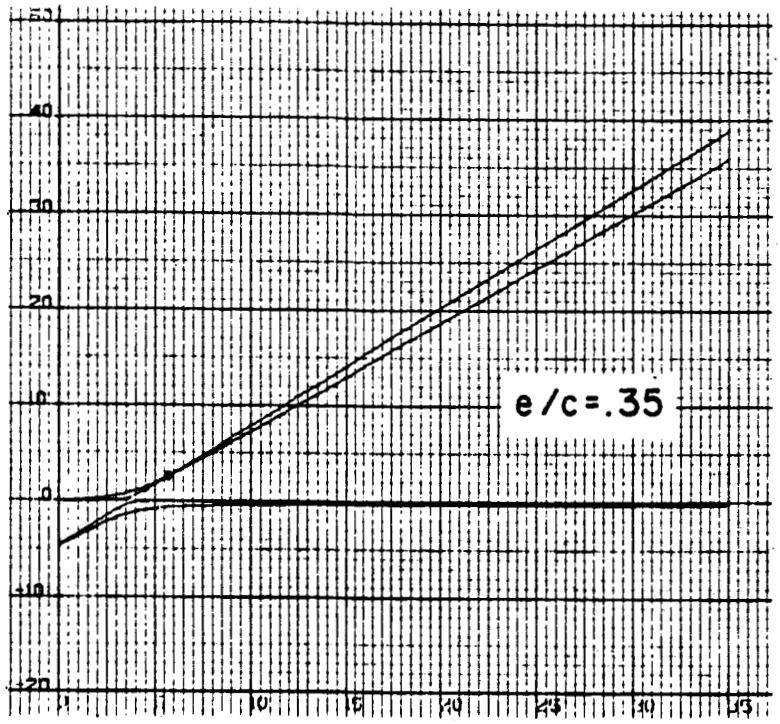

(a) e/c = .35

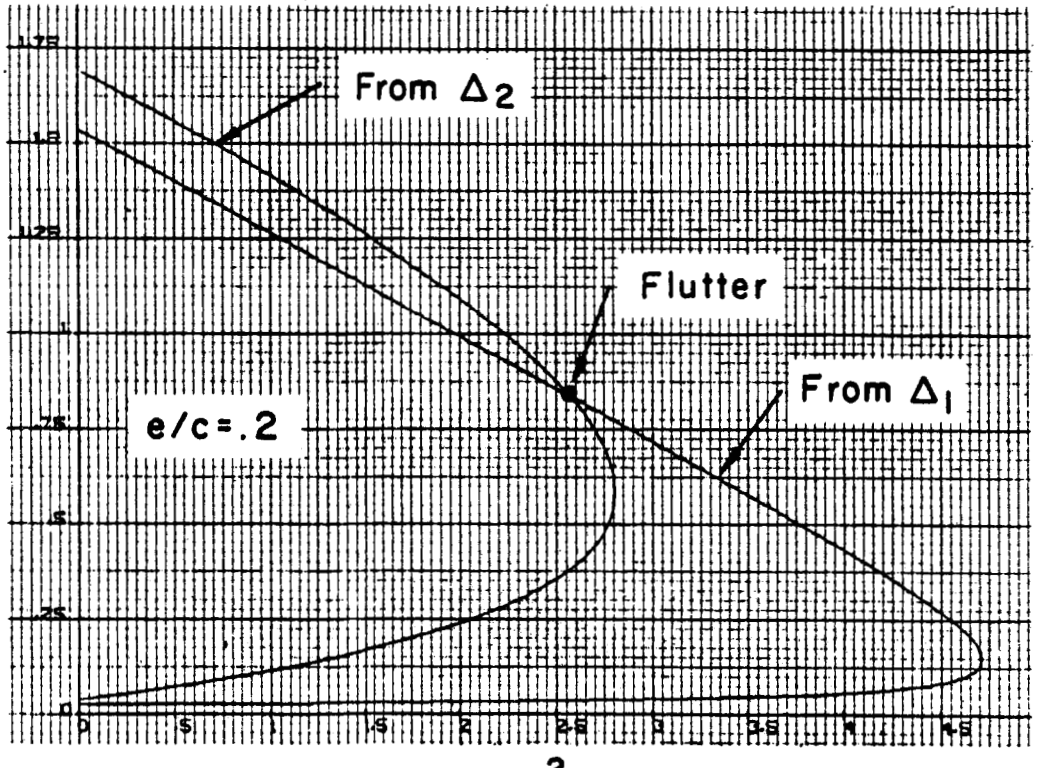

(b) e/c = .2

Fig. 12.- Various behavior patterns associated with the roots of Δ_1 and Δ_2 ; $\omega_t = 5\omega_b$.

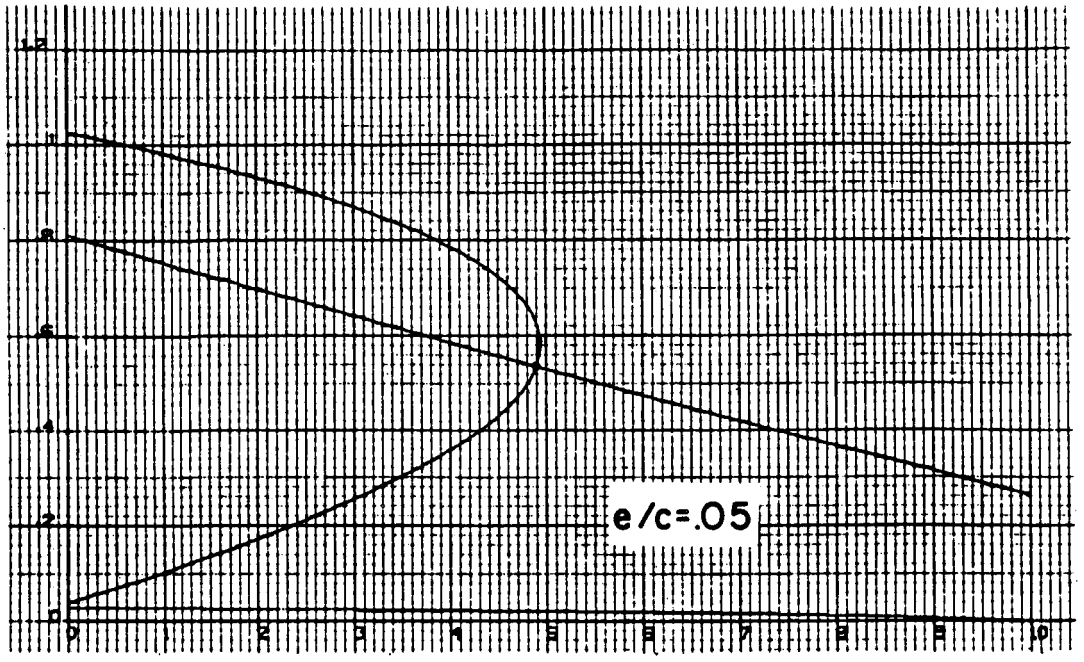

(d) e/c = .05

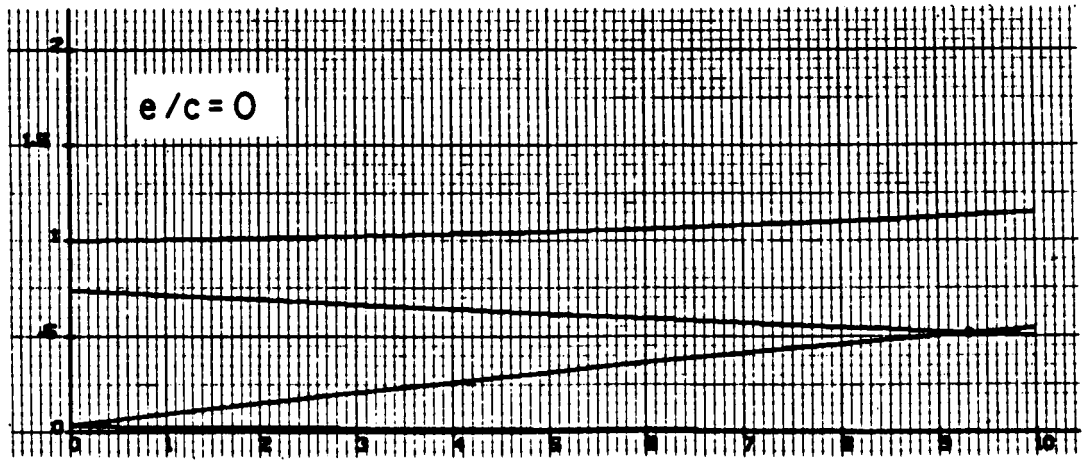

(e) e/c = 0

Fig. 12.- (Cont.)

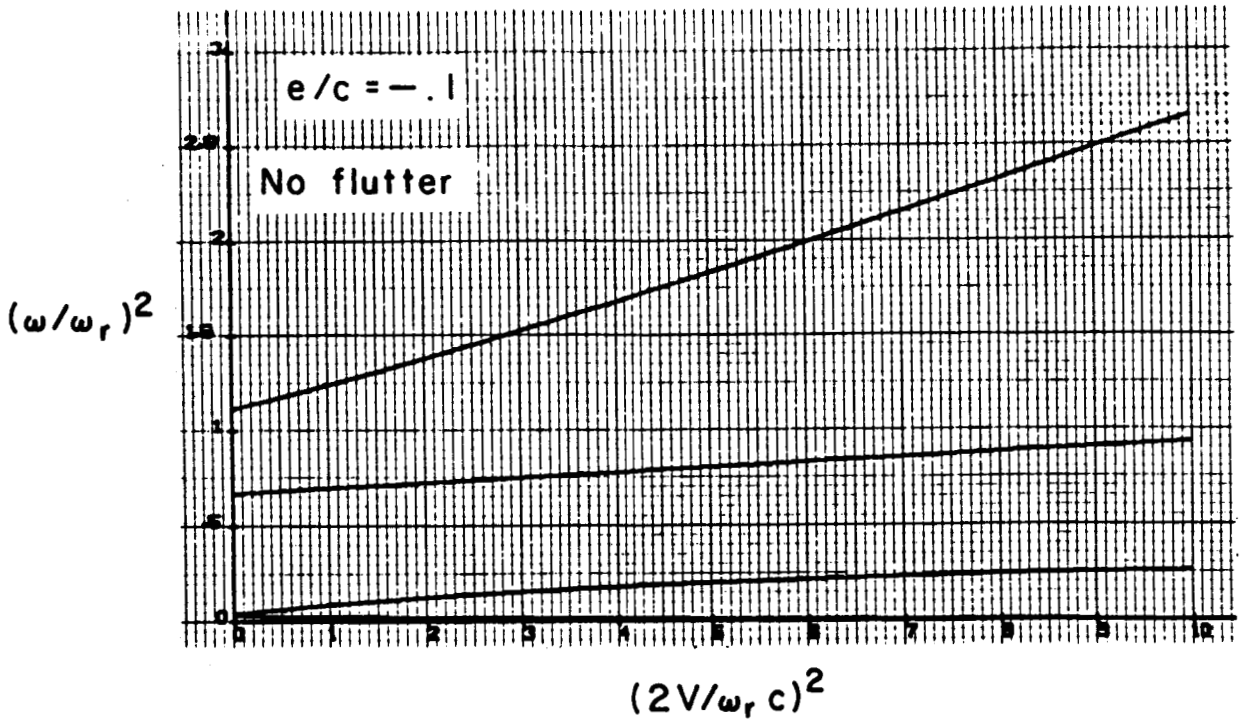

(e) e/c = - 0.1

Fig. 12.- (Concluded)

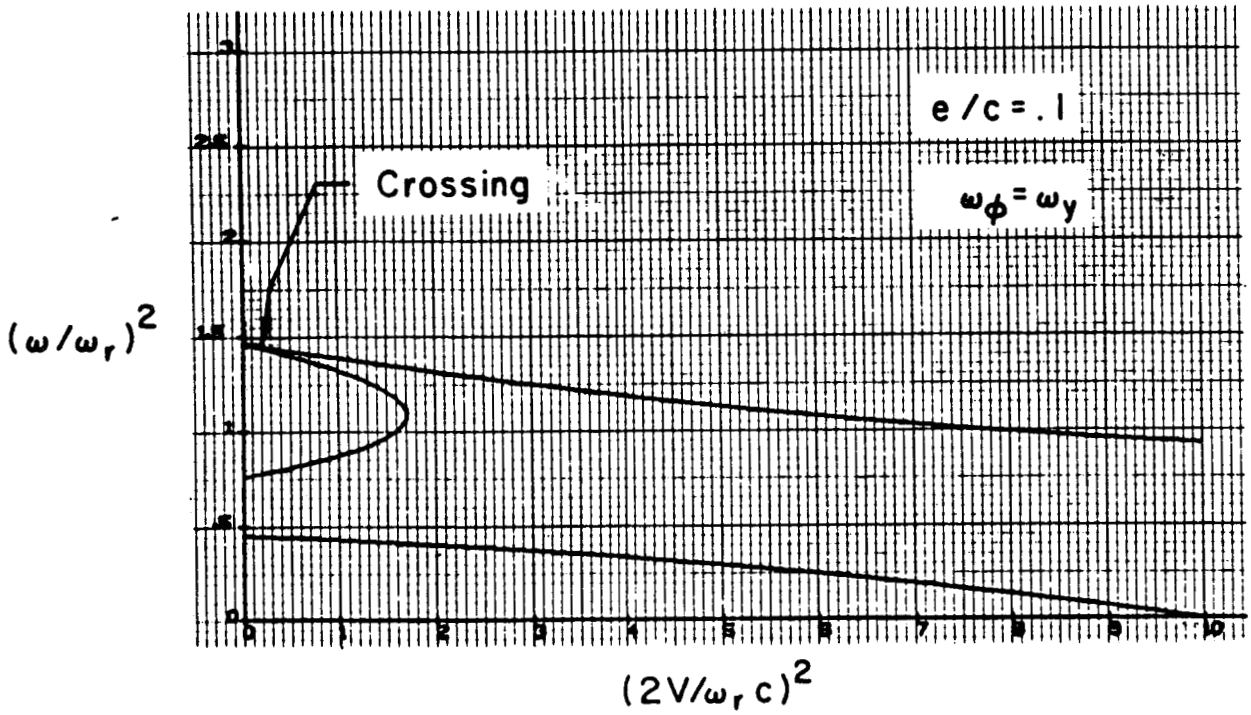

Fig. 13.- Roots of Δ_1 and Δ_2 for system with very low flutter speed; $\omega_\phi = \omega_y$.

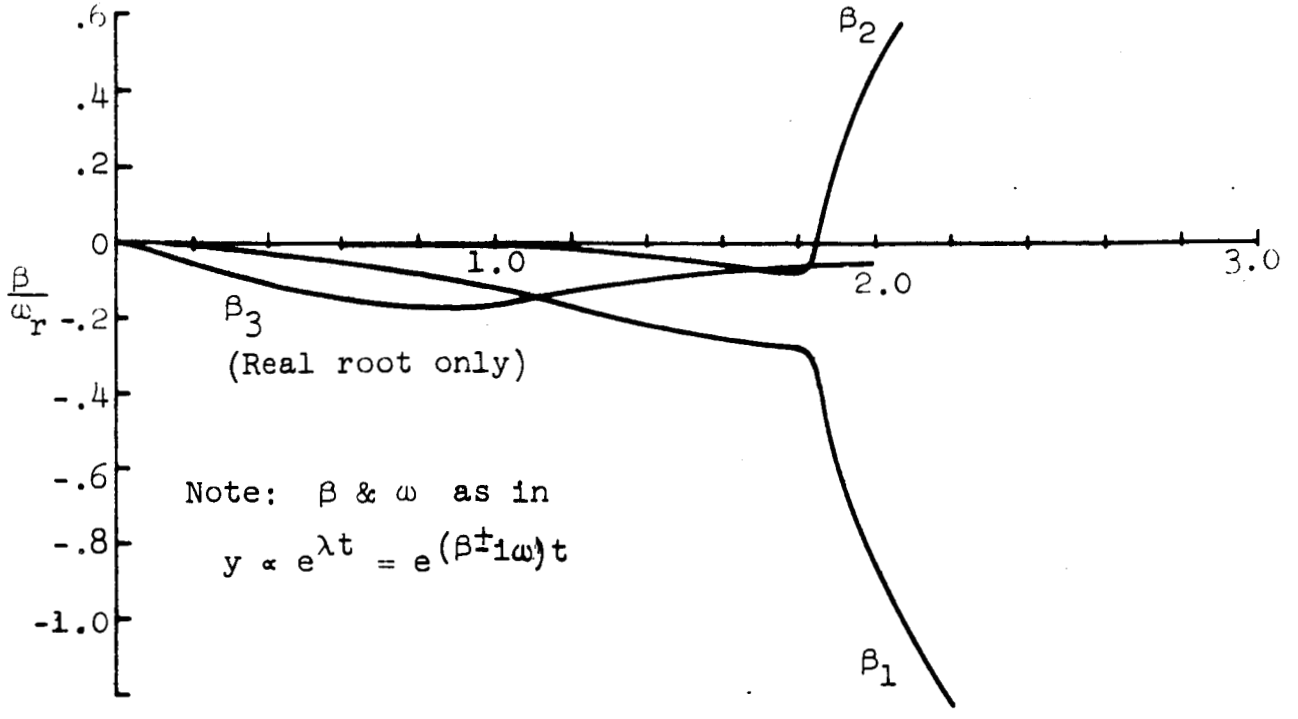

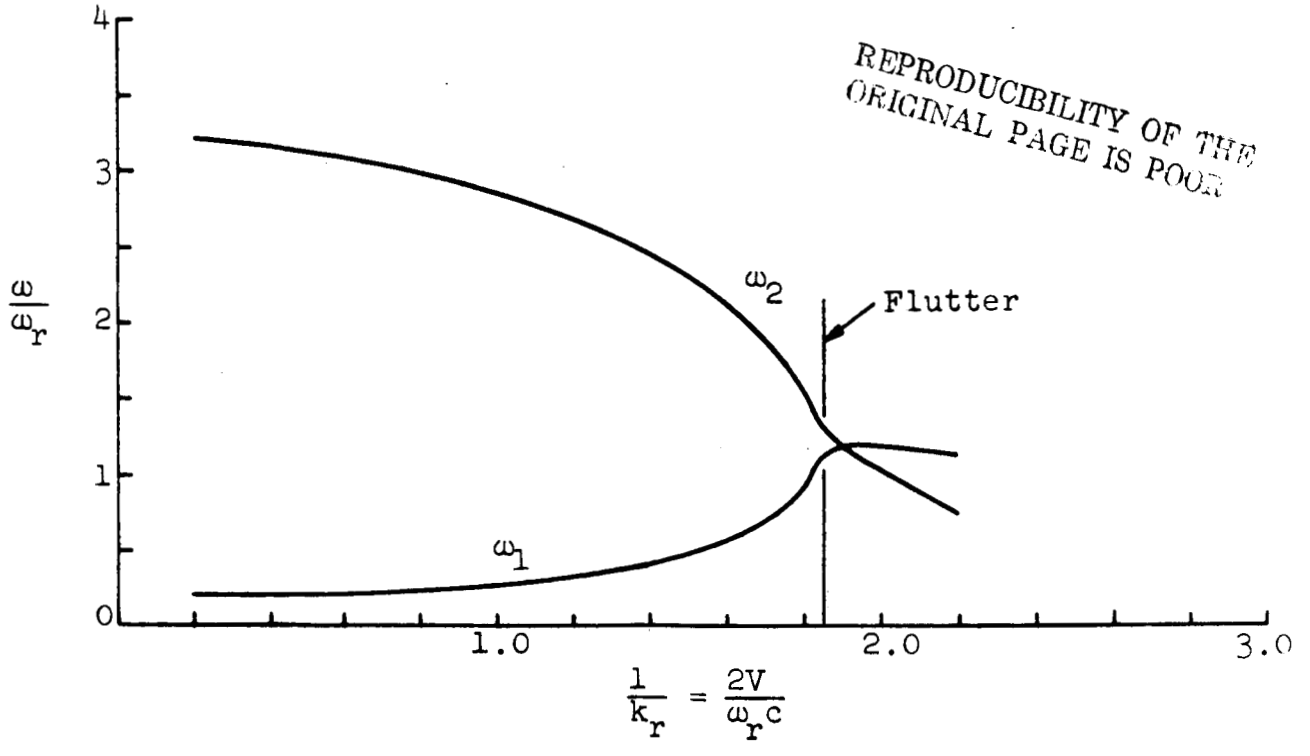

a) $\frac{e}{c} = .3$

Fig. 14.- Roots of Characteristic Equation.

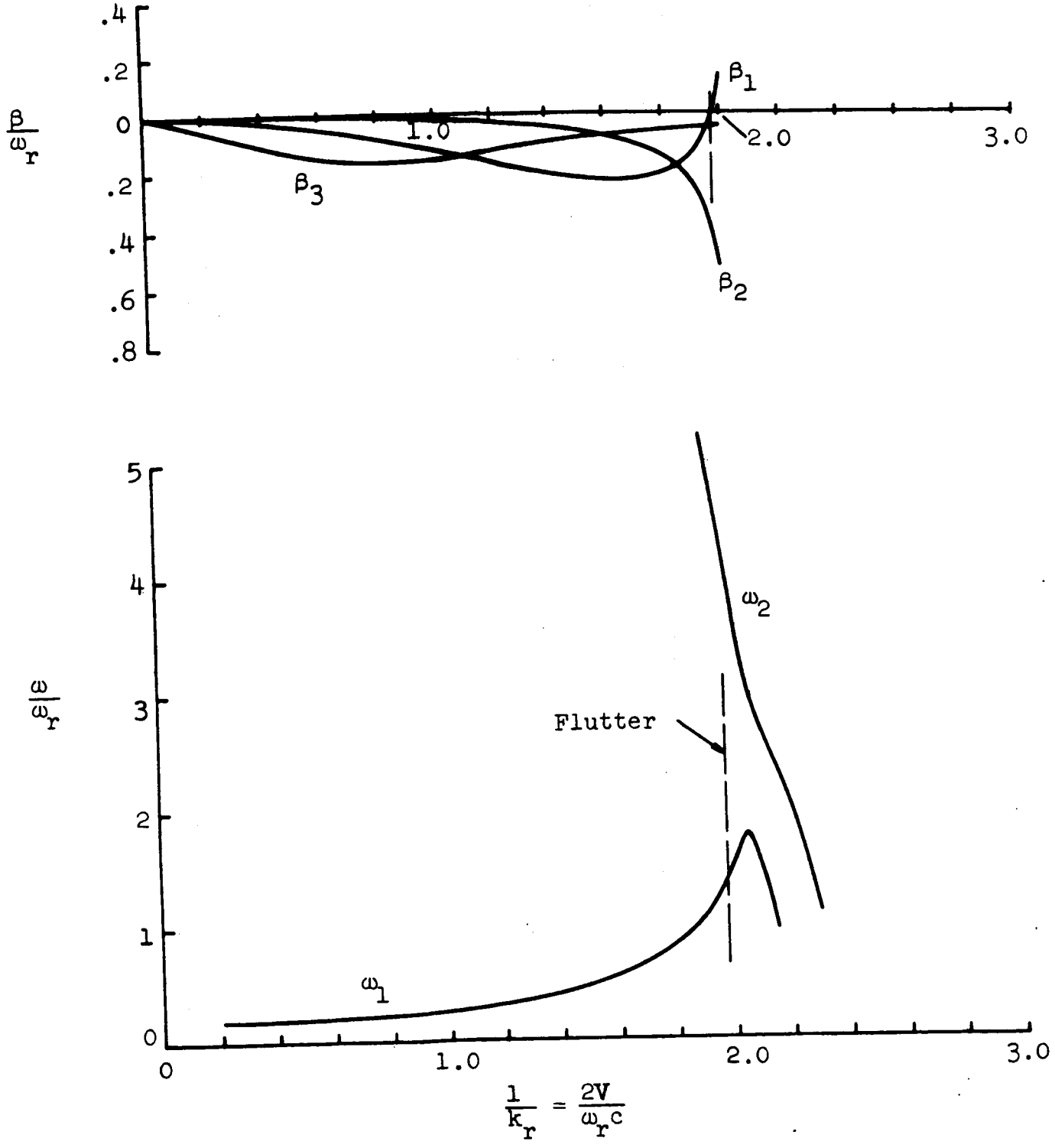

(b) $\frac{e}{c} = .315$

Fig. 14.- (Cont.)

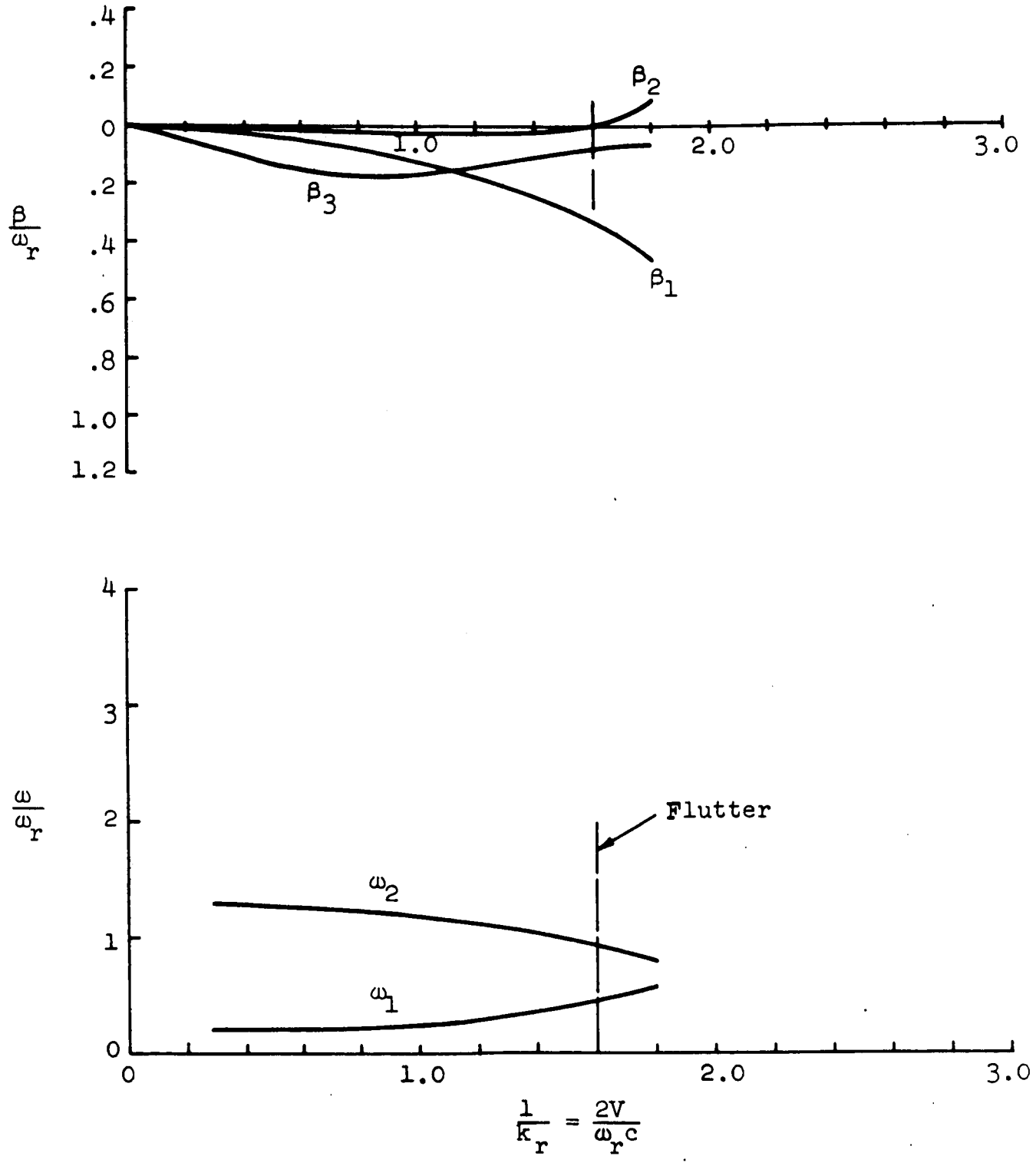

(c) $\frac{e}{c} = .2$

Fig. 14.- (Cont.)

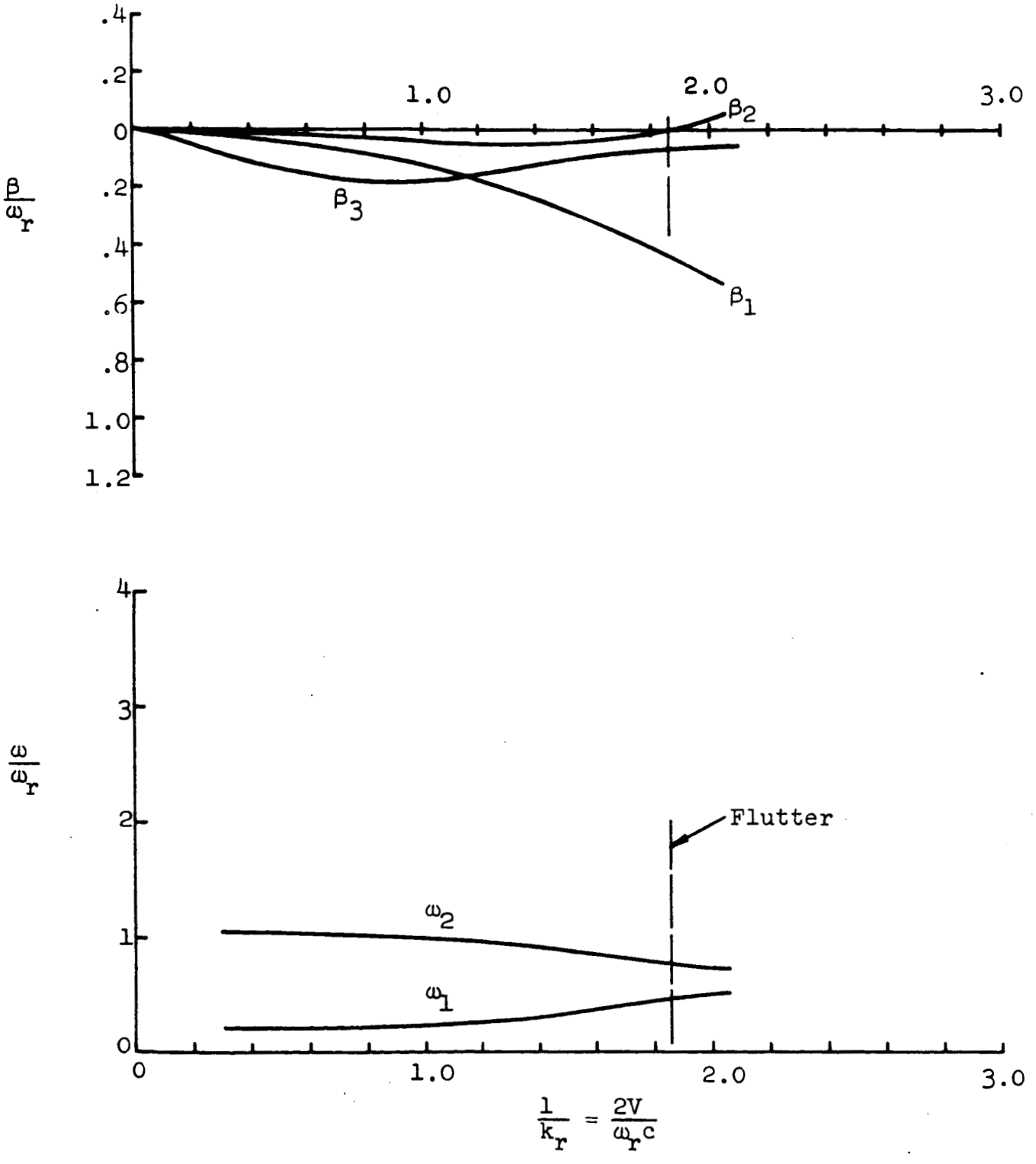

(d) $\frac{e}{c} = .1$

Fig. 14.- (Cont.)

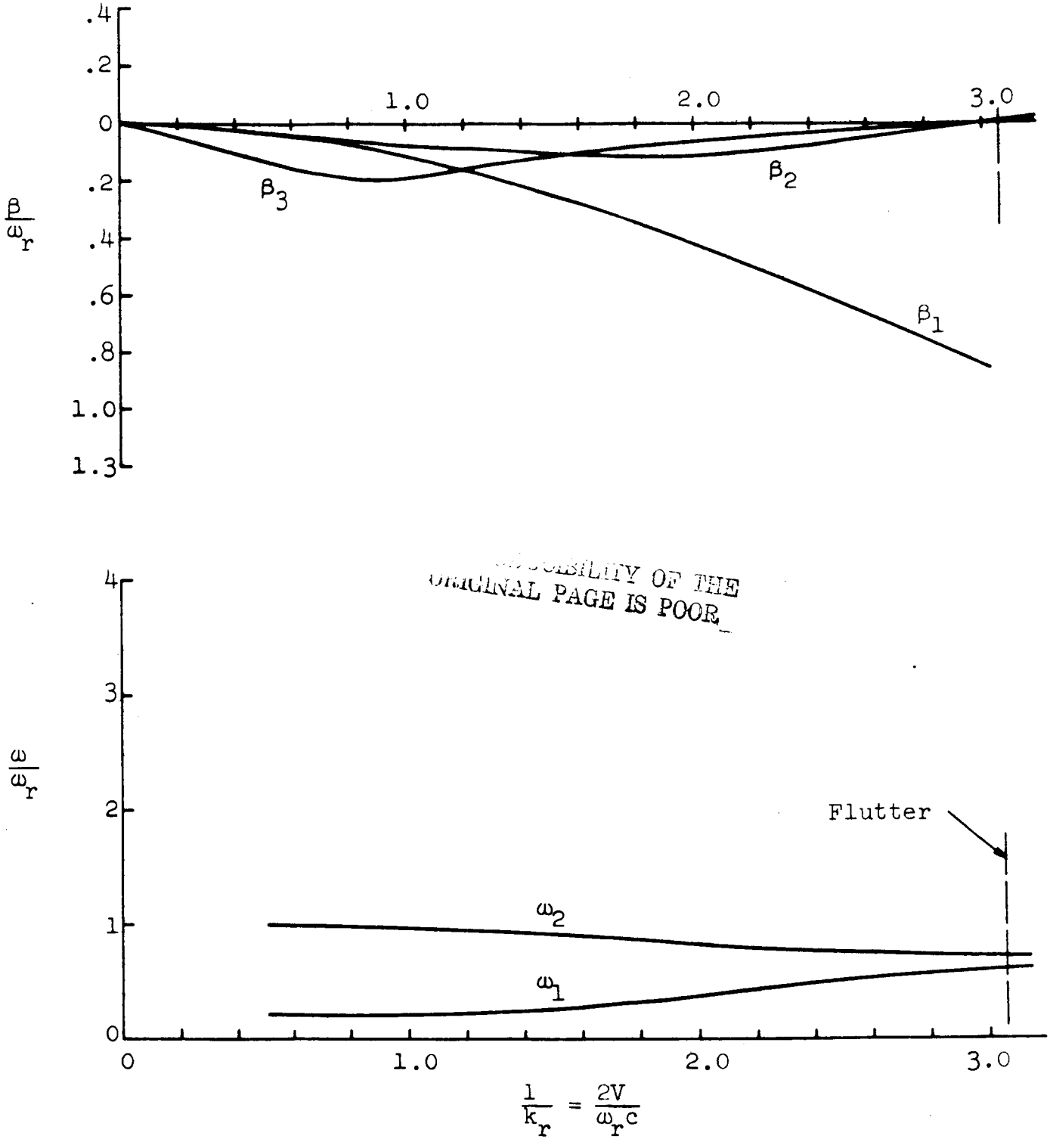

(e) $\frac{e}{c} = 0$

Fig. 14.- (Concluded)

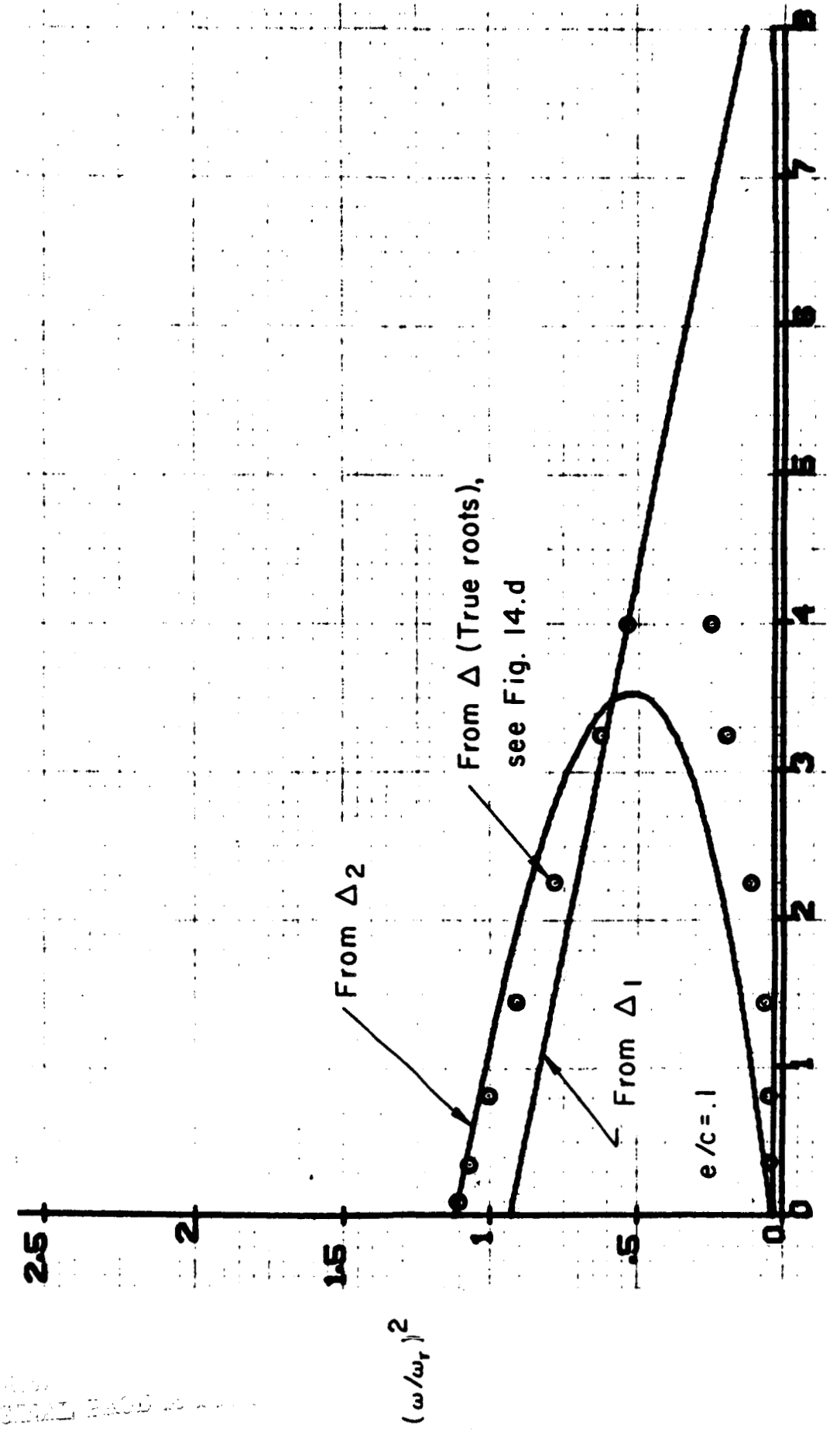

(a) $\frac{e}{c} = .1$

Fig. 15.- True and "quasi" roots of characteristic equation.

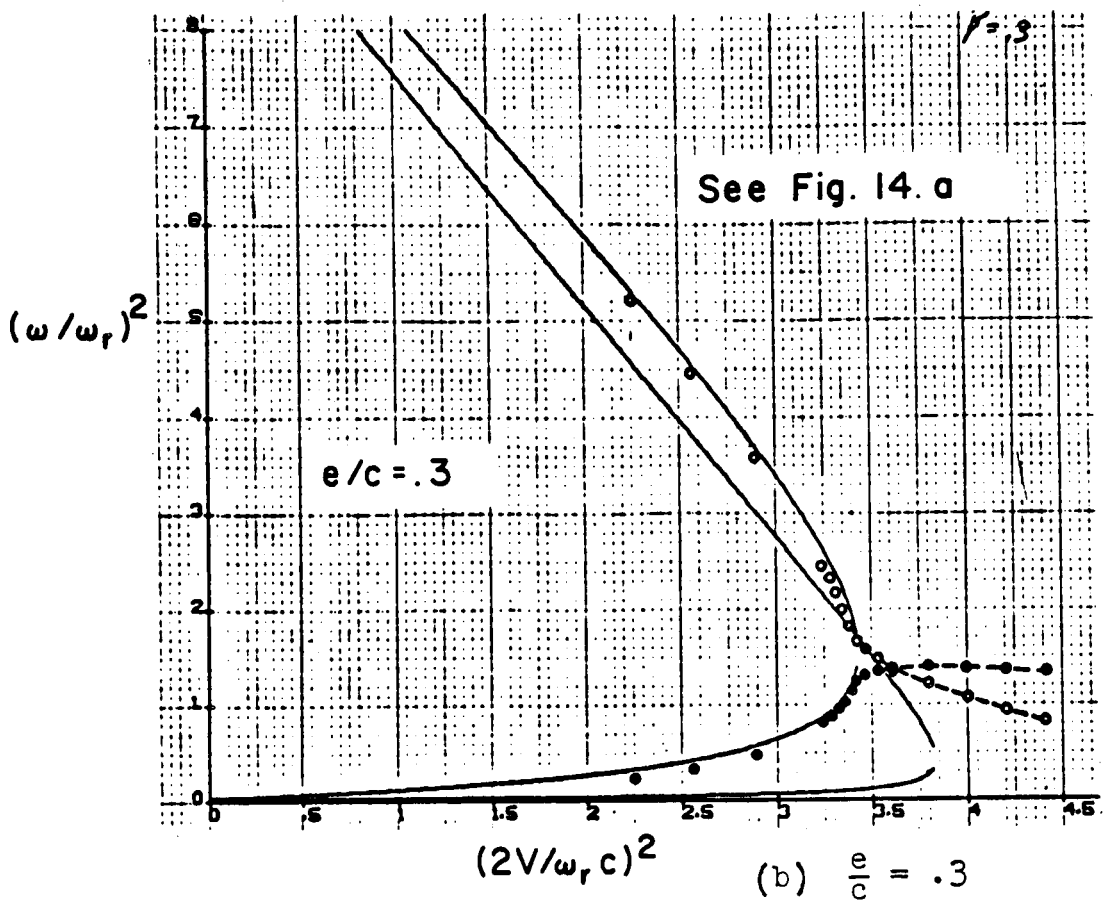

(b) $\frac{e}{c} = .3$

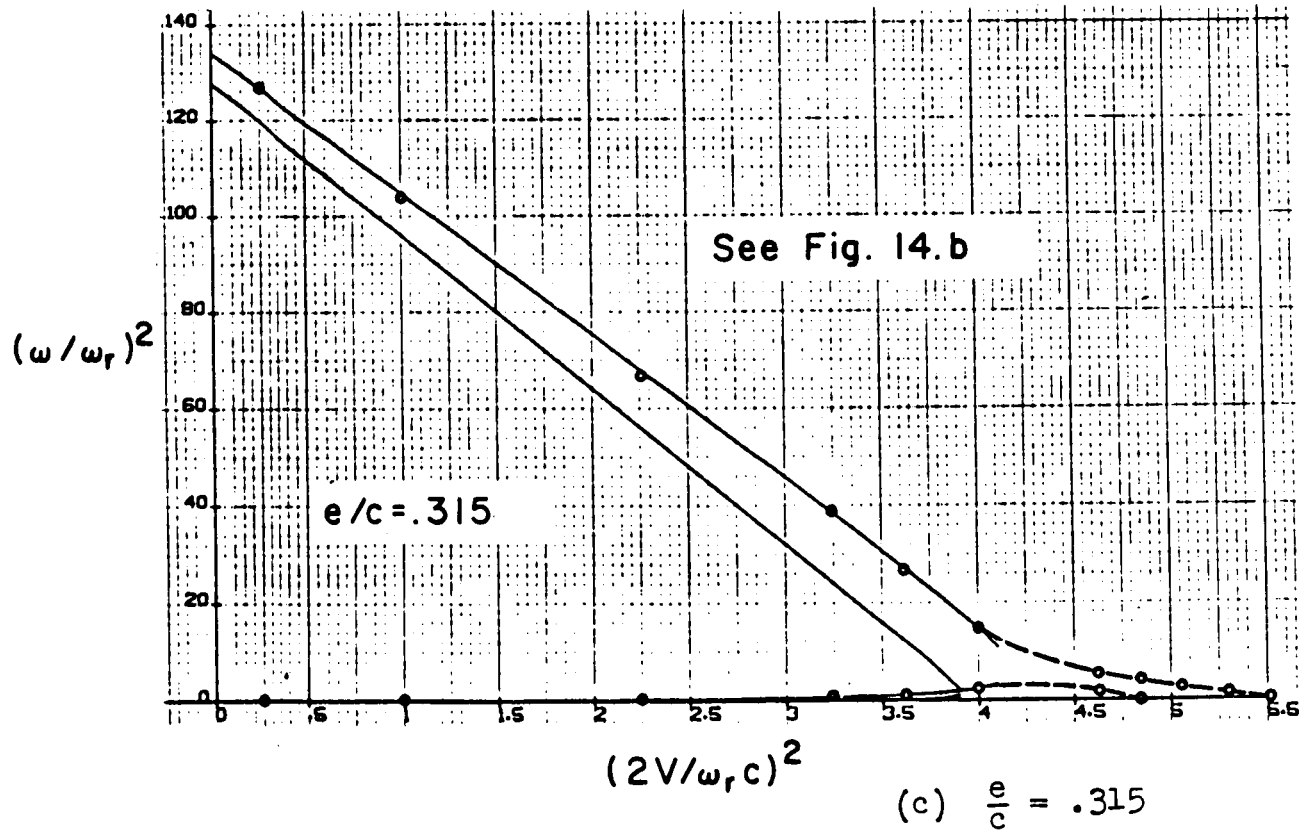

(c) $\frac{e}{c} = .315$

Fig. 15.- (Concluded)

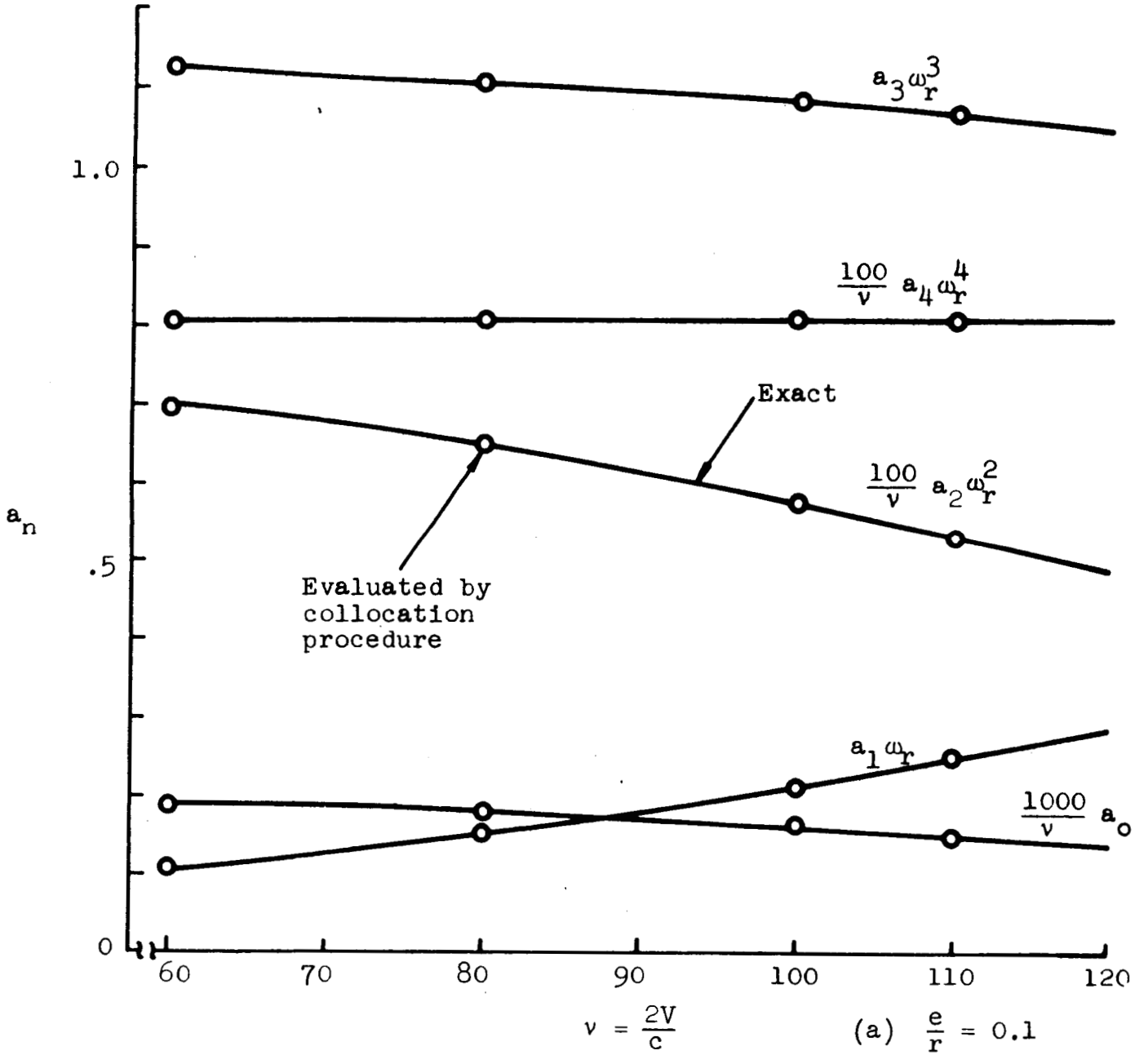

Fig. 16.- Exact a_n values compared with values deduced from frequency response function.

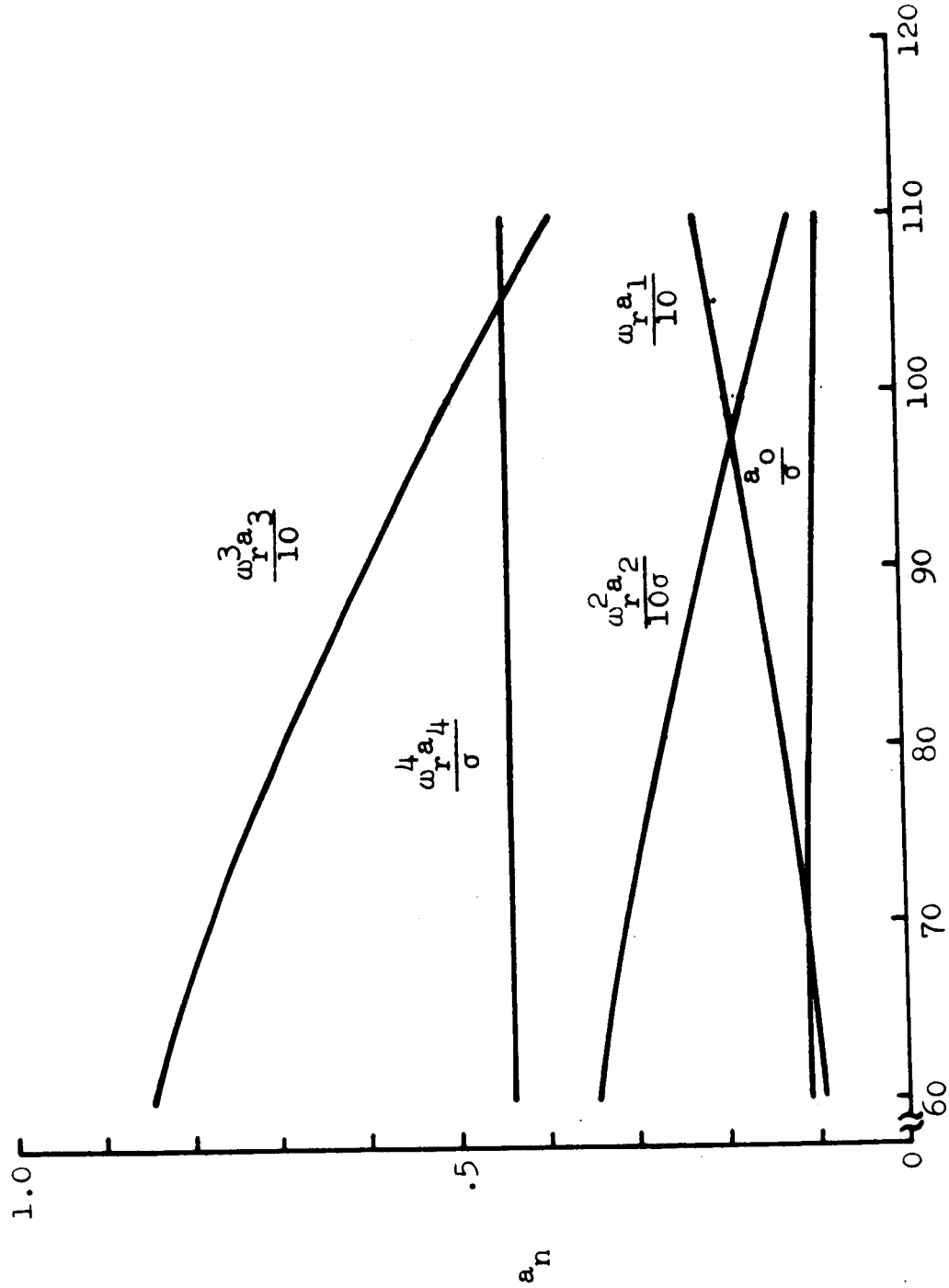

(b) $\frac{e}{c} = 0.3$

Fig. 16.- (Concluded)

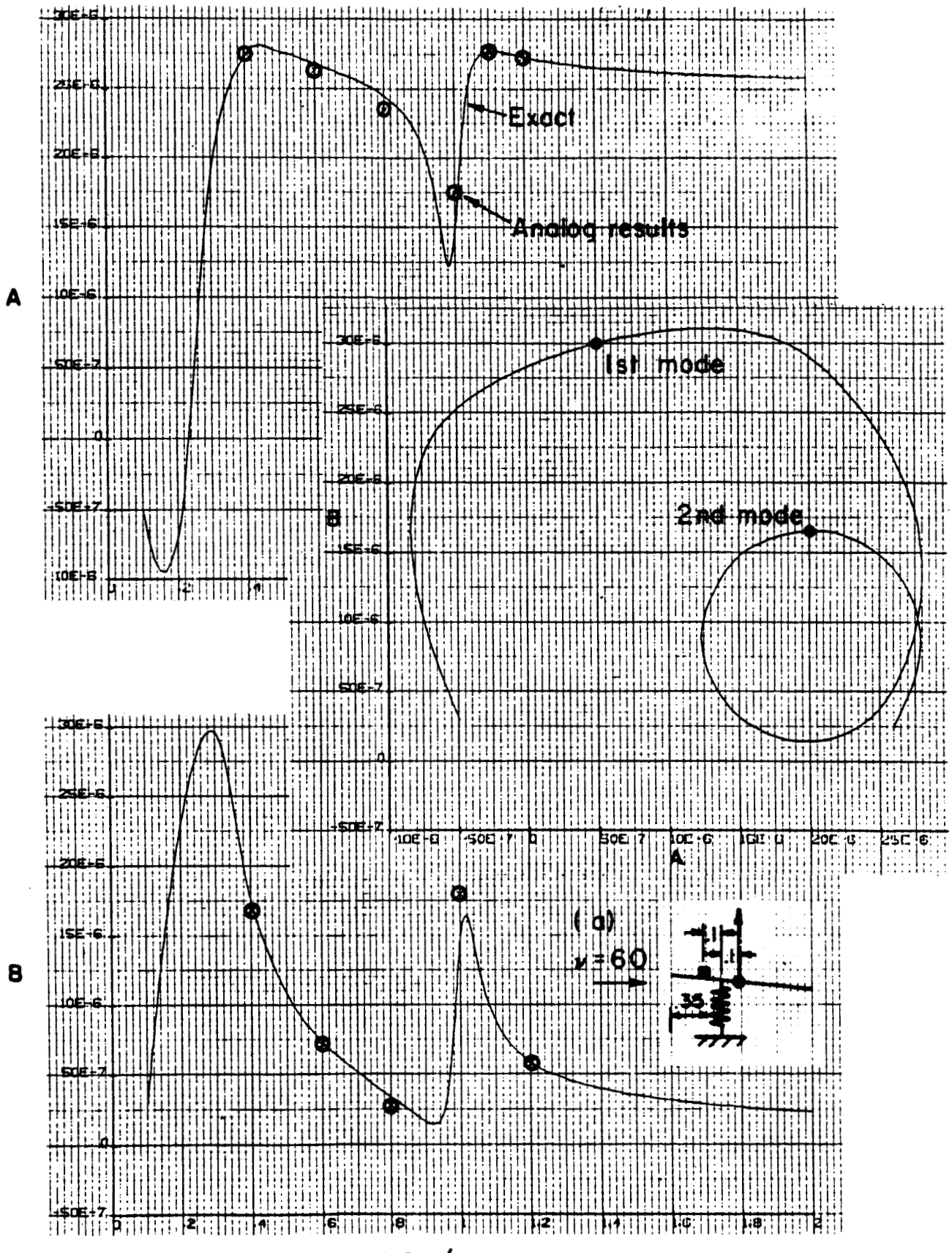

(a)

Fig. 17.- Illustrative frequency response plots.

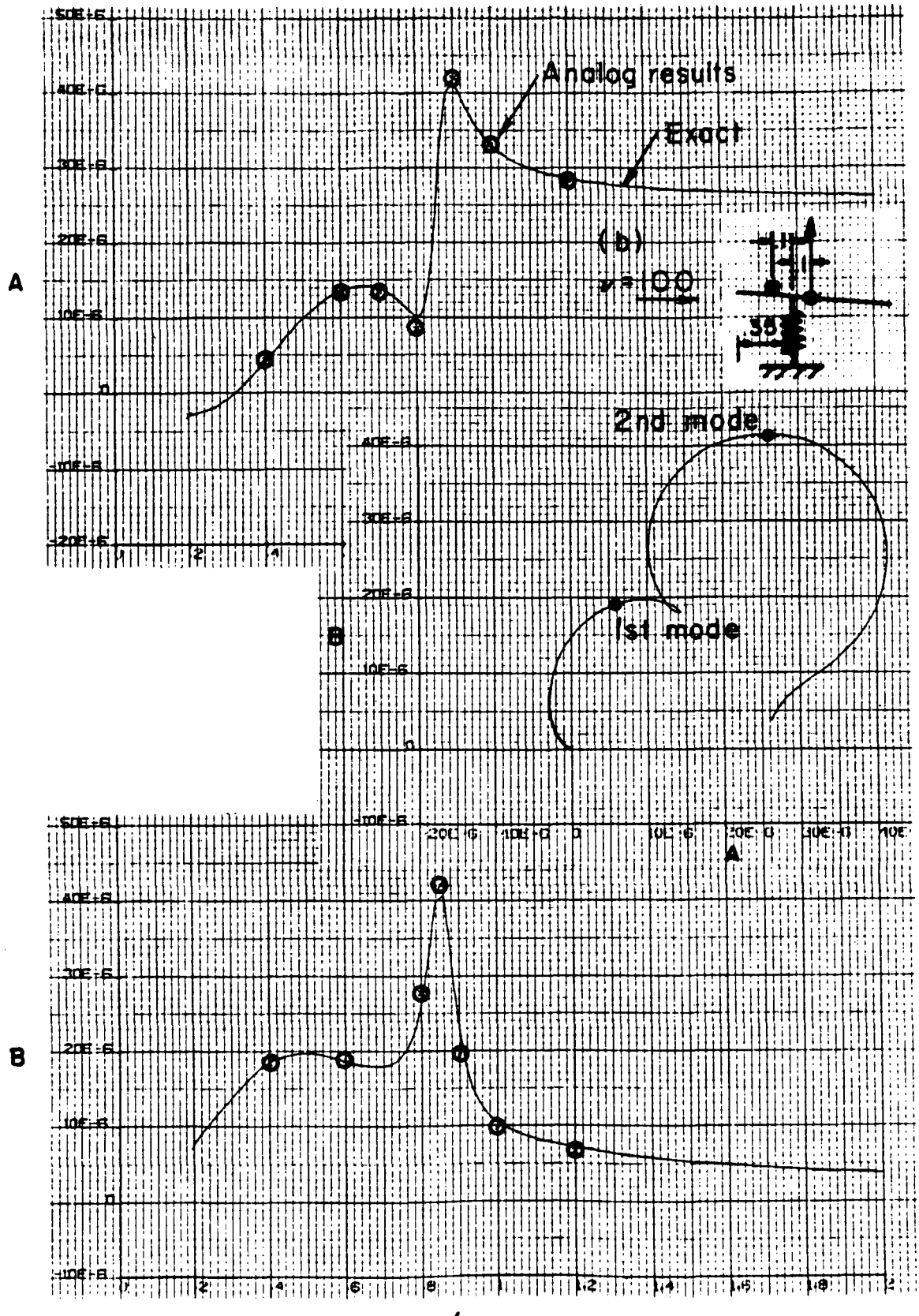

(b)

Fig. 17.- (Cont.)

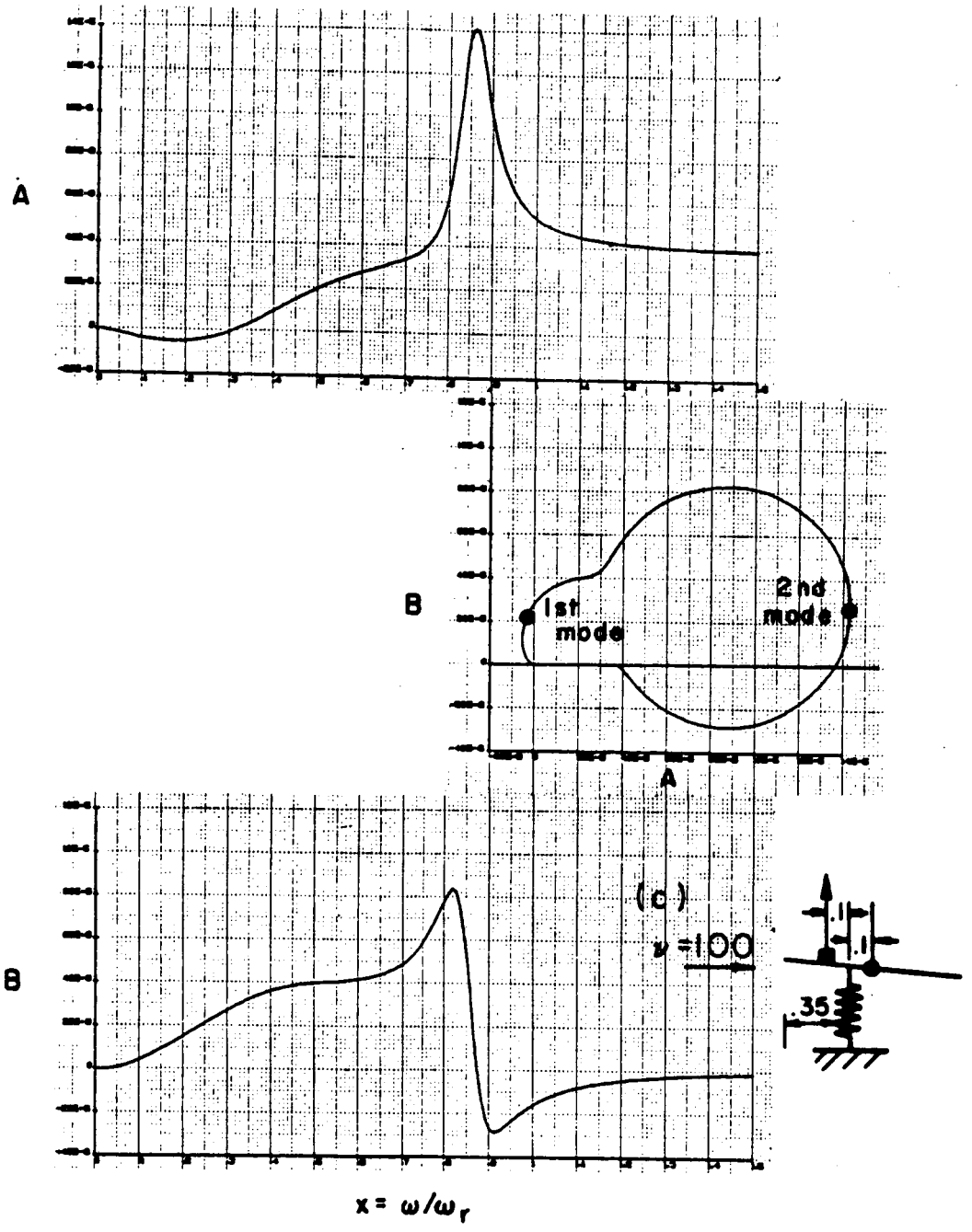

(c)

Fig. 17.- (Cont.)

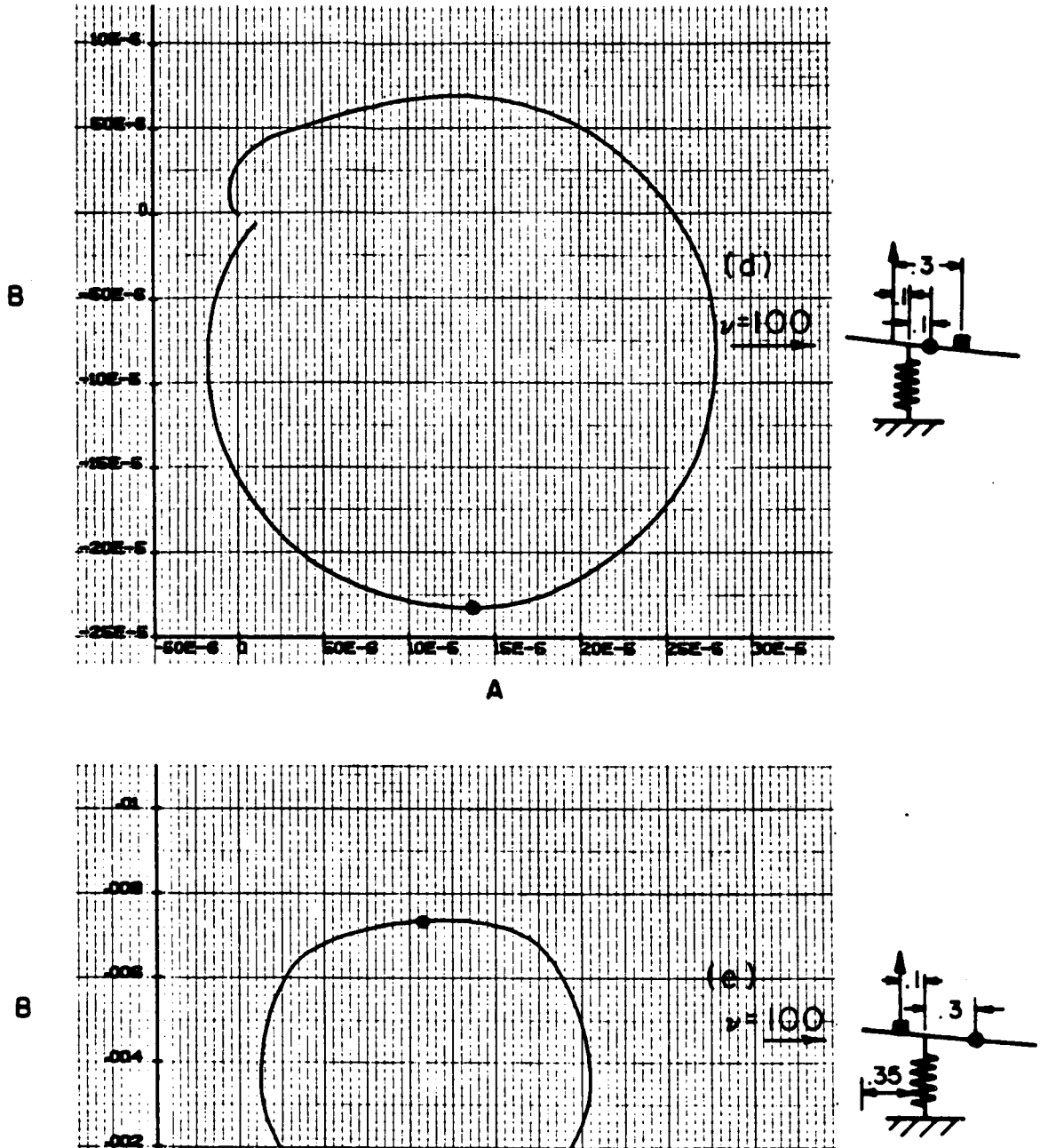

(d)

Fig. 17.- (Concluded)

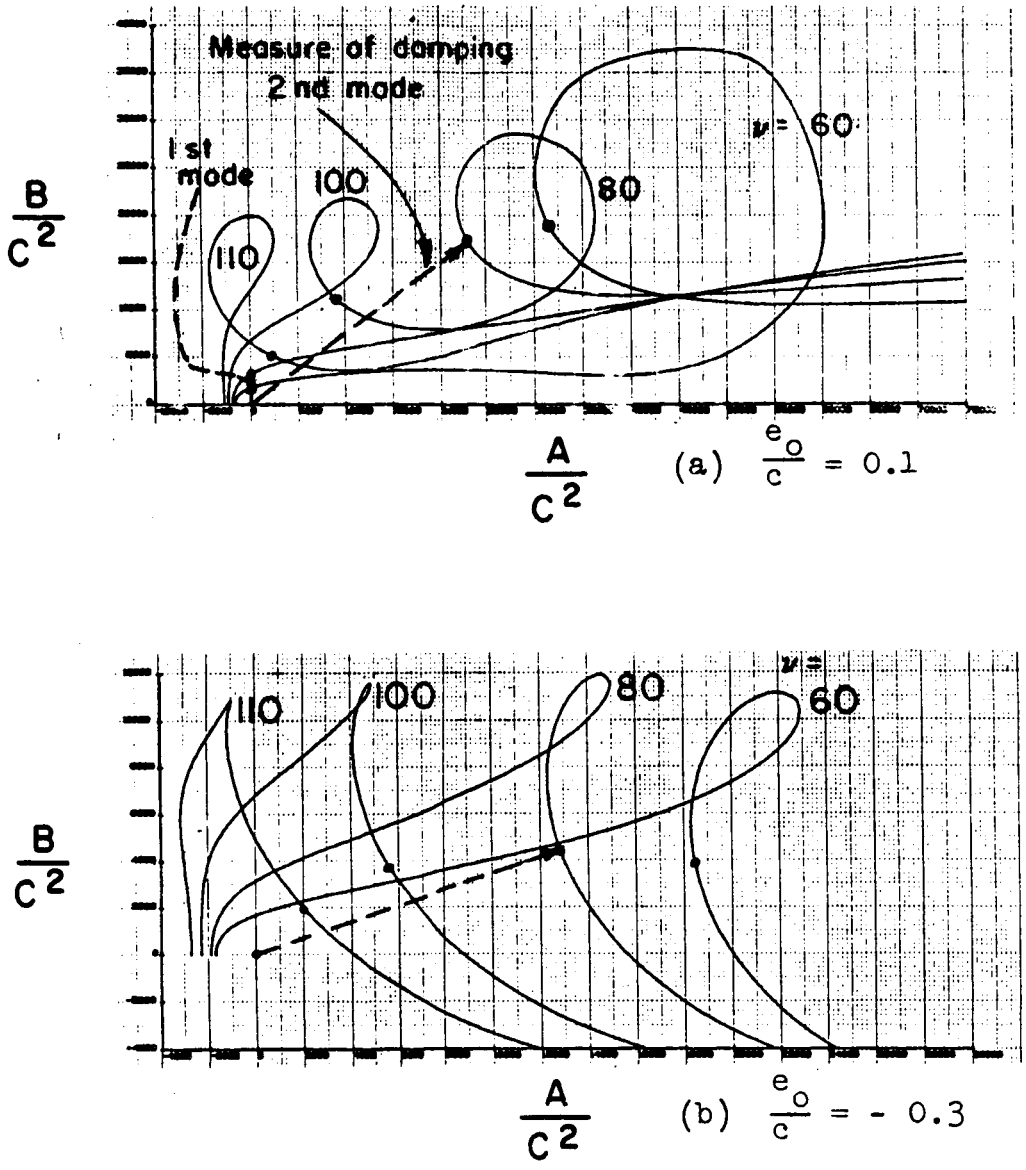

Fig. 18.- Illustrative impedance loci plots.

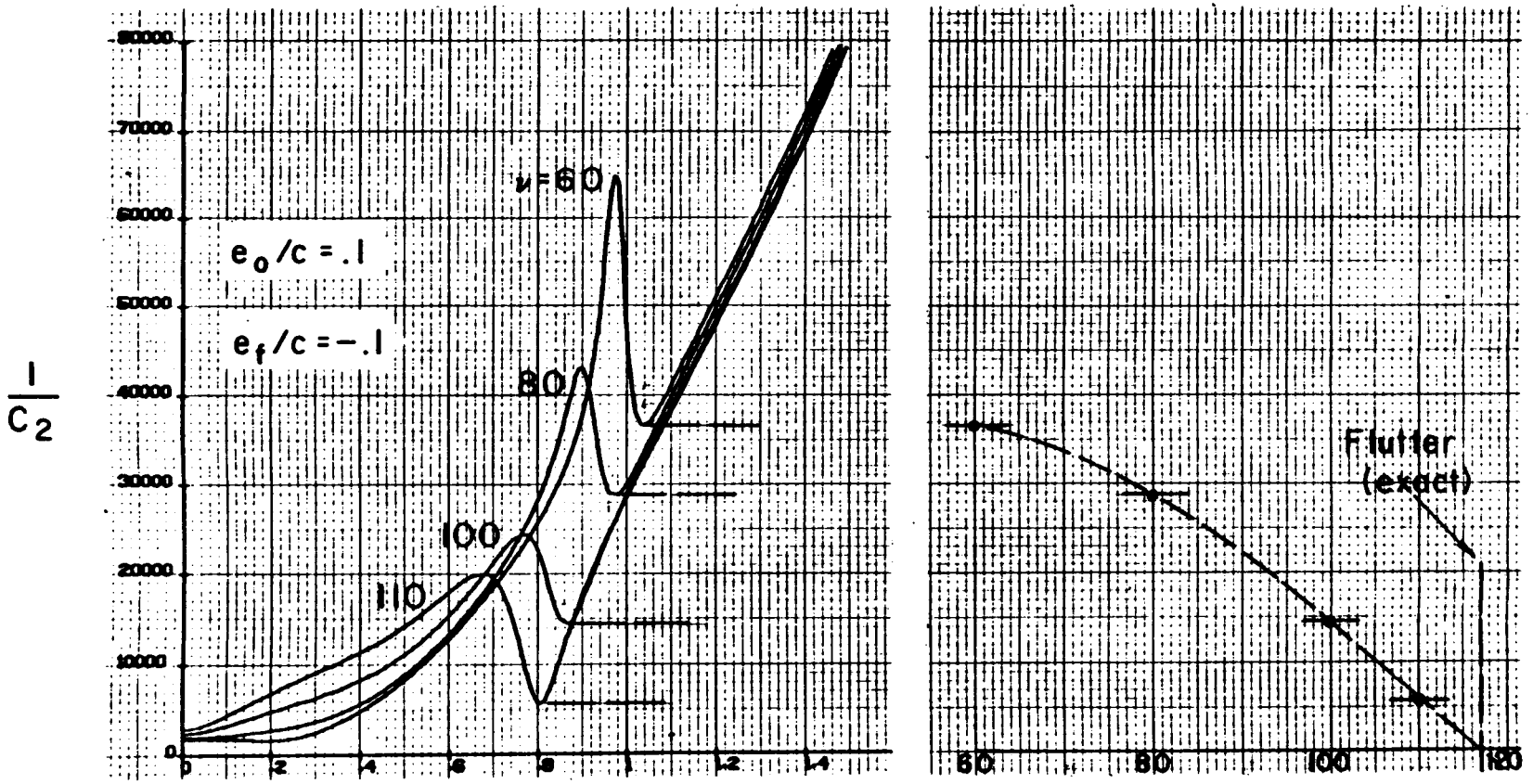

(a) $\frac{e}{c} = .1$; mild flutter

Fig. 19.- Extrapolation of low impedance values to predict flutter.

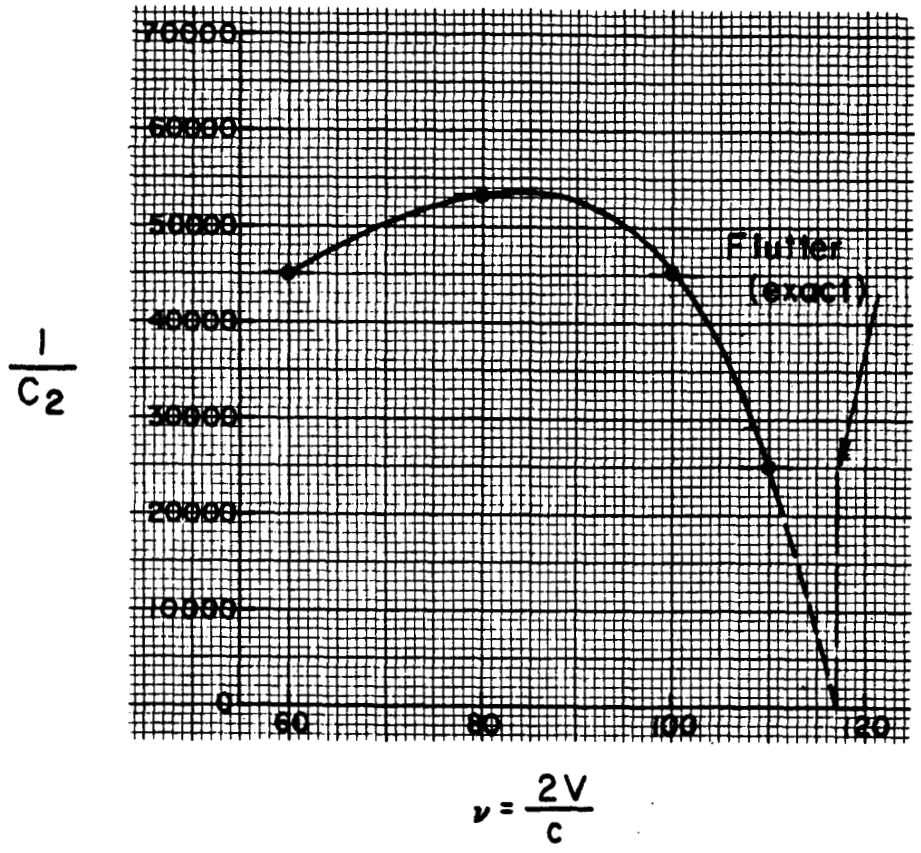

(b) $\frac{e}{c} = .3$; explosive flutter

Fig. 19.- (Concluded)

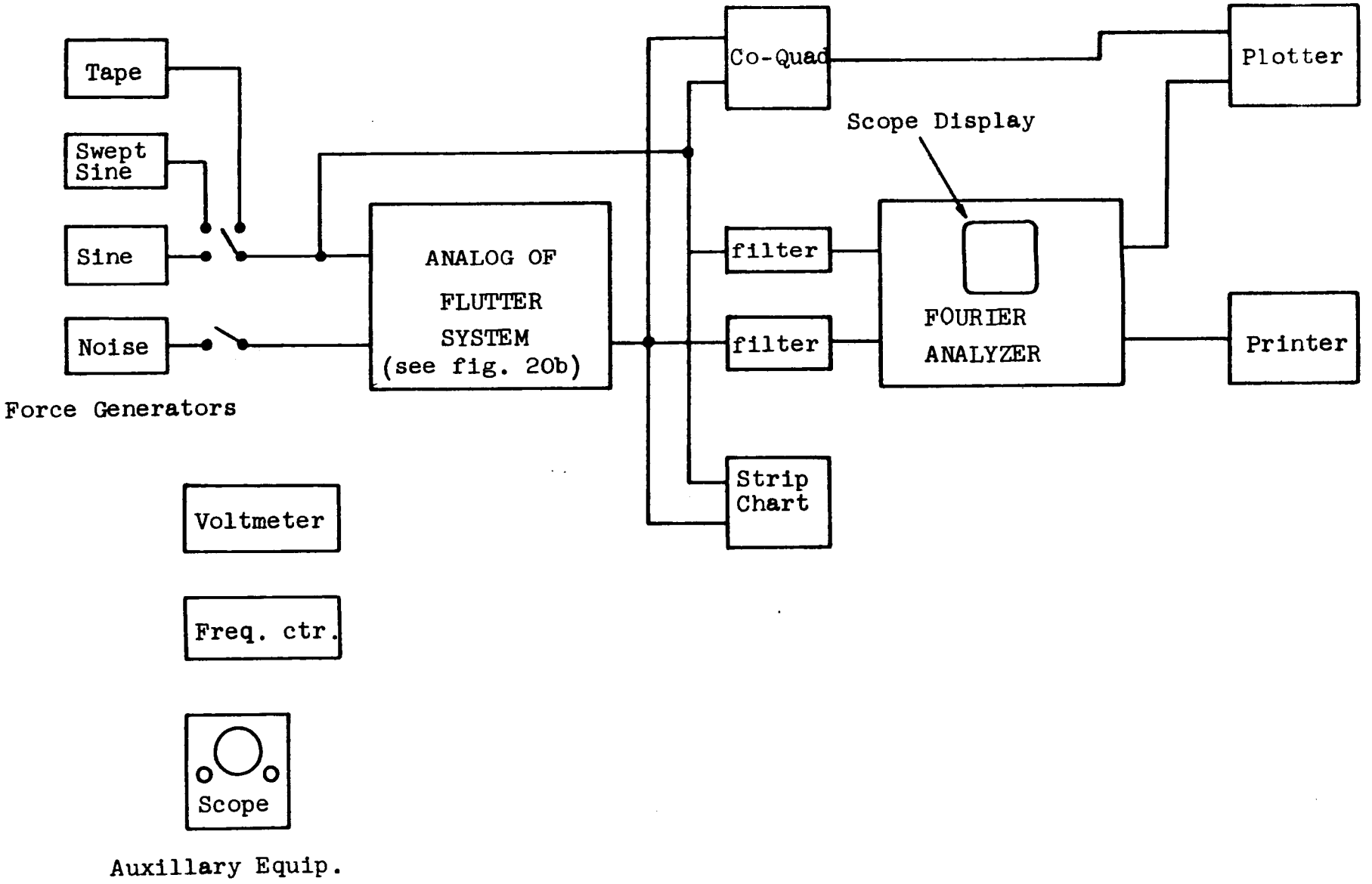

(a) General layout

Fig. 20.- Equipment used to study response characteristics of aeroelastic system.

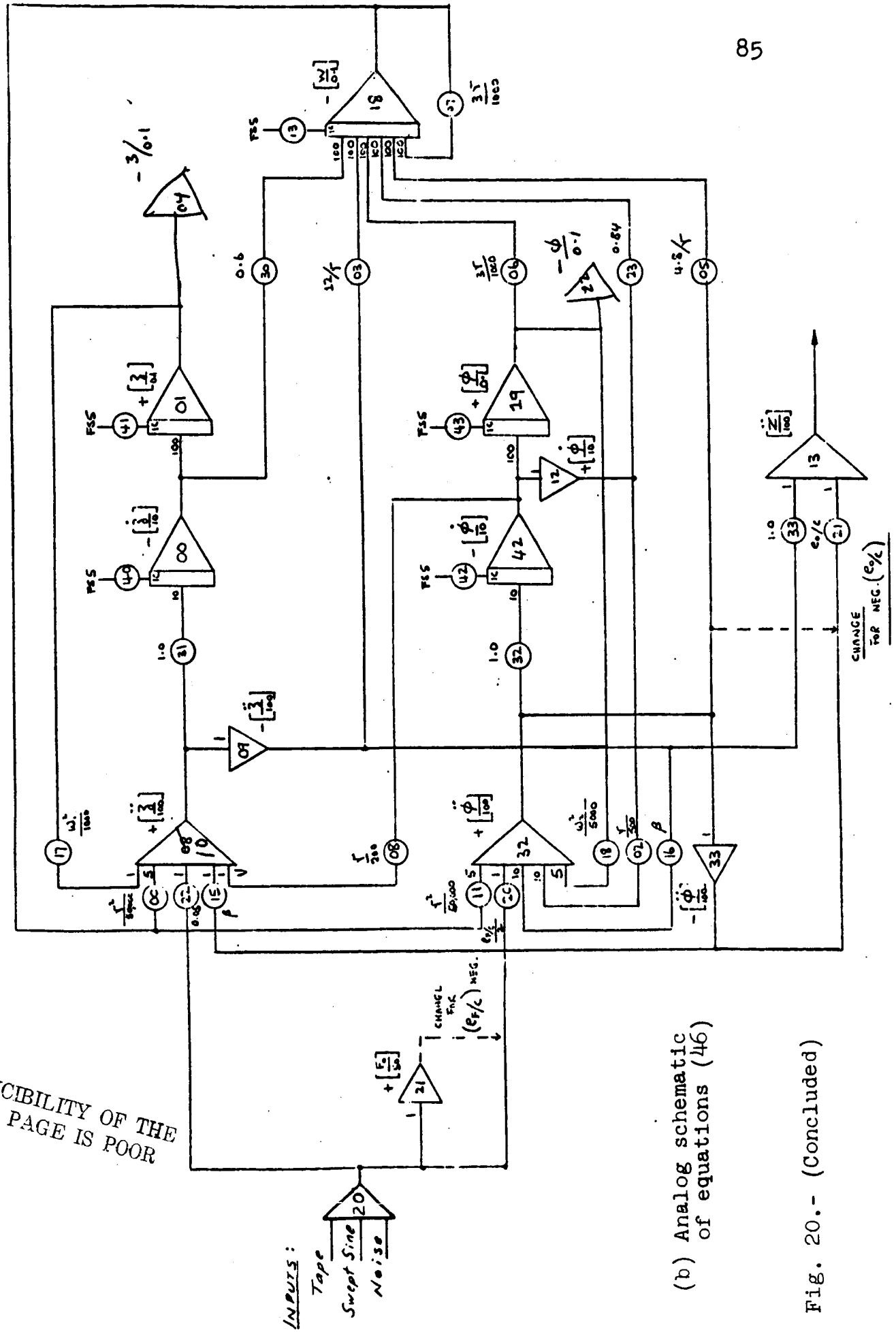

(b) Analog schematic of equations (46)

Fig. 20.- (Concluded)

Figure 21.- Analog computer, Fourier analyzer and auxiliary equipment used for simulated subcritical flutter testing experiments.

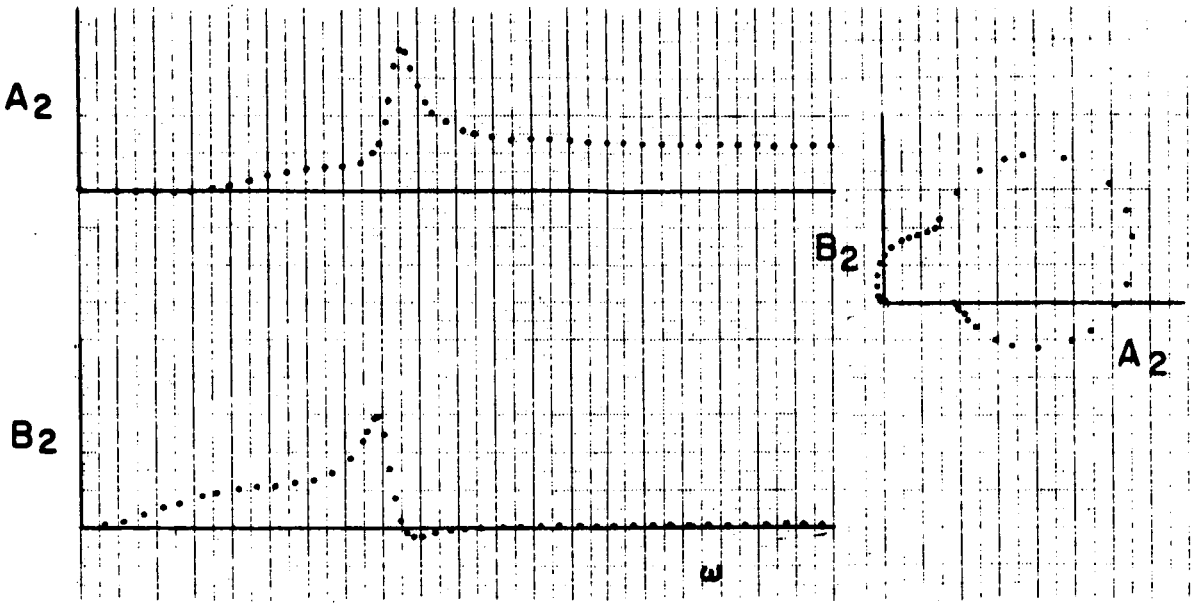

Fig. 22.- Ideal frequency response function (no noise) obtained by frequency dwell technique.

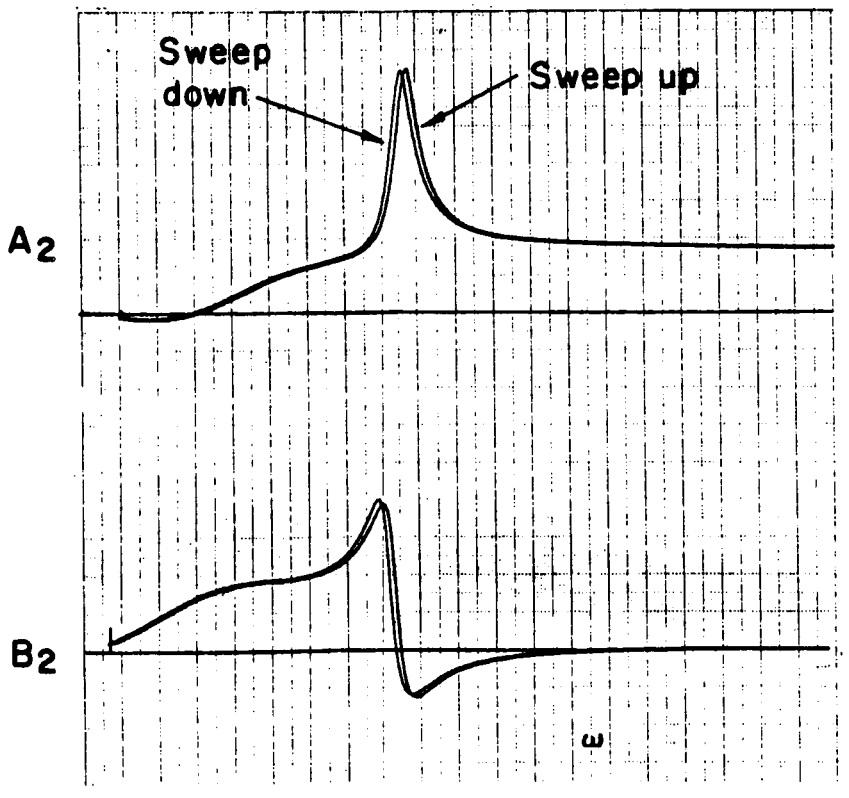

Fig. 23.- Frequency response functions obtained by slow sweeps.

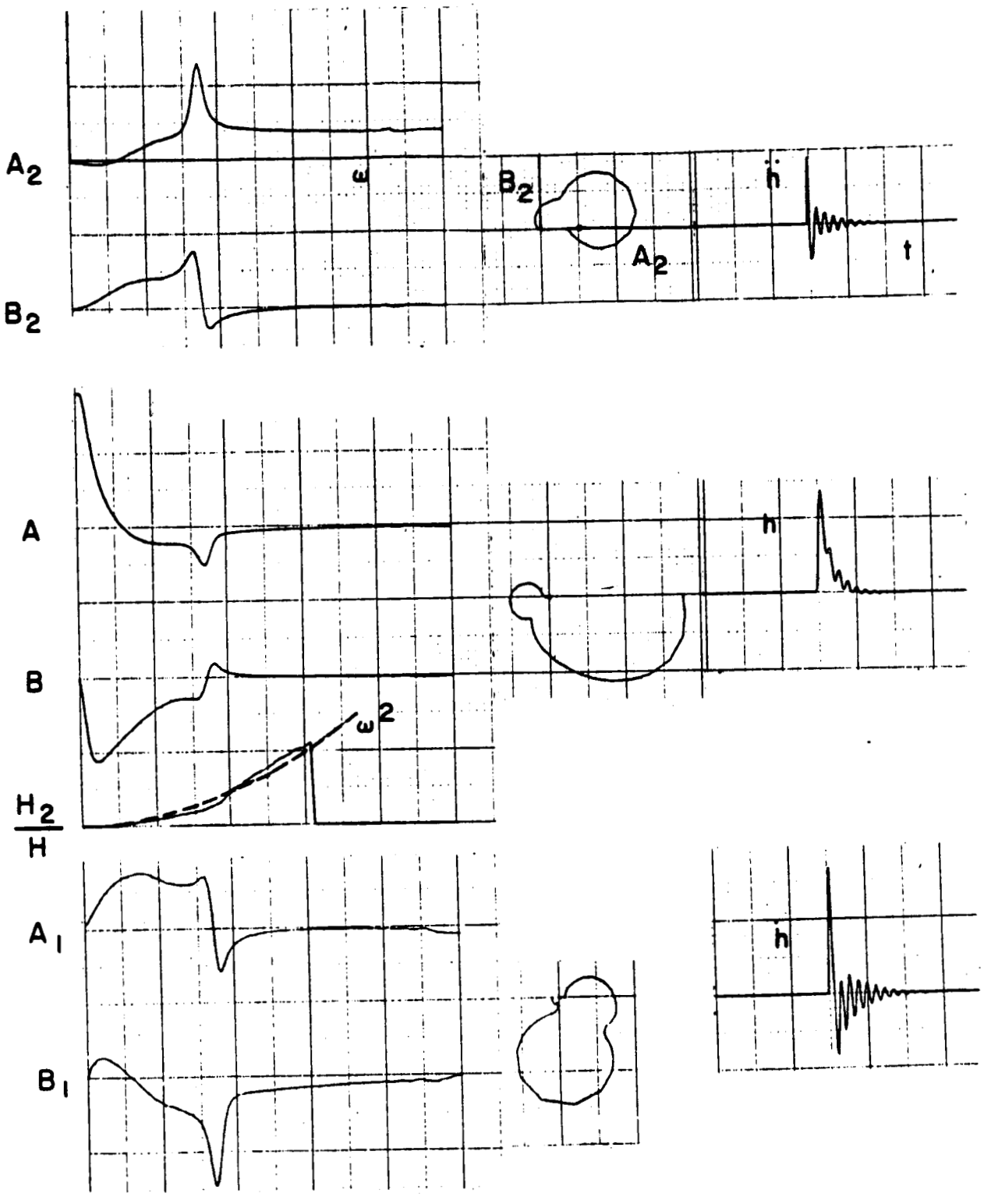

Fig. 24.- Frequency response and h functions obtained from $\frac{F_y}{F_F}$

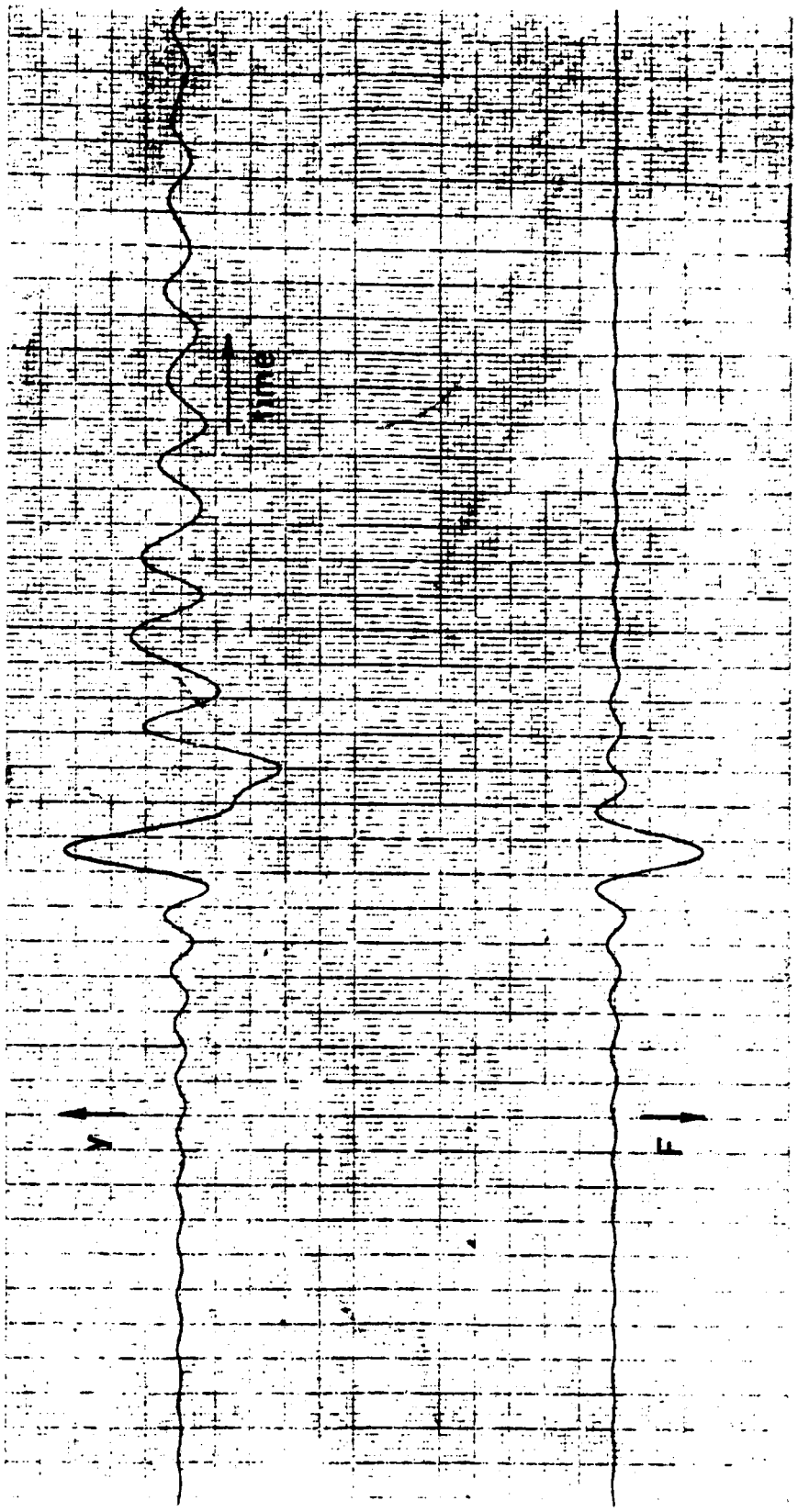

Fig. 25.- Response of 5th-order system to impulsive sine input.

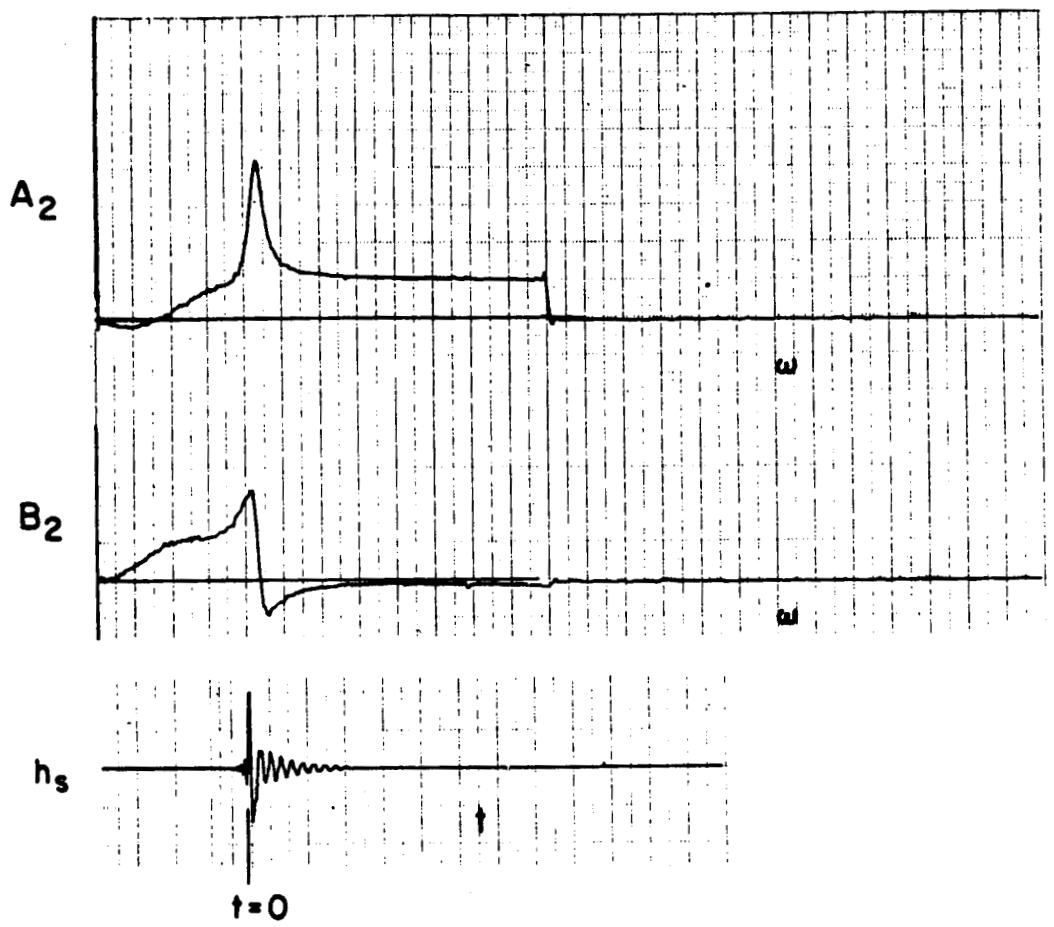

Fig. 26.- Frequency response function and h_s as obtained from an impulse sine input.

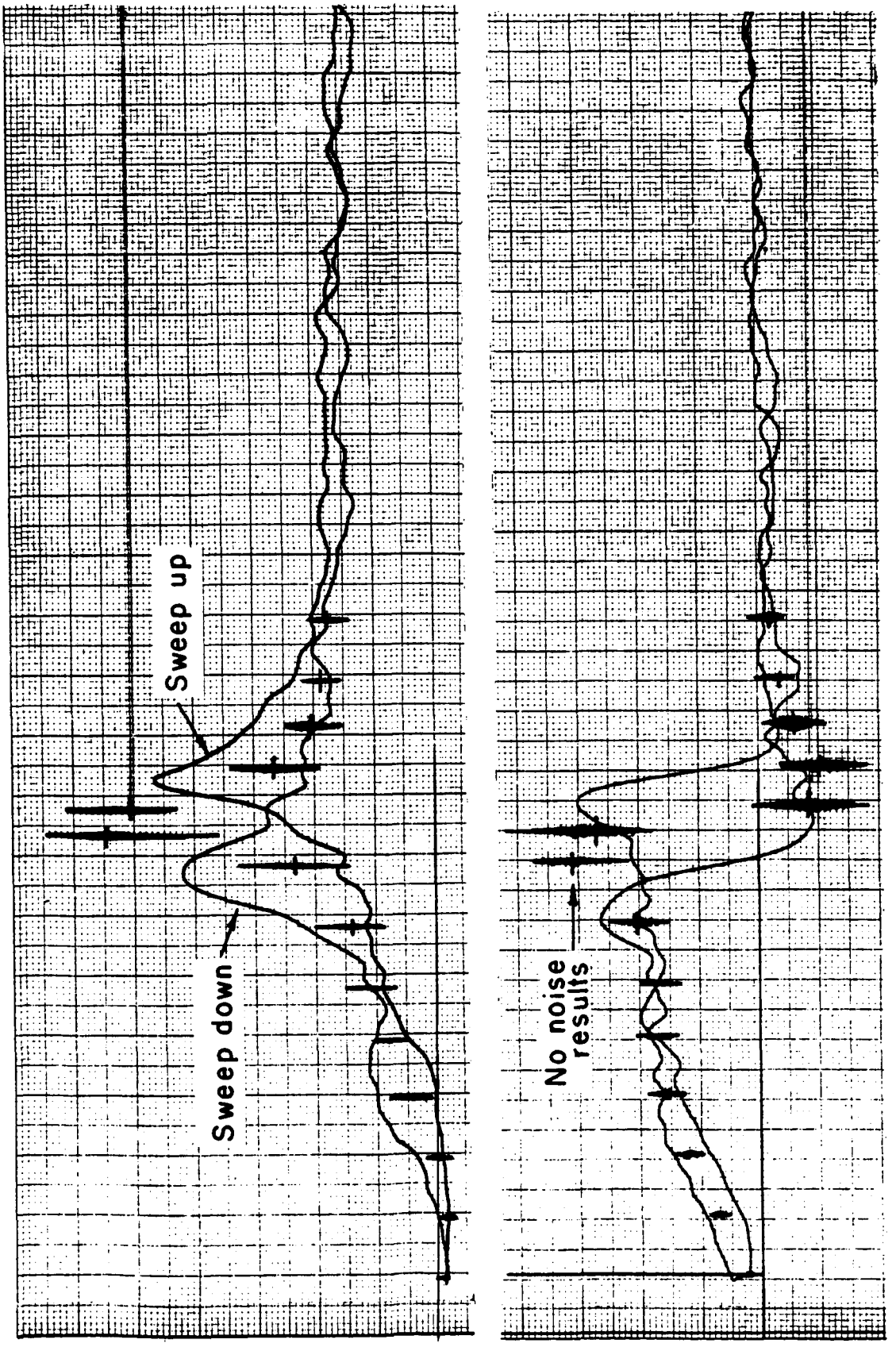

Fig. 27.- Frequency response function obtained by frequency dwell, with unknown noise in the input.

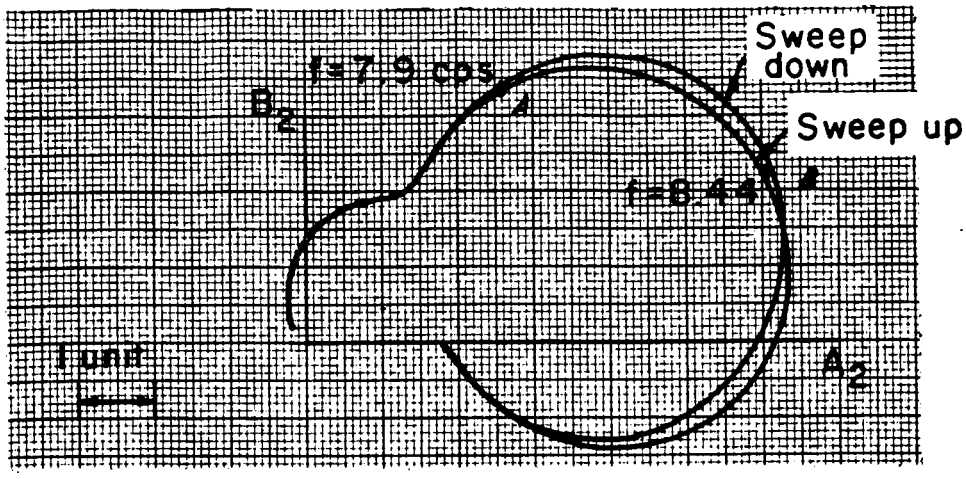

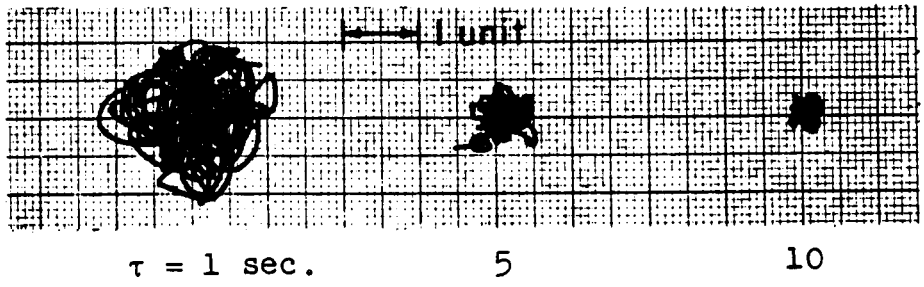

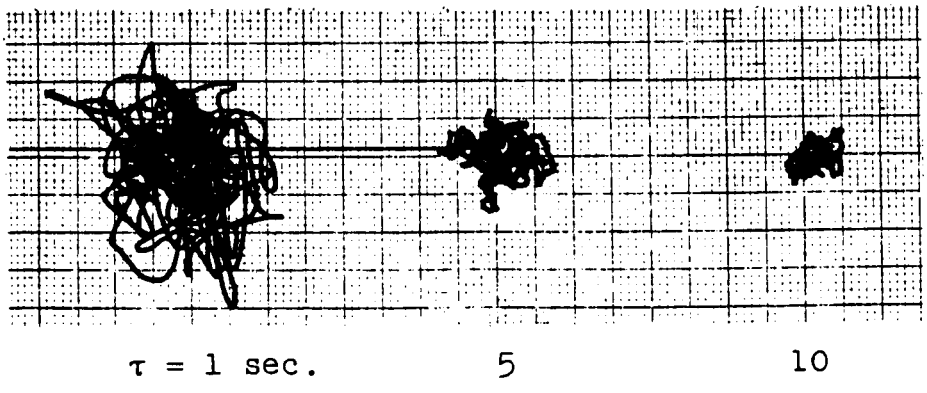

Fig. 28.- Dwell results obtained with noisy input for various averaging times in Co-Quad analyzer.

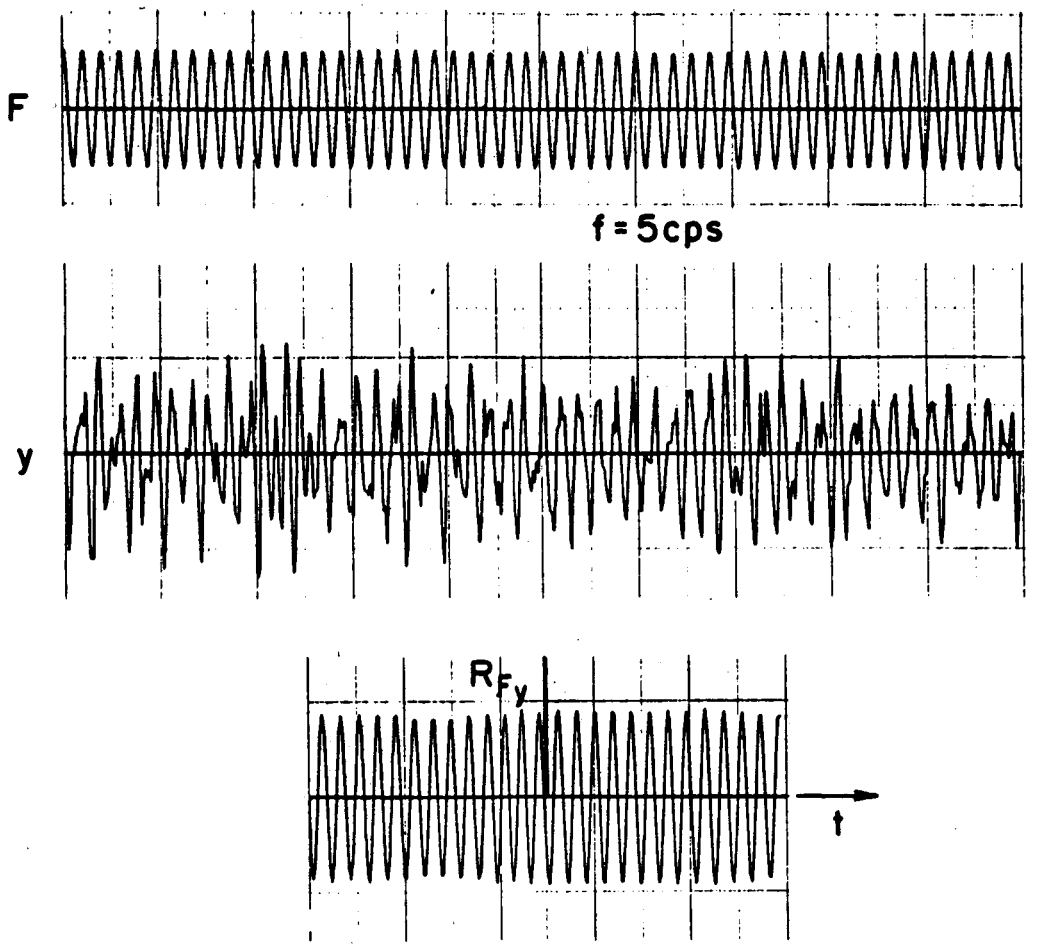

Fig. 29.- Noise elimination by cross-correlation for frequency dwell technique.

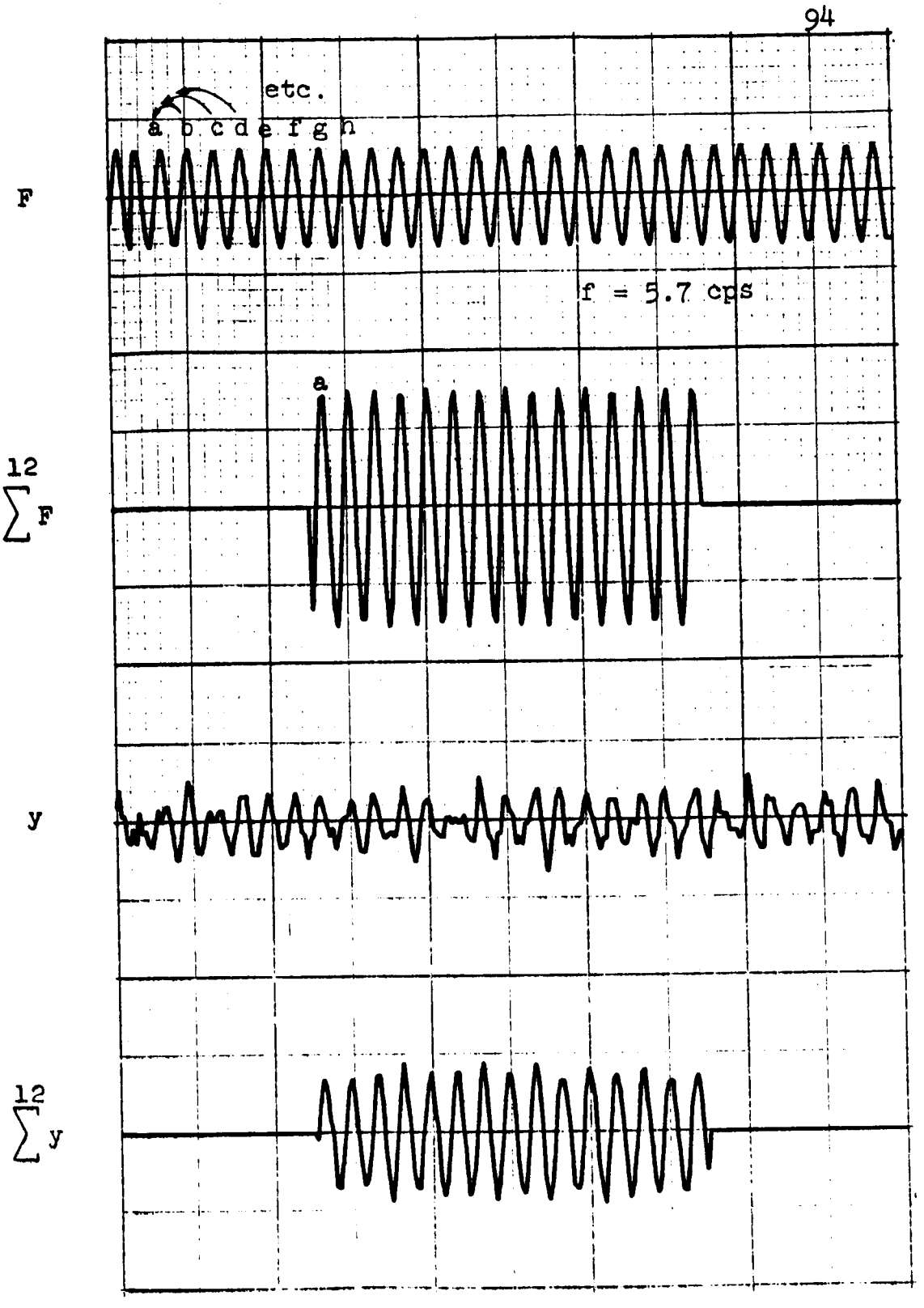

Fig. 30.- Noise elimination by peak shifting for frequency dwell technique.

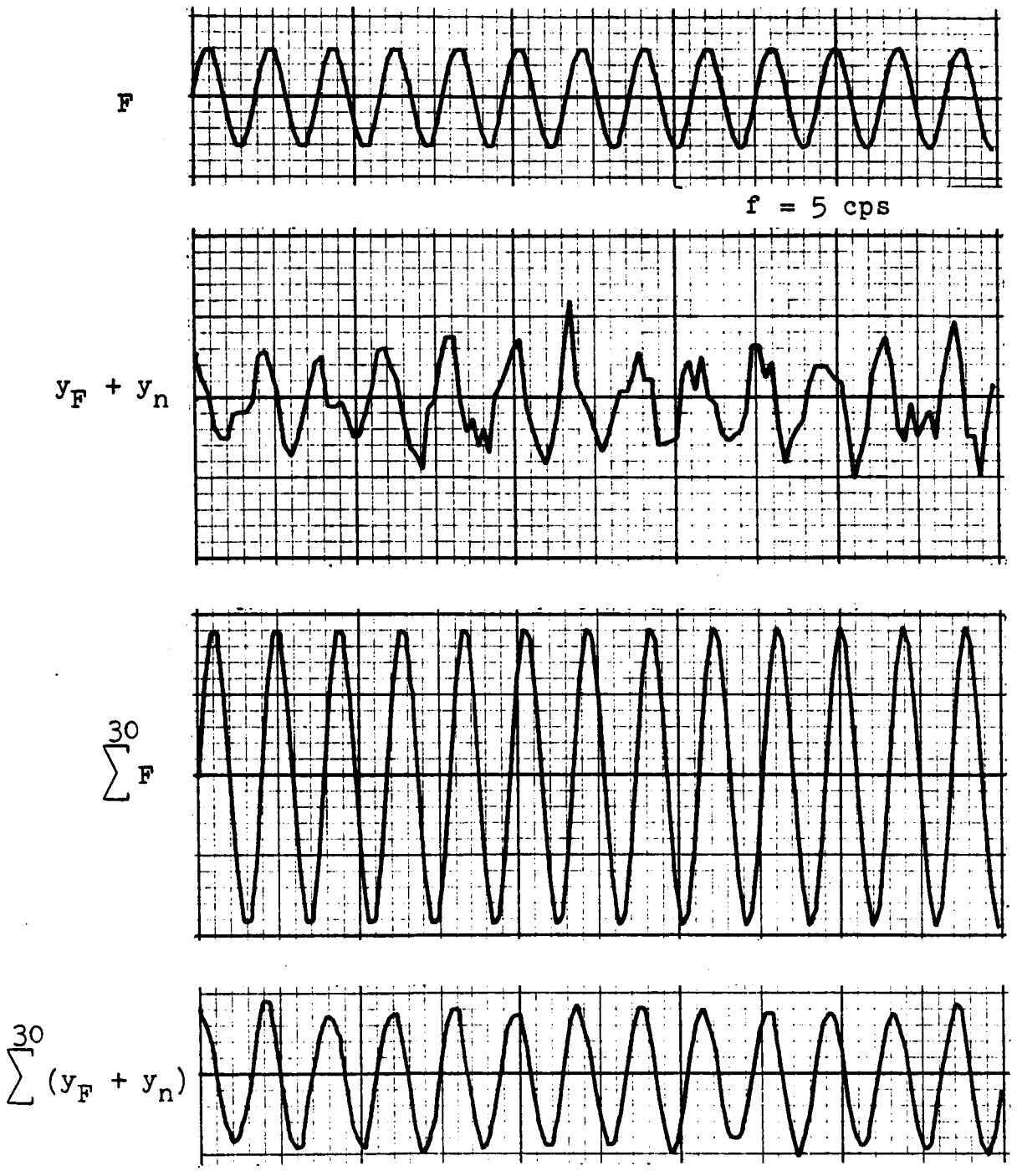

Fig. 31.- Noise elimination by ensemble averaging for frequency dwell technique.

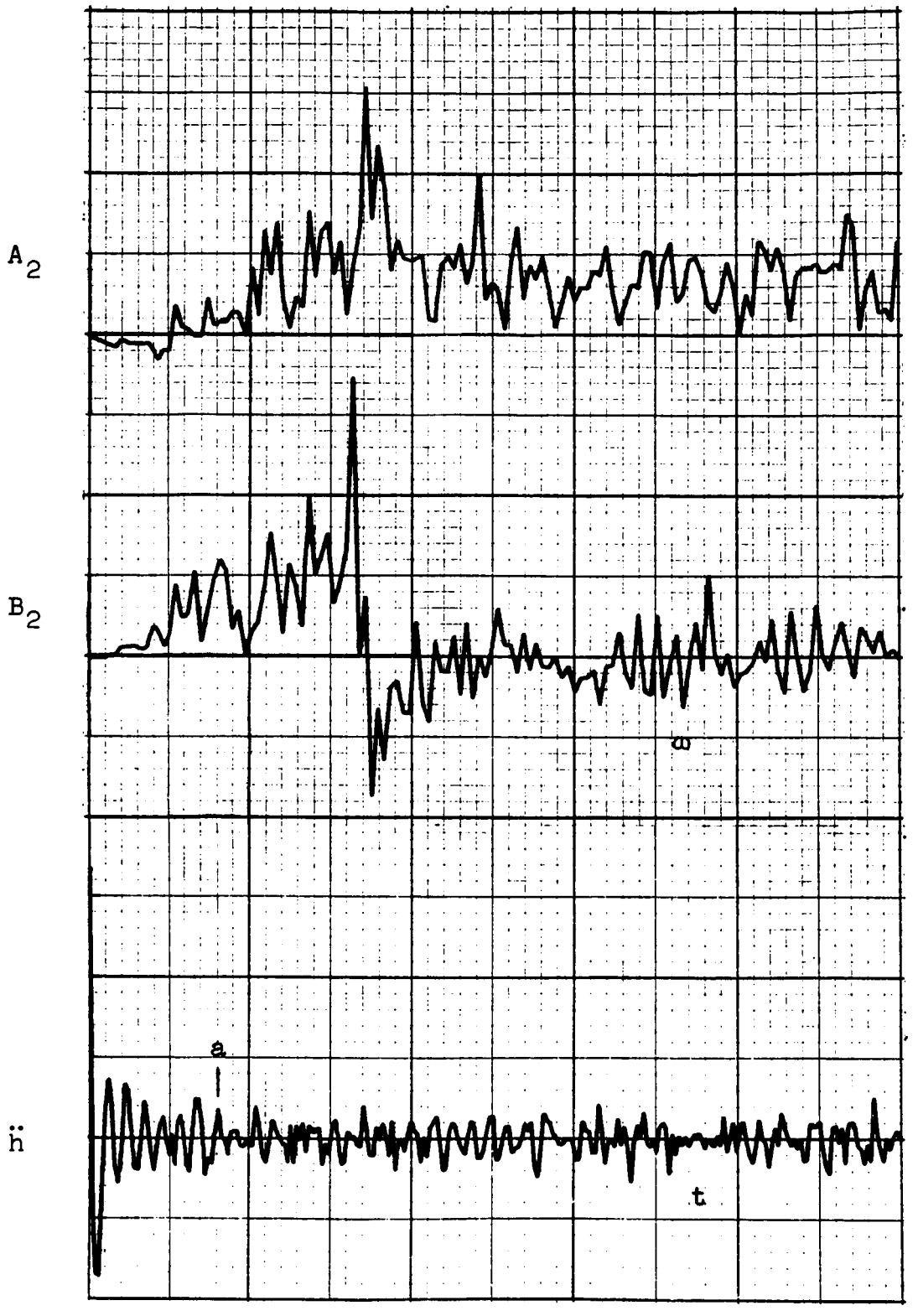

Fig. 32.- Frequency response and $\ddot{h}$ functions obtained by single swept sine run with noise in input.

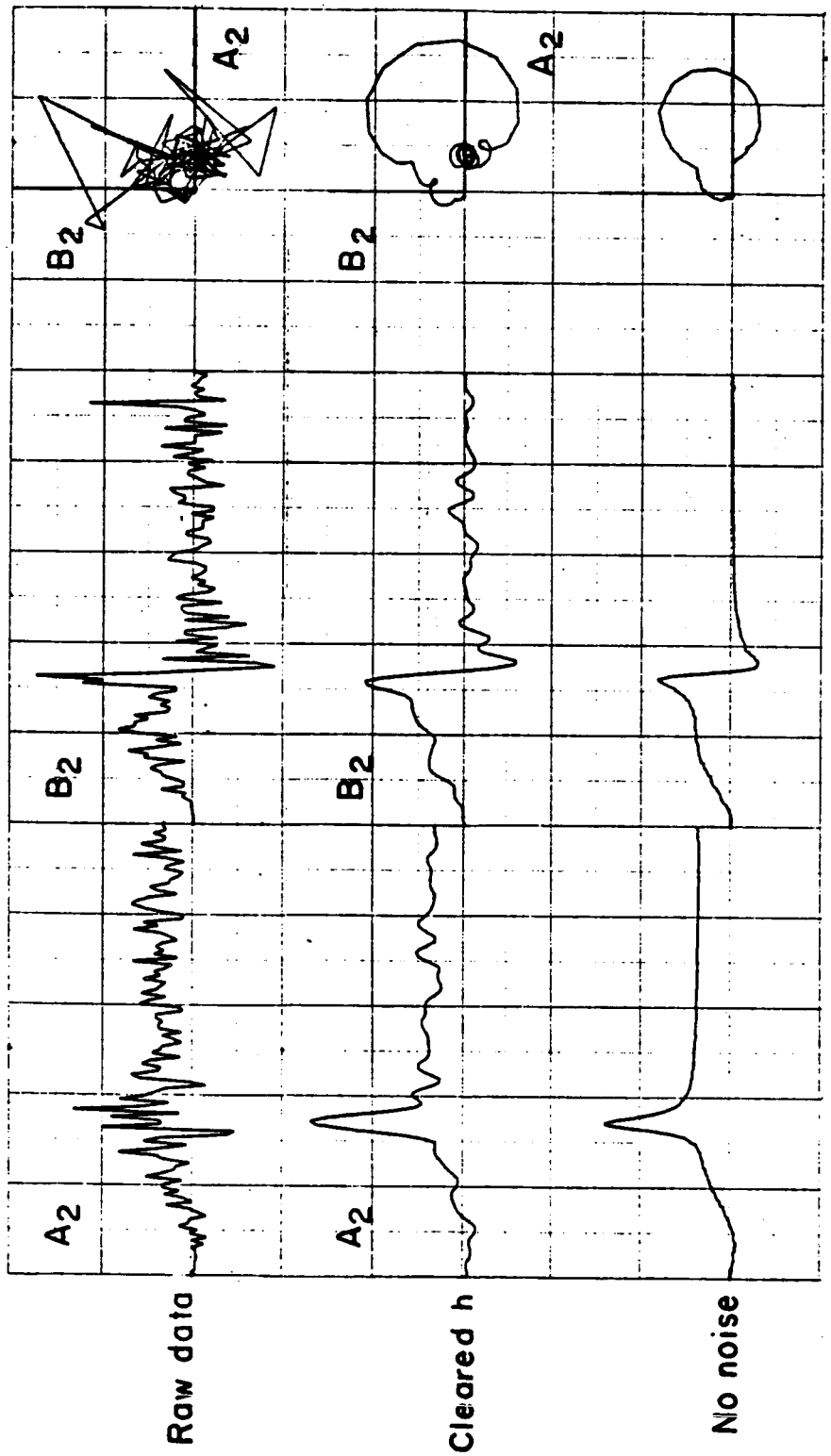

Fig. 33.- Improved frequency response function by clearing h function.

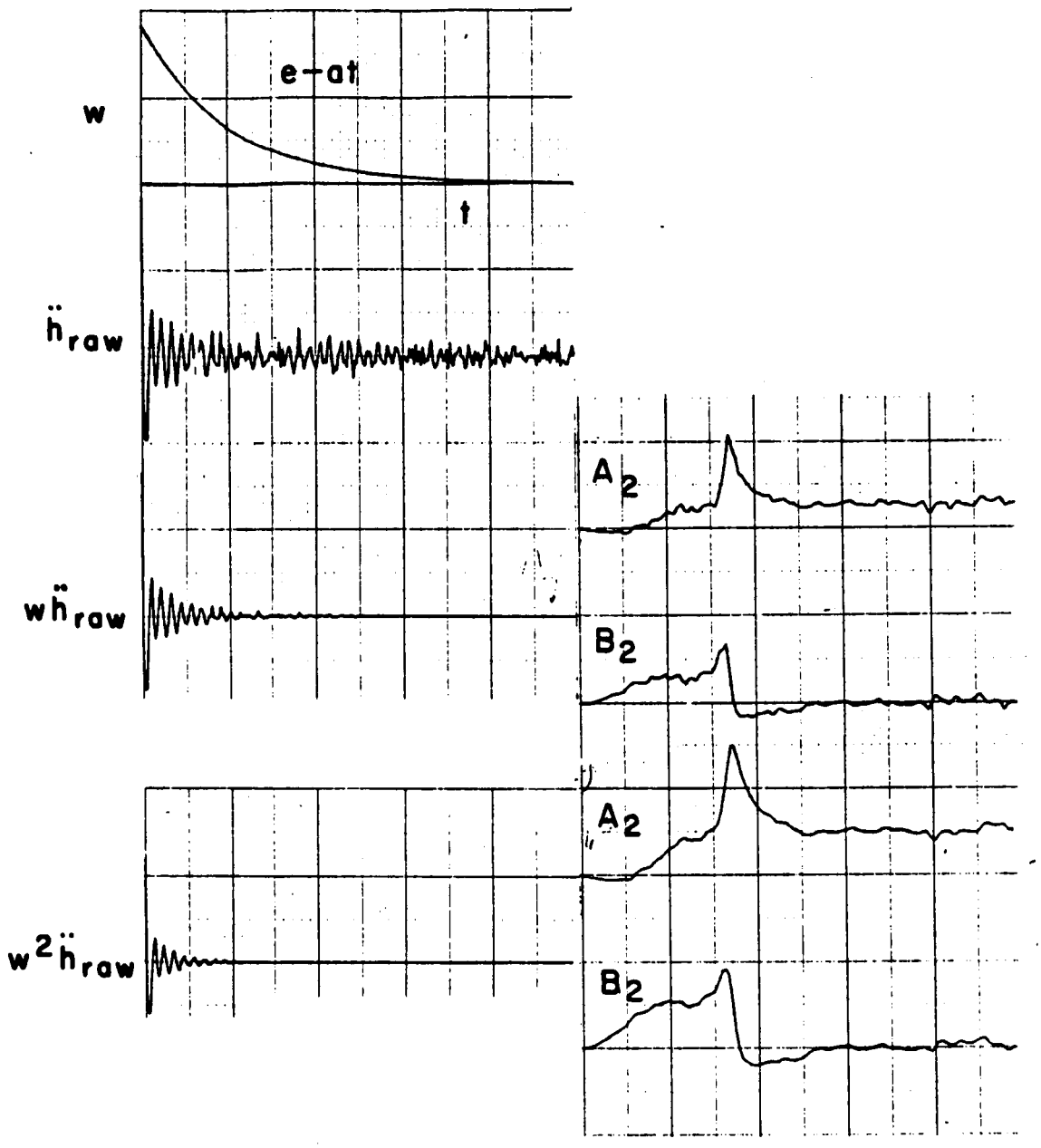

Fig. 34.- Improved frequency response function by exponential weighting of h function.

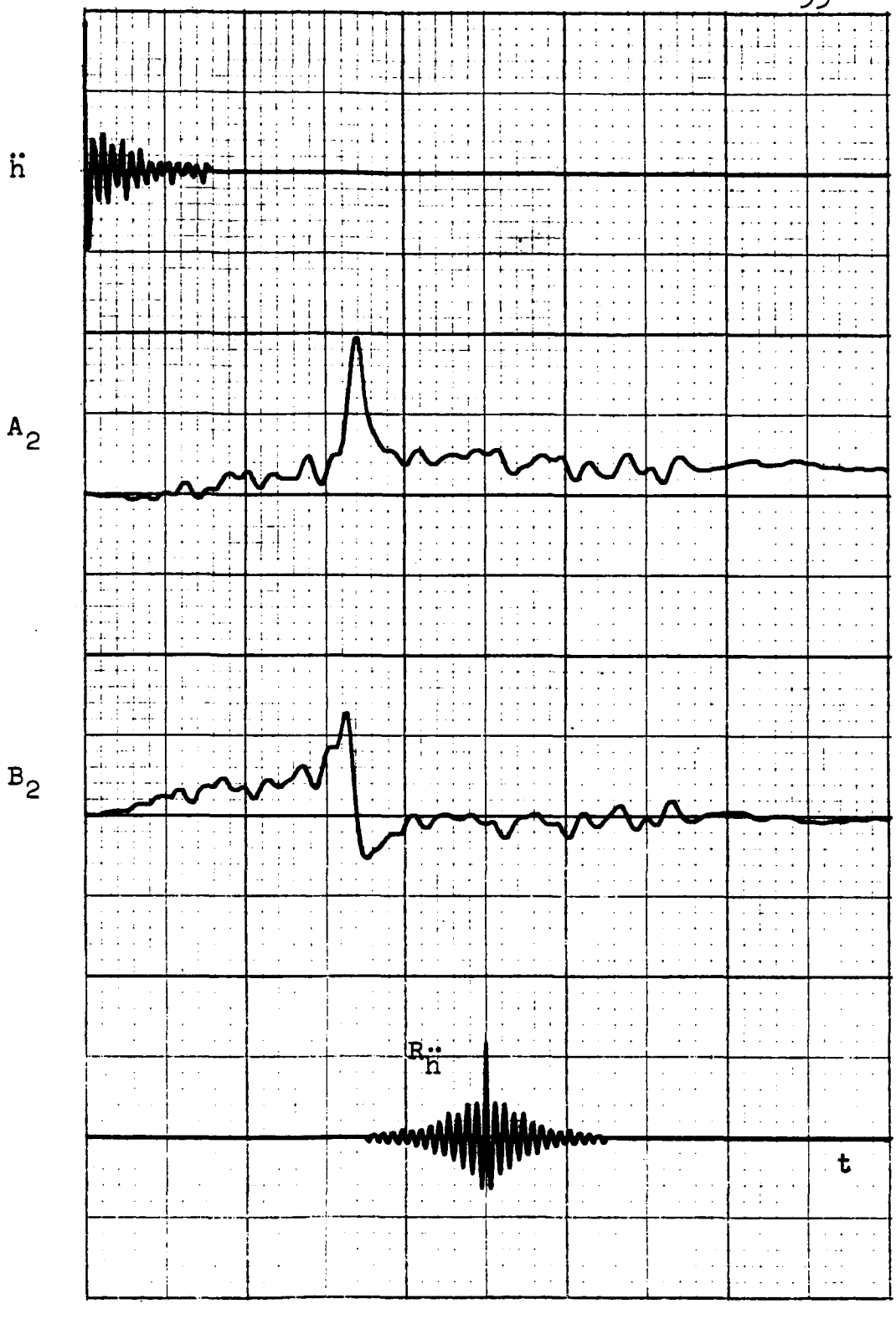

Fig. 35.- Use of cross-correlation between input and output to eliminate noise.

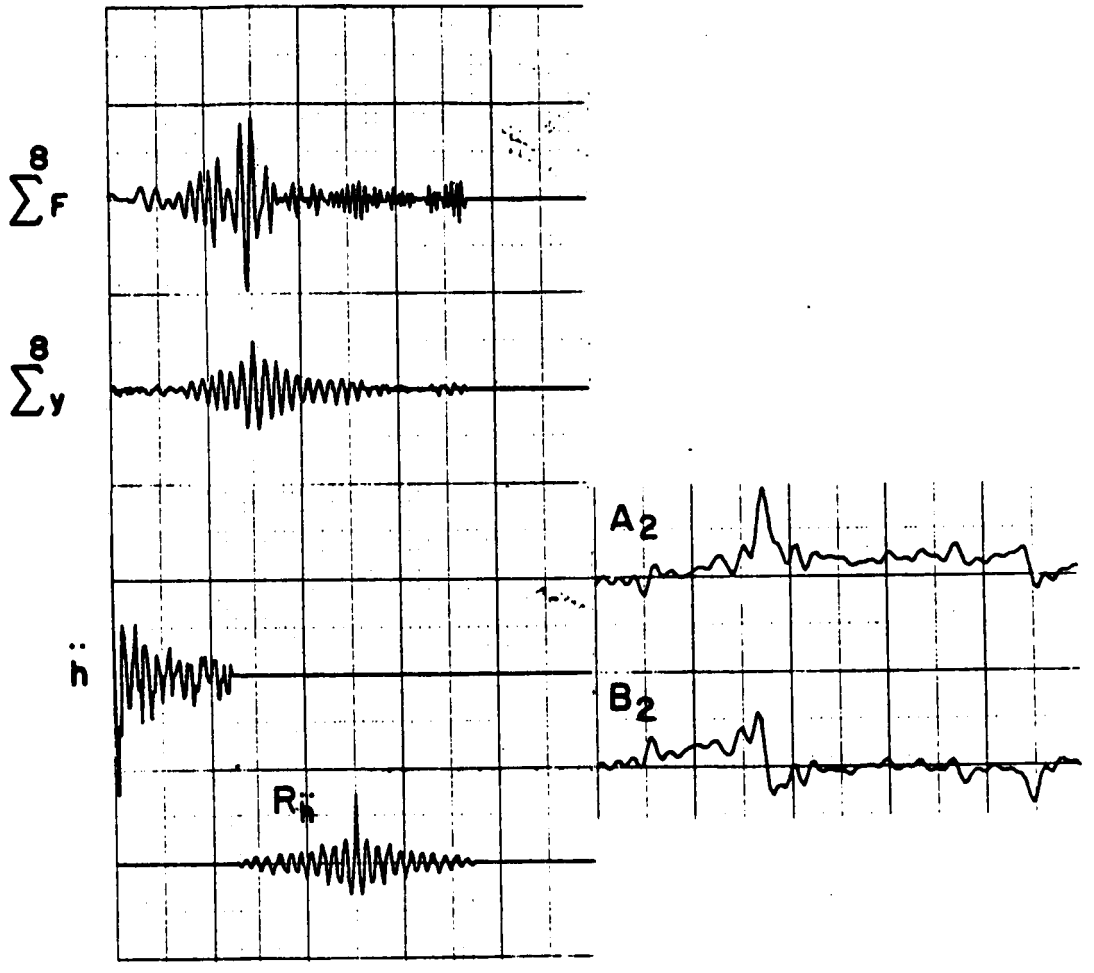

Fig. 36.- Use of peaking shifting technique for swept sine run to eliminate noise.

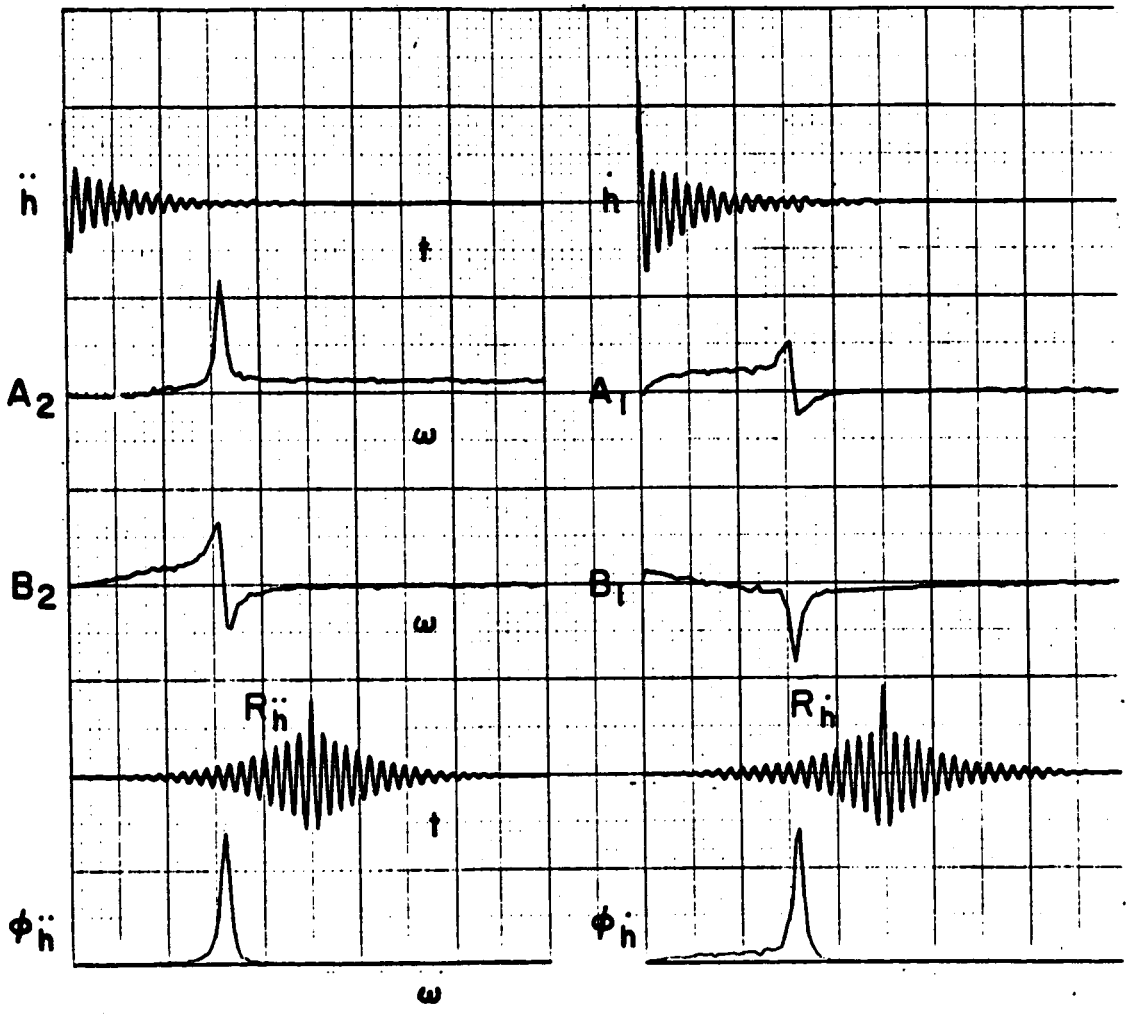

a) ν = 110 ; average of 20 runs

Fig. 37.- Use of ensemble averaging of sine sweep runs to eliminate noise.

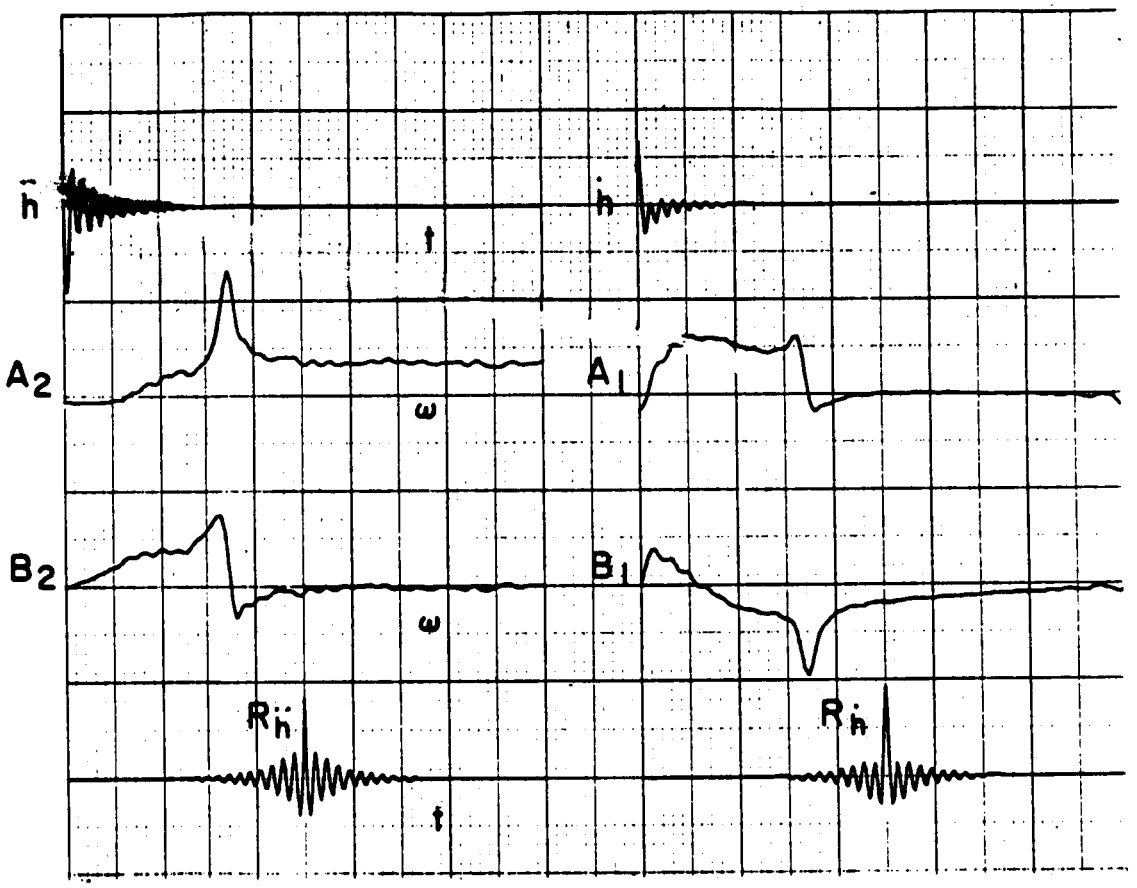

b) $\nu = 100$, average of 20 runs

Fig. 37.- (Cont.)

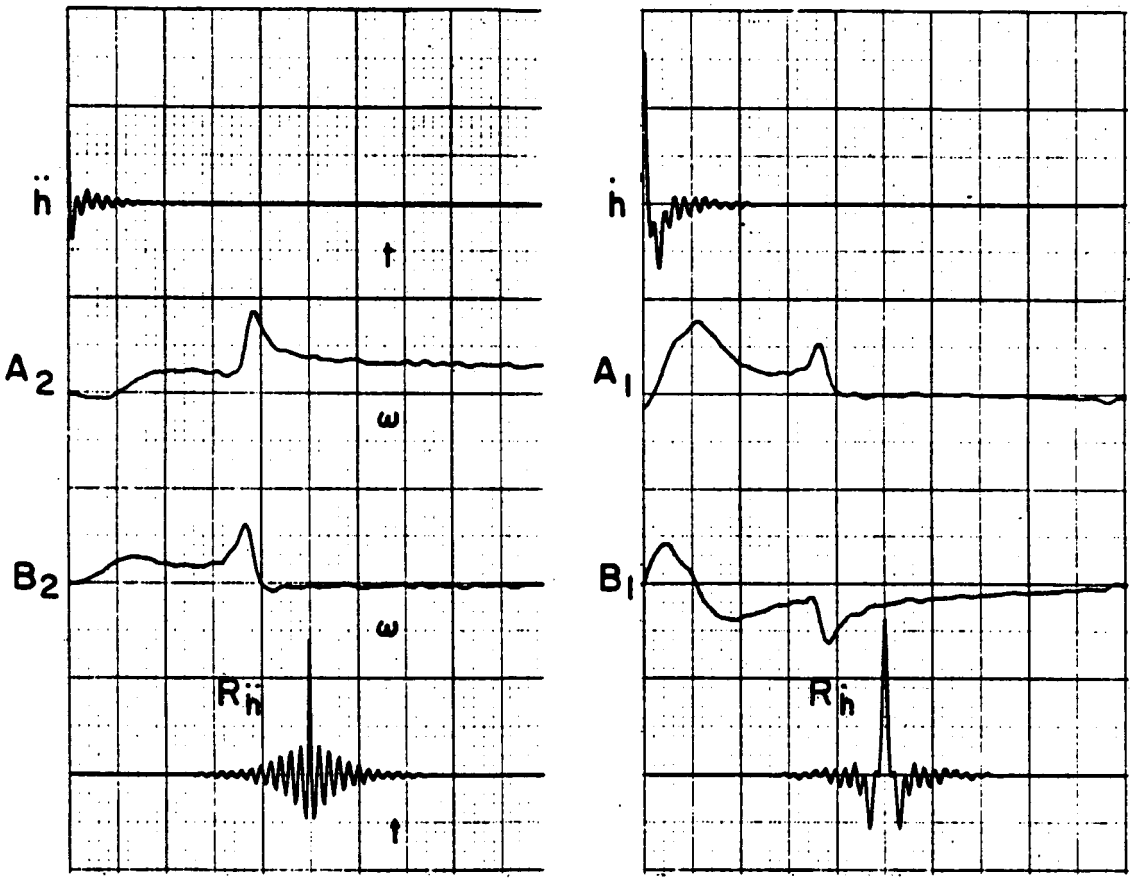

c) $\nu = 80$; average of 20 runs

Fig. 37.- (Cont.)

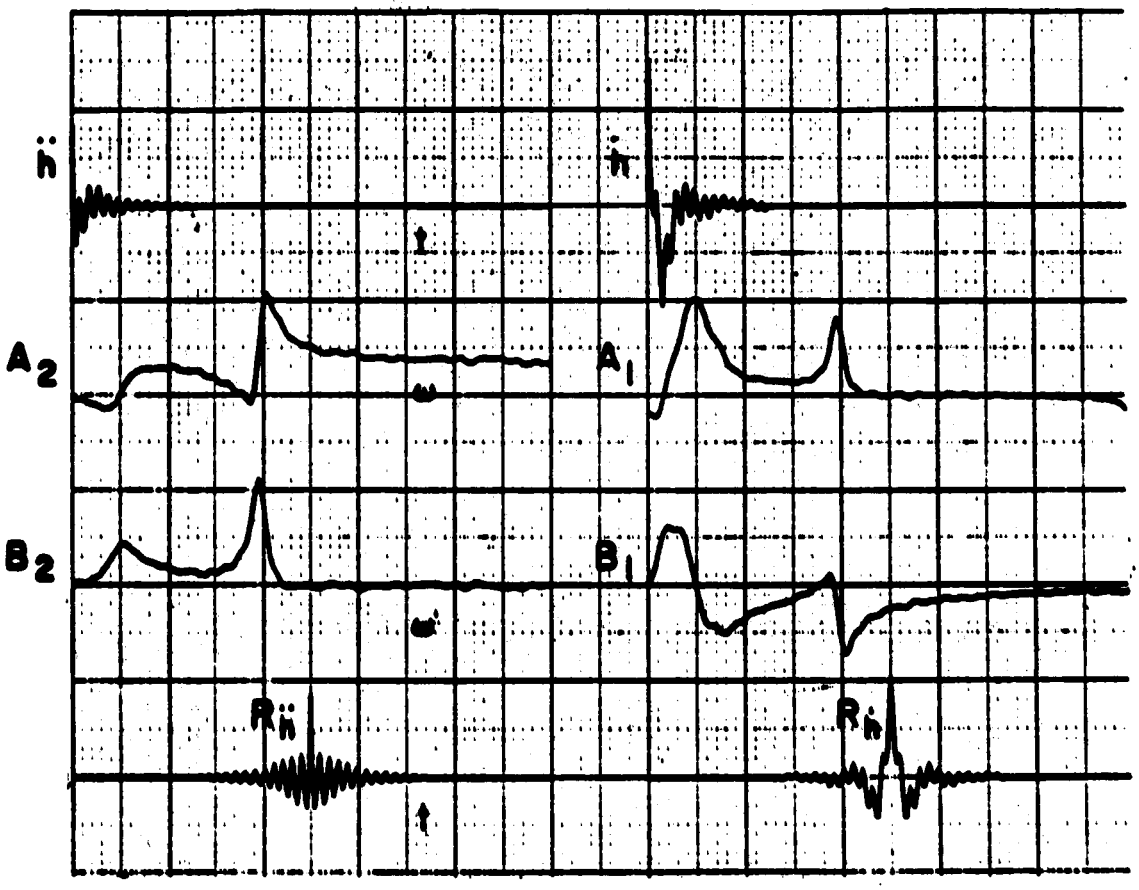

d) v = 60 ; average of 20 runs

Fig. 37.- (Concluded)

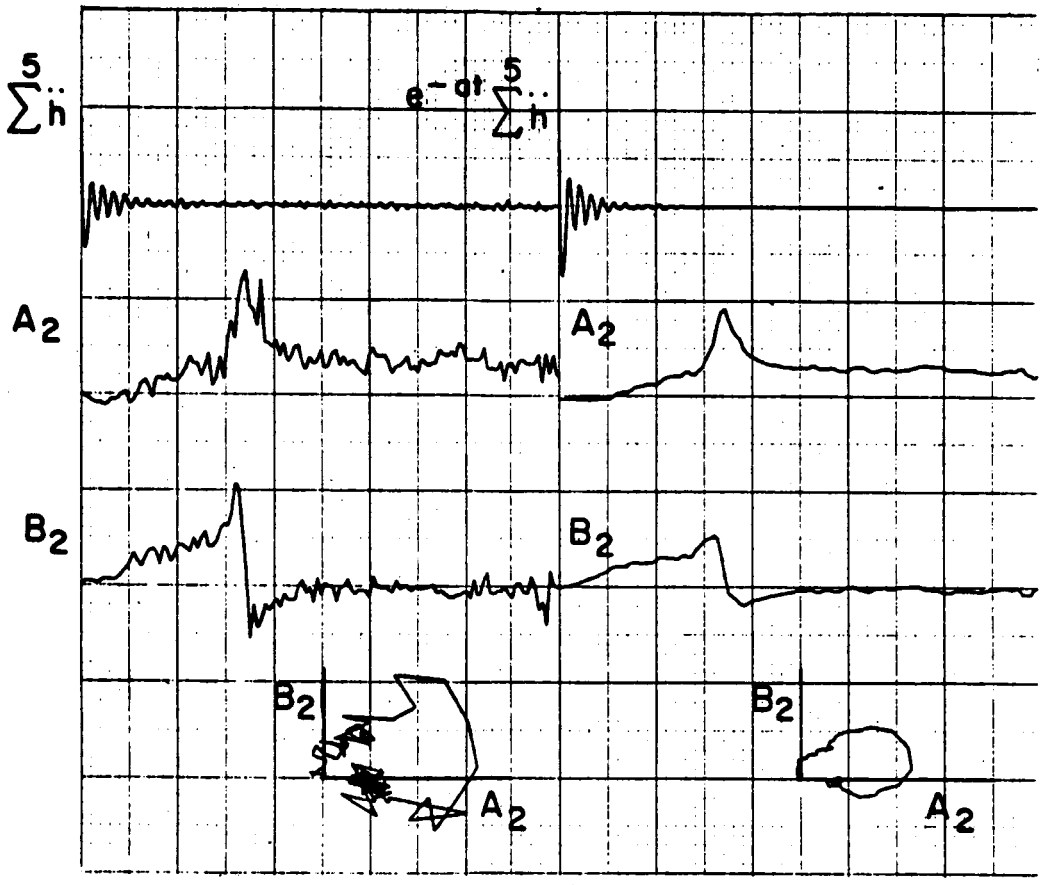

Fig. 38.- Combination use of ensemble averaging and weighting of h function to eliminate noise, $\nu = 100$.

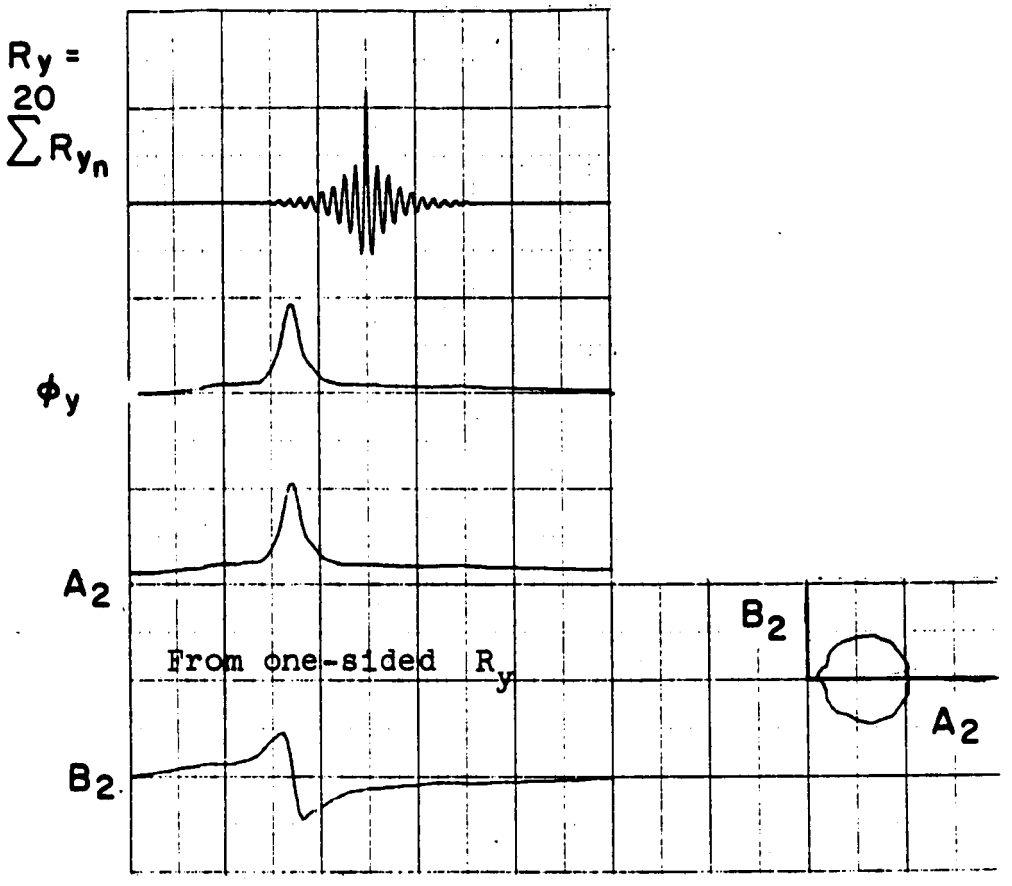

Fig. 39.- Ensemble averaging of the correlation functions for acceleration response due to noise input only, $\nu = 100$.

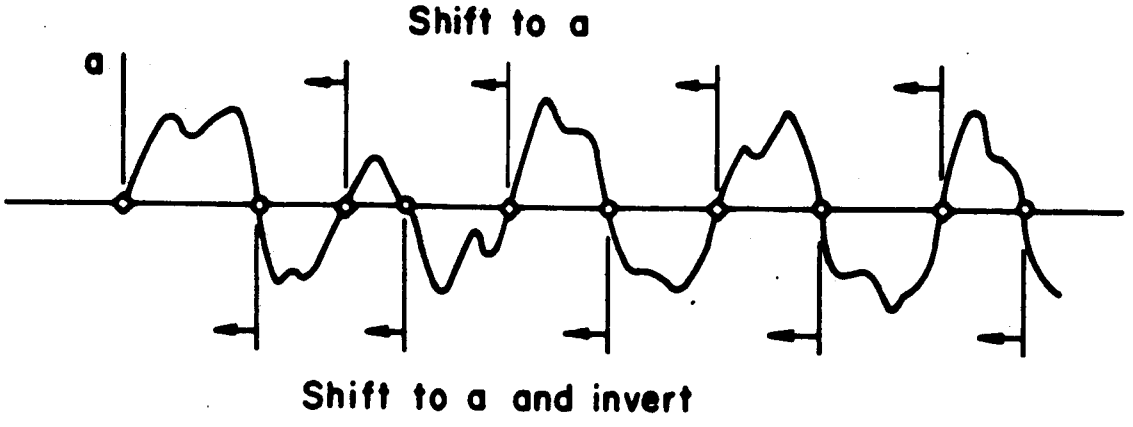

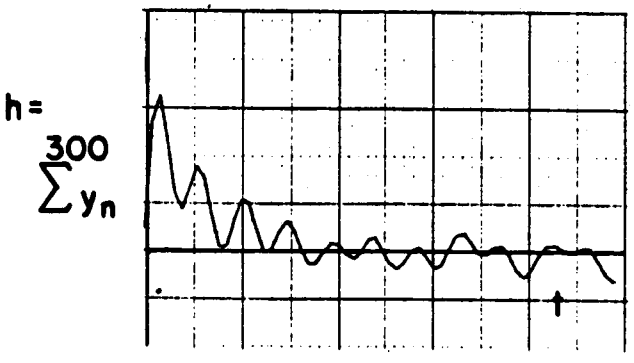

Fig. 40.- Randomdec signature obtained from response to noise only, $\nu = 100$.

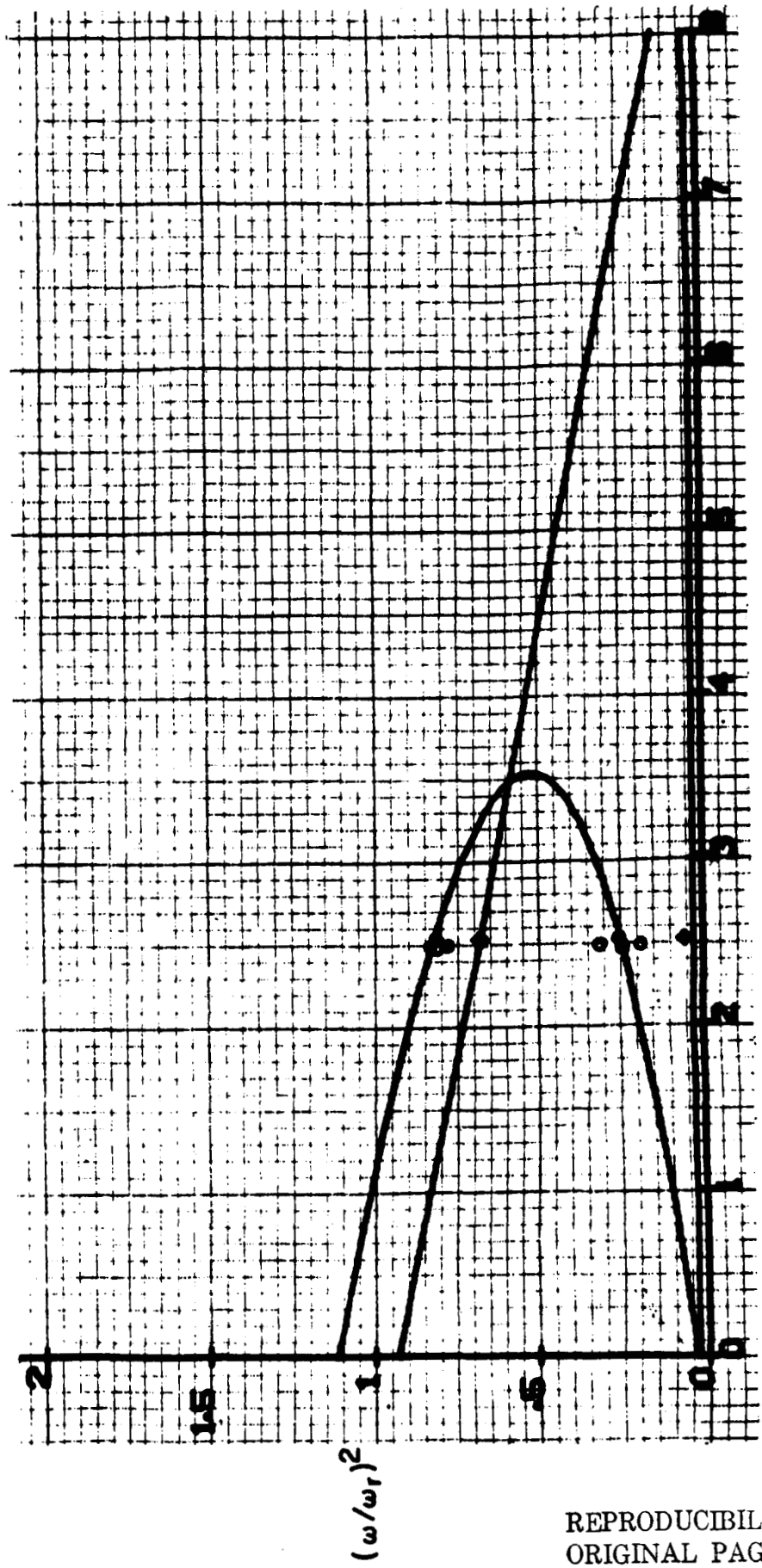

Fig. 41.- Quasi-roots obtained from experimentally deduced differential equation coefficients.

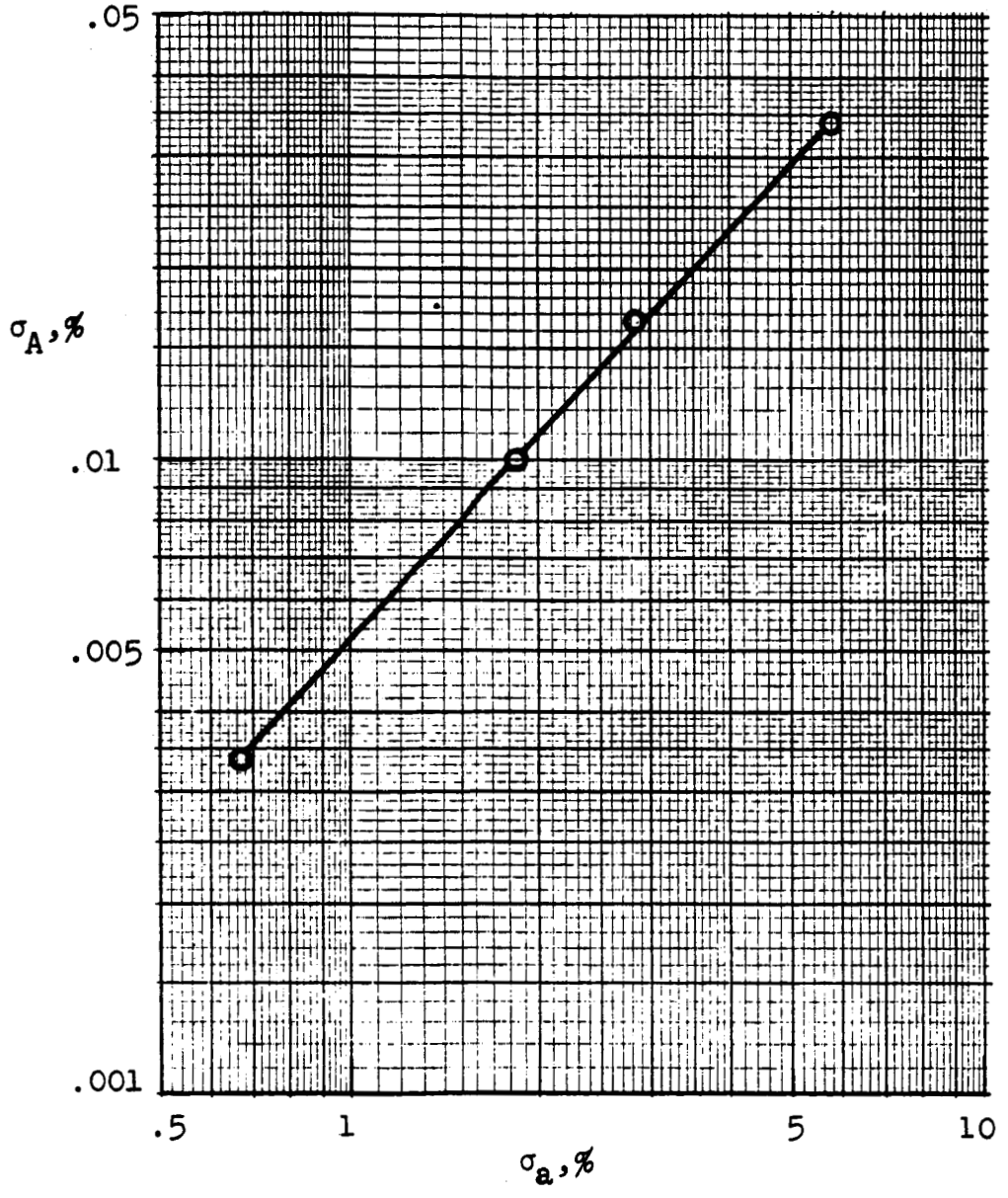

Fig. 42.- Sensitivity study of deduced differential equation coefficients.

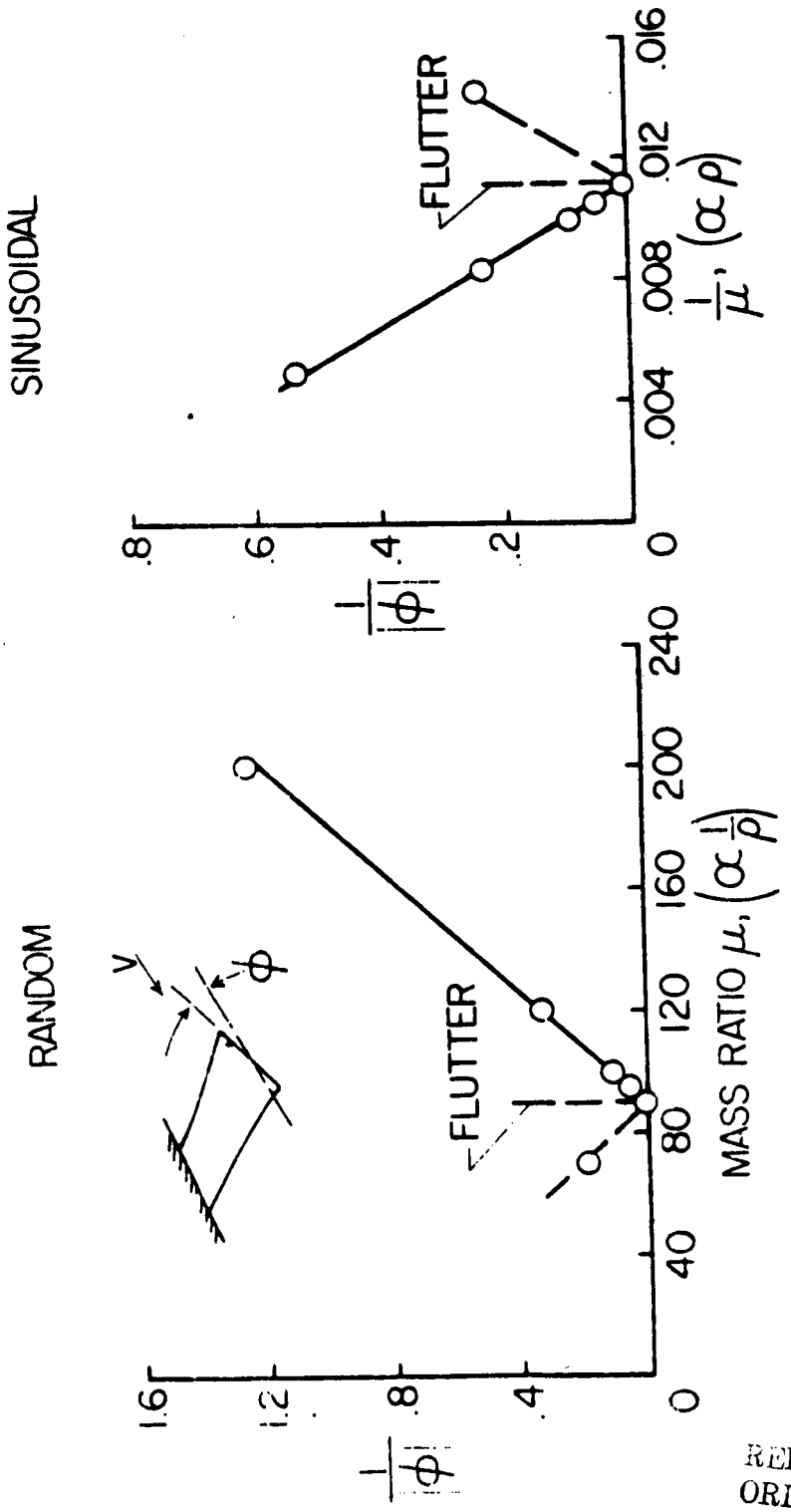

Fig. 43.- Extrapolation technique based upon density.